Development and Characterisation of Neutralising Mouse-Human Chimeric Anti-SARS-CoV Monoclonal Antibodies

by

Kevin Anthony Hay

A Thesis submitted to the Faculty of Graduate Studies of

The University of Manitoba

in partial fulfilment of the requirements of the degree of

MASTER OF SCIENCE

Department of Immunology

University of Manitoba

Winnipeg

THE UNIVERSITY OF MANITOBA

FACULTY OF GRADUATE STUDIES

*****

COPYRIGHT PERMISSION

Development and Characterisation of Neutralising Mouse-Human

Chimeric Anti-SARS-CoV Monoclonal Antibodies

BY

Kevin Anthony Hay

A Thesis/Practicum submitted to the Faculty of Graduate Studies of The University of

Manitoba in partial fulfillment of the requirement of the degree

MASTER OF SCIENCE

DEDICATION

To my father, whose perseverance and hope is a shining beacon.

ACKNOWLEDGEMENTS

I would like to thank my supervisor, Dr. Jody Berry, for his constant help and support in undertaking this Masters Degree. The Immunology Department at the University of Manitoba, both faculty and students, were supportive and enhanced my learning. In particular I would like to thank Kent HayGlass, Aaron Marshall, and John Wilkins for taking the time to be a part of my Masters committee. The laboratory members of the Monoclonal Antibody Lab Unit at the National Microbiology Laboratory were a source of support and expertise whenever I required help, especially Xin Yuan and Francesca Airey. Two cooperative education students, Mark Vendramelli and Melanie Blanchard assisted in the laborious purification protocols, which was great appreciated! My fellow graduate student, Darren Boese, worked through the hard times of chimeric antibody production with me. Christoph Rader at the NIH provided me with invaluable information on using the pIGG vector he developed. James Rini at the University of Toronto supplied me with the antigen necessary to do the vast number of my experiments. I wish to thank Anton Andonov for teaching me how to perform neutralisation assays in a Level 3 facility, and spending his time on this project. Thanks are also extended to my community at St. Margaret's Anglican Church and my roommates who have made Winnipeg 'home' for me.

TABLE OF CONTENTS

TABLE OF FIGURES AND GRAPHS

LIST OF ABBREVATIONS USED

ACE2	ANGIOTENSIN-CONVERTING ENZYME 2
CTL	CYTOTOXIC LYMPHOCYTE
C_K	KAPPA CONSTANT DOMAIN
DC-SIGN	DENDRITIC CELL SPECIFIC INTERCELLULAR ADHESION MOLECULAR GRABBING NONTERGRIN
ELISA	ENZYME-LINKED IMMUNOSORBENT ASSAY
ER	ENDOPLASMIC RETICULUM
FDA	FOOD AND DRUG ADMINSTRATION
FIPV	FELINE INFECTIOUS PERITONITIS VIRUS
HACA	HUMAN ANTI-CHIMERIC ANTIBODIES
HAHA	HUMAN ANTI-HUMAN ANTIBODIES
HAMA	HUMAN ANTI-MOUSE ANTIBODIES
HIV-1	HUMAN IMMUNODEFIENCY VIRUS 1
IRES	INTERNAL RIBOSOME ENTRY SITE
LDH	LACTATE DEHYDROGENASE
L-SIGN	LIVER/LYMPH-NODE SPECIFIC INTERCELLULAR ADHESION MOLECULAR GRABBING NONTERGRIN
MAB	MONOCLONAL ANTIBODY
MBL	MANNOSE-BINDING LECTIN
ORF	OPEN READING FRAME
RBD	RECEPTOR BINDING DOMAIN
RDRP	RNA-DEPENDENT RNA-POLYMERASE
SARS	SEVERE ACUTE RESPIRATORY SYNDROME
SARS-COV	SEVERE ACUTE RESPIRATORY SYNDROME CORONAVIRUS
SCFV	SINGLE-CHAIN VARIABLE FRAGMENT
SGRNA	SUB-GENOMIC RNA
SNV	SINGLE NUCLEOTIDE VARIATION
TRS	TRANSCRIPTIONAL REGULATORY SEQUENCE
UTR	UNTRANSLATED REGION
V_H	HEAVY CHAIN VARIABLE DOMAIN
V_L	LIGHT CHAIN VARIABLE DOMAIN
WHO	WORLD HEALTH ORGANISATION

1 Introduction

1.1 Abstract

Introduction: Severe Acute Respiratory Syndrome coronavirus (SARS-CoV) is the etiological agent behind a pandemic in 2002/2003 that caused ~8000 infections with a 10% case-fatality rate. The health community reacted quickly to contain the pandemic, and no further outbreaks of the disease have been recorded. However, no vaccine is currently available and treatment options are limited in the event another outbreak occurs. Passive immunity via neutralizing monoclonal antibodies would provide a unique and immediate treatment option.

Methods: Using recombinant DNA technology, the variable regions of four anti-SARS-CoV monoclonal antibodies (mAb) of the F26 series were inserted into the pIGG expression vector and transiently expressed in 293T cells. The resulting chimerics were purified and characterised by immunochemical and immunobiological assays. The parental mouse mAbs were characterised in parallel, and the results compared.

Results: ELISA and Western Blotting on parental and chimeric F26 series mAbs demonstrate that the antibodies bind the ACE2 receptor-binding domain of the SARS-spike glycoprotein. The binding characteristics are maintained between the chimeric and parental mAbs. F26G18 (murine) and 18H18L (chimeric) neutralise the *in vitro* infectivity of the TOR2 strain of SARS-CoV with identical titres (0.31 and 0.37 μg/mL respectively) in the same assay system.

Conclusions: A series of neutralising chimeric antibodies specific for SARS-CoV have been developed using recombinant DNA technology. In particular, the chimeric 18H18L retains the high neutralising titre of the parental version, giving it the potential to be used therapeutically in the event of a SARS outbreak.

1.2 Brief History of the SARS Epidemic

On February 11th, 2003 the World Health Organization (WHO) received a report indicating that there were 305 cases of 'infectious atypical pneumonia' in the Guangdong province of China, over 100 being healthcare workers[1]. Five deaths had already resulted[2]. This 'infectious atypical pneumonia' caused severe acute respiratory distress, leading to the name SARS, or severe acute respiratory syndrome for this new disease. Hong Kong responded with increased surveillance for atypical pneumonia especially on people who had recently travelled to mainland China. This surveillance detected a case of H5N1 avian influenza A, sparking the WHO to declare a state of global pandemic alert. However, H5N1 was not detected in any other cases, alleviating fears of an influenza pandemic while raising fears of an unknown agent[3].

Meanwhile, the "Hotel M" in Hong Kong received a guest on February 21st. This guest, a sixty-five year old doctor (Patient A) who had recently visited Guangdong, had been sick since February 15th. Unbeknownst to him, he carried the infectious agent for SARS and infected at least seventeen contacts within the hotel. These contacts then travelled home to locations such as Singapore, Hanoi, and Toronto. In addition, Patient A was taken to the Prince of Wales Hospital in Hong Kong, and an outbreak of SARS

occurred there among the healthcare workers. The rapid worldwide spread of SARS lead to the WHO issuing a global alert on March 12th, followed by a travel advisory on March 15th.[2]

On March 17th the WHO created the Multicentre Collaborative Network for SARS, an international linkage of laboratories to determine the causative agent of SARS[2]. By the end of the month the virus, SARS coronavirus (SARS-CoV), had been isolated by three different laboratories and diagnostic tests were in development. [4-6] By the middle of April, the virus genome was sequenced[7, 8] and the link between SARS and the novel coronavirus was established enough for the WHO to declare SARS-CoV as the causative agent of SARS.

Human-human transmission ended July 5th, with the final cases being reported in Taiwan. In all SARS affected over 8000 patients worldwide with 774 fatalities reported to the WHO[3]. The epidemic was brought under control through a concerted effort by the WHO and national health organisations across the globe, instituting measures to reduce the spread of the disease. In many ways the SARS epidemic served as a prototype of how health organisations and laboratories can work together tightly to achieve the protection of the general population.

1.3 The Clinical Disease

The severe acute respiratory syndrome caused by SARS-CoV is unique. Initially, it presents with fairly ubiquitous symptoms such as fever, malaise, myalgia (muscle pain), and coughing [2]. SARS can be differentiated from some other types of infectious

atypical pneumonias, such as those caused by chlamydia or mycoplasma, by the fact that it rarely presents with upper respiratory symptoms [2]. Later in the course of the illness, the coughing turns into shortness of breath and/or tachypnea (rapid breathing). Pleurisy (inflammation of the pleural cavity lining) and watery diarrhoea can also occur, affecting 40-70% of patients[9]. Radiology of the lung shows abnormalities; mainly ground-glass opacifications or focal consolidations of the peripheral, subpleural, and lower zones of the lungs[10]. Approximately 20-30% of patients require intensive care and mechanical ventilation[2].

Autopsy analysis of the lung in patients who died within ten days of illness onset demonstrates 'diffuse alveolar damage, desquamation of pneumocytes, an inflammatory infiltrate, edema, and hyaline-membrane formation'[2]. Patients who died later in the course of the illness (greater than 10 days) had squamous metaplasia and multinucleate giant cells in the lung along with the diffuse alveolar damage. Respiratory failure caused by acute respiratory distress syndrome was the main cause of death in all cases[2].

The mean incubation period of SARS is about four and a half days, a slightly longer period compared to other respiratory viral infections. The viral load reaches its peak around ten days after disease onset[11]. Blood work shows lymphocytopenia in the majority of cases, with elevated levels of serum alanine aminotransferase and lactate dehydrogenase (LDH)[9]. The lymphocytopenia affects $CD4^+$ more than $CD8^+$ T cell populations and reaches a nadir seven to nine days after infection, before recovering to normal[12]. Thromobocytopenia occurs in some cases[12]. The main spread of virus is by aerosol inhalation; however, virus has been detected in the feces of patients with diarrhoea, providing another potential route for viral spread[9].

Predisposing adverse outcome predictors in infected patients include advanced age, high concentration of LDH, and a pronounced lymphocytopenia[2]. Older patients seem to be more susceptible, with case fatality rates increasing as a function of age: 0-24 (0%), 25-44 (6%), 45-64 (15%), and ≥65 years old (52%)[11]. The disease severity was lower in youths, suggested by the fact that none of the children younger than 12 required intensive care or mechanical ventilation. One study showed that more females than males were infected, but this is probably due to the high proportion of female nurses, a primary group affected by the SARS outbreak[13].

Complications occur in some patients who successfully clear SARS-CoV. These include respiratory impairment, muscle weakness, post-traumatic stress disorder, and depression[14, 15].

1.4 Virology of SARS-CoV

1.4.1 Morphology and Classification

SARS-CoV belongs to the family *Coronaviridae*, so named for the related viruses that have a distinctive crown-like morphology of club-shaped peplomers radiating from the envelope[16]. *Coronaviridae* is within the order Nidovirales, a group of positive-stranded RNA viruses that translate their proteins via a nested set of subgenomic (sg) mRNAs[16]. *Coronaviridae* also can be subdivided into two genuses; *Coronavirus*, which SARS-CoV belongs to, and *Torovirus*. Unlike coronaviruses, members of the genus *Torovirus* produce rod- and kidney- shaped virions as well as the common spherical

structure[16]. Coronaviruses are the only members of Nidovirales that have been seen to be important pathogens in humans[16].

Serologically, the coronaviruses can be divided into three main groups. Group I and II have been isolated from mammals, while so far Group III has been restricted to birds. The human coronaviruses are spread between Groups I and II. Initial sequencing studies based on the highly conserved polymerase gene placed SARS-CoV within its own group (Group IV) [7, 8]. Later analysis based on an even more conserved region further downstream in the ORF1b region using the genus *Torovirus* to root the tree demonstrated that SARS-CoV is better understood as an early split-off from Group II, a view that has been further confirmed by others[17].

Coronaviruses cause a wide variety of diseases from the common cold and enteritis to fatal multi-organ involvement. Although the coronaviruses as a group infect a broad range of species, from birds to primates and cows, individual viruses tend to only infect one animal species[18]. SARS-CoV is unique among the coronaviruses for its ability to cross species readily, productively infecting Himalayan palm civets, cats, dogs, rodents, and primates[16].

1.4.2 Genomic Organisation

At 30 kilobases, coronaviruses contain the largest RNA genome of all known viruses. The SARS-CoV genome is a single positive-stranded RNA with a 5' replicase region (265-21,485) and a 3' structural region (21,485-29,740) [17]. Capped and polyadenylated, the genomic RNA can and does serve as mRNA, demonstrated by the fact that the purified genomic RNA alone is infectious[16]. The replicase and structural

regions are flanked by 5' and 3' untranslated regions (UTRs) 192 and 340 nucleotides in length respectively. These UTRs are further enclosed on the 5' end by a 72-nucleotide leader sequence, and the polyadenylate tract on the 3' end[17]. The leader contains a transcriptional regulatory sequence (TRS) six nucleotides in length that is repeated eight more times throughout the genome: 5'-ACGAAC-3'[19]. The viral RNA-dependent RNA polymerase (RdRp) uses the TRSs to transcribe the nested set of mRNAs (see section 1.4.6).

SARS-CoV contains a total of fourteen open reading frames (ORFs), two within the replicase region (ORF1a and 1b) which covers two-thirds of the genome and the remainder in the structural region[7]. Within the structural region four of the ORFs are assigned to conserved structural proteins. The eight ORFs unaccounted for are found interspersed between the structural protein ORFs and encode putative accessory proteins[8]. Each coronavirus has a set of accessory proteins that are unique to it, and may or may not have some homology to other coronaviruses. The accessory proteins of SARS-CoV show no significant homology to any other coronavirus accessory protein[17].

1.4.3 Nonstructural Proteins

The replicase region ORFs (1a & 1b) are read through together by a -1 ribosomal frameshift mechanism to produce a single polyprotein. The frameshift occurs through the combination of a 'slippery' sequence and a downstream pseudoknot structure to stall the ribosome[19]. The polyprotein is cleaved into the 16 nonstructural proteins (Nsp) by two internal viral proteinases; a chymotrypsin-like protease (M^{pro}) that is found in all coronaviruses and a papain-like cysteine protease (PL^{pro}). PL^{pro} is involved in cleavage

of the N-terminal of the ORF1a region, while M^{pro} cleaves the C-terminal ORF1a and the entire ORF1b region[16].

While all the Nsps have not been well characterised structurally or biologically, some information is known. Nsp1 seems to suppress host protein synthesis by targeting the mRNA for degradation[20]. Nsp2 is 638 amino acids in length, and has no known function[21]. Nsp3 and Nsp5 are the PL^{pro} and M^{pro} proteases respectively, while Nsp4 and Nsp6 are putative membrane proteins[21]. A multidomain protein, Nsp3 functions also as an ADP-ribose 1'-monophosphatase through its X domain and contains three other domains of unknown function[16]. Nsp7 and Nsp8 form a cylinderical structure that bind RNA through the Nsp8 unit, and can act as a secondary RNA dependent RNA polymerase (RdRp) [22]. Nsp9 is a single-stranded RNA-binding protein (ssRBP), while Nsp10 assembles into a dodecameric structure, binds nucleic acid, and effects mitochondrial function through interacting with proteins involved in the oxiditive electron transport chain[21]. Nsp11 is a short 13aa peptide with unknown function[21].

Nsp12 is the main RdRp and Nsp13 is a helicase with NTPase, dNTPase and 5'triphosphatase activity. Exo- and endo- ribonuclease activity are performed by Nsp14 and Nsp15 respectivity, while Nsp16 is a ribose 2'-O-methyltransferase[21].

1.4.4 Structural Proteins

Spike (S) protein is the glycoprotein that forms the club-shaped peplomers on the surface of the virion. Encoded by ORF2, this 1255 amino acid protein has 12 N-linked glycosylation sites and a molecular mass of approximately 180 kiloDaltons[19]. The large external domain can be subdivided into two functional domains, termed S1 and S2, while

the C-terminal is comprised of the transmembrane and cytoplasmic domains[16]. Studies suggest that S exists *in vivo* as a trimer which forms in the ER and then is transported to the Golgi to make EndoH-resistant complex N-glycans[23]. The globular head is formed by S1, which contains the ACE2 receptor binding domain between amino acids 318-510[24]. S2 forms the stalk and possesses two heptad repeat motifs of a coiled-coil structure and acts in membrane fusion[25], much like gp41 does for HIV-1.

Host cell receptors that bind S protein have been identified. Angiotensin-converting enzyme 2 (ACE2), a membrane-bound host protein, binds S protein and mediates virion entry, making it the primary receptor for the virus[26]. The lysines at 353, and to a lesser extent 82 and 84 of ACE2 seem to be important for binding to S protein. Studies have shown that S protein also binds to liver/lymph-node specific intercellular adhesion molecular grabbing nontegrin (L-SIGN) [27] and dendritic cell SIGN (DC-SIGN) [28]. While L-SIGN mediates virion entry, albeit at a lower efficacy than ACE2, DC-SIGN does not mediate entry and therefore may play a potential role in the systematic spread of the virus by acting as a 'Trojan horse'.

Envelope (E) protein is a small (9 kiloDalton) 76 amino acid protein that associates with the viral envelope and is encoded by ORF4. E protein has two transmembrane domains with both N- and C- termini in the virus lumen. Although E protein is not essential to virion assembly, it probably serves an important role in creating the spherical structure, since virions assembled in the absence of E are aberrantly shaped[16]. E has also been shown to deform lipid bilayers, leading to curvature. In addition to virion assembly functions, E seems to act as an ion channel, altering membrane permeability[29]. The purpose of this function is currently unknown.

Membrane (M) protein is encoded by ORF5 and associates with the viral envelope. The N-terminal ectodomain is linked to a triple-membrane spanning domain, then an α-helical domain followed by the C-terminal endodomain[16]. The ectodomain is N-glycosylated. M protein does not get transported to the plasma membrance but rather stops at the Golgi complex[30]. It also interacts with both S and nucleocapsid (N) proteins, playing an important role in virion assembly[31].

Nucleocapsid (N) phosphoprotein is a 46 kiloDalton multifunctional protein. Encoded by ORF9a, N phosphoprotein binds to viral genomic RNA to form the helical nucleocapsid. It performs this through its RNA-binding domain which binds to the leader sequence of viral RNA[16]. N phosphoprotein also aids in virion packaging through associating with the M protein, and is implicated in the control of viral RNA production. Cellular localisation experiments support these functions, with N phosphoprotein accumulating at the sites of RNA production and assembly[16].

1.4.5 Accessory Proteins

SARS-CoV contains the largest number of accessory proteins of any of the known coronaviruses. None of these proteins are essential for virus replication *in vitro*[32]. The structure and function of these proteins is still an area of considerable research, since in most coronaviruses their elimination leads to marked viral attenuation. By making recombinant forms of the proteins, it was seen that SARS patient sera contained antibodies directed against all of them[33]. These proteins may play a virulence factor role in human infections as they are clearly expressed *in vivo*.

The most studied accessory proteins are 3a, 3b, 6, and 7a, called by the ORF that produces them. After studies demonstrating that it is a transmembrane protein that integrates into the mature virion, 3a has been classified as a novel structural protein unique to SARS-CoV[34, 35]. Two forms of 3a are detectable, a major 37kDa O-linked glycoslyated form and a minor 31kDa unglycoslyated form, though only the 37kDa form is incorporated into the virions. 3a interacts with S, M, and E suggesting a putative role in virus assembly[36]. 3b is a 154 amino acid protein that contains two nuclear localisation signals and has been shown to be targeted to the nucleus[37]. It may play a role in pathogenesis through disregulating the cell cycle[38]. When accessory protein 6 was inserted into the an attenuated murine coronavirus (MHV) genome, the strain became markedly more virulent[39]. This suggests that accessory protein 6 plays a role in enhancing virion production and pathogenesis. 7a localises in the intermediate compartments between the Golgi and ER and has a putative role in inducing capase-dependent apoptosis[40].

1.4.6 SARS-CoV Replication

SARS-CoV attaches to cells by binding ACE2, with possible assistance from L-SIGN (in *cis*) and/or DC-SIGN (in *trans*). In order for fusion of the virus and cell membranes to occur, a protease must digest S protein into the S1 and S2 fragments[41]. If the virus undergoes endocytosis, cathepsin L in the acidic endosomes can perform the cleavage process[42]. However, there is some evidence that secreted proteases can cleave S protein before it encounters a cell, thereby allowing it to fuse directly with the cell

membrane[11]. This information helps clarify conflicting reports on whether or not SARS-CoV fusion is pH-dependent.

After attachment and cleavage, the viral fusion peptide in the S2 region is embedded into host membrane and the heptad repeat regions come together into a six-helix bundle, fusing the membranes and freeing the nucleocapsid into the cytoplasm. The N phosphoprotein then disassociates from the nucleic acid through an unknown mechanism and the full length genomic RNA serves as the mRNA for the ORF1a/1b polyprotein. Upon cleavage, these units form the RNA replicase-transcriptase complex[16].

In order to transcribe the remaining ORFs and replicate the genome, negative sense RNA is first formed, which then serves as the template for more full length genomic RNA as well as the sub-genomic (sg) nested set of mRNAs that give rise to the remaining proteins. This nested set of eight sgRNA molecules contains the same 3' end with a common 5' leader and different middle lengths. With the exception of sgRNAs 3, 7, 8, and 9, only the 5' most ORF is transcribed. For 3, 7, 8, and 9 an internal ribosome entry site (IRES) to allow for expression of ORF3b, 7b, 8b, and 9b products respectively. Although a set of negative sense sgRNAs have been identified in infected cells, it is still unknown whether or not the set of positive sense sgRNAs are made from the corresponding set of negative ones, or if the main route is from full length negative sense RNA to positive sense sgRNA [16].

Creation of the nested set is made possible through the transcription regulatory sequences (TRS) present in the leader and at the start of each sgRNA. If the sgRNA are made during positive sense transcription, then the transcriptase complex starts by transcribing the leader at the 3'end of the negative sense full genome, encounters the

TRS, then jumps to another TRS on the genome and continues transcription. If negative sene sgRNA is made first, then the discontinous transcription occurs in the reverse fashion, jumping to the TRS in the leader sequence[16]. The only protein of the ORF1a/1b polyprotein that has been shown to not be essential for replication is Nsp2[43].

Once the sgRNAs are produced, the host ribosomal machinery is hijacked to manufacture the viral proteins. As N phosphoprotein accumulates, it starts to associate with viral RNA in the cytoplasm, both positive and negative sense as well as full length and subgenomic. This association seems to regulate the viral RNA replication process, as accumulation leads to a shift from sgRNA to full-length genomic RNA[16]. The newly formed helix nucleocapsid is then packaged into the virions through a RNA packaging domain at nucleotides 19715-20294, as well as interactions of N with M protein[44].

Although some S protein travels to the cell surface of infected cells and can cause fusion, the majority of S, E, and M (as well as 3a, but in extremely low levels) localises to the ER/Golgi Intermediate Complex (ERGIC) [16]. It is here that virions form by curvature of the membranes and bud with nucleocapsid inside. The virions then accumulate in large vesicles within the cells, which then in turn fuse with the plasma membrane, releasing the virus.

1.5 Host / Pathogen Interactions

1.5.1 Tissue Tropism

ACE2, the primary receptor for S protein on SARS-CoV, has a wide tissue distribution. It is a metallopeptidase homolog of ACE. ACE2 inactivates angitotensin II,

turning off the rennin-angiotensin system and controlling cardiac function and blood pressure[11]. Some of the organs it is present in include the lung (alveolar type I and II pneumocytes), small intestine (enterocytes), kidney (brush border proximal tubular cells), and endothelial vessels[45]. ACE2 is not expressed on B and T lymphocytes or splenic macrophages. There is considerable debate currently about the expression of ACE2 in the upper respiratory tract, with one group reporting expression in only the basal layer of the nonkeratinised squamous epithelium[45], and another finding abundant ACE2 expression on the luminal surface of ciliated cells[46].

The tissue tropism of SARS-CoV for the lung, small intestine, and kidney can be explained by the receptor distribution[47]. However, virus has been detected in the colon and on hepatocytes, even though colonic enterocytes and liver cells reportedly lack ACE2[48]. Also, there is no evidence of arterial or vein endothelial cell infection, even though they have expression of the receptor. This presence of virus in cells lacking the receptor and absence of virus in cells with the receptor suggests that other factors, such as a co-receptor, are important in infection of these cells.

Upon autopsy, virus can also be detected in brain, spleen, and lymph nodes. *In vitro* studies have shown that PBMCs[49], DCs[50], and monocyte derived macrophages[50] can be infected with SARS-CoV, but the infection tends to be abortive, i.e. viable virus progeny is not produced. Recently, it has been reported that replication can occur in PMBCs for a short period of time, about 8 days [12].

1.5.2 Host Immune Response

The host immune response to SARS-CoV involves all arms of the immune system, innate and adaptive, cell-based and humoral. Plasma proteomic analysis demonstrates that acute-phase proteins, like serum amyloid A and mannose-binding lectin (MBL) are elevated in infected individuals[51]. MBL in particular can be seen as a first defence against the virus since it can bind to S protein through its carbohydrate recognition domains leading to protective effects that are mannan-inhibitable. A study of MBL gene polymorphism showed a significant difference in the distribution, with certain haplotypes that were associated with low or deficient MBL serum levels being linked to patients that developed SARS compared to healthy controls [52].

Cytokines can play an important role coordinating the immune system and leading to the appropriate protective response. In fatal SARS cases expression of IL-6, IL-8, and MCP-1 was detected in the lung. IP-10, IL-8, MIG, and MCP-1 are elevated in SARS patients' lungs and peripheral blood, though there is a noted absence of type 1 IFN and TNFα [53]. This lack of type I IFN and TNFα is a distinctive difference between SARS-CoV and influenza infections, which induce a large amount of these cytokines [11]. IFNγ is shrouded in contradictory reports; two series from Hong Kong suggested that it was elevated and possibly plays a role in immunopathogenesis [54, 55], while several other studies report no elevated IFNγ levels [53, 56, 57].

In vitro studies done on the abortive infection of macrophages and DCs by SARS-CoV demonstrates that IP-10, MCP-1, MIP-1a, and RANTES are upregulated upon infection of these cells [58, 59]. Immunohistochemistry (IHC) on IP-10 shows that it is present in pneumocytes and alveolar macrophages[53]. Overall, however, there is a lack of

evidence as to which cells in particular are producing the cytokine and chemokine response to SARS-CoV, and further investigation is required.

Cytotoxic lymphocytes (CTL) and helper T cells both seem to play an important role in cell-based immunity. One study in SARS survivors showed that two HLA-A2 restricted epitopes present in the S protein were high immunogenic and created a specific T cell response[60]. T cell responses in patients to N phosphoprotein were seen to persist for at least two years after clearance of the virus[61]. When SARS patients were restimulated with inactivated SARS-CoV a memory CTL response was induced, and there was a selective expansion of Vγ9Vδ2 effector/memory populations[62]. These Vγ9Vδ2 T cells are able to provide anti-SARS-CoV activity in an IFNγ dependent manner by killing infected target cells. NK cells may or may not be important in disease; mouse model studies suggest NK cells are disposable[63], while some human studies suggest that they could have a role in reducing the severity of the disease.

The humoral antibody response also plays a role in host defence. By day 14 of the illness, most patients have seroconverted[64]. However, immunofluorescence assays and ELISA developed with N phosphoprotein can detect serum IgG as early as day 4. A follow-up study of 56 subjects demonstrated that total SARS-CoV specific and neutralising IgG antibodies peaks at approximately 4 months before dropping[65]. After 24 months, 11% no longer had SARS-CoV specific antibodies detectable by ELISA; however, neutralising antibodies were still present. A larger study of 623 subjects showed that the neutralising antibodies were able to neutralise pseudotype viruses created from the S proteins of four different strains, demonstrating that neutralising antibodies can be cross reactive[66]. S protein is the only structural protein that elicits neutralising

antibody, though there has been some work showing that antibodies against the accessory/structural protein 3a are neutralising[67]. The *in vivo* significance of this work, however, is unknown. Amino acids 441-700 of S protein contain the epitopes that are immunodominant for antibody response, as shown by the screening of SARS patient sera against truncated fragments of the S protein[68].

1.5.3 Pathology and Immunopathology

A current area of research in SARS-CoV host/pathogen interactions is the exact mechanisms of lung damage leading to respiratory failure, as well as the contribution of an excessive or misled immune response to the pathology. The lung damage seen is described as acute lung injury leading to diffuse alveolar damage. Two main mechanisms seem to result in lung damage: a direct destruction of the alveolar and bronchial epithelial cells and macrophages, and an indirect destruction caused by immune mediators.

Direct destruction can be simply described as the damage the virus performs on the cells as a result of infection. In terms of directly impacting cellular function, some of the accessory proteins play important roles in disregulating the cell cycle. For example, 3a (studied in Vero E6) [69] and 7a (studied in lung, kidney, and liver cell lines) [70] proteins both induce capase-dependent apoptosis. 7a also inhibits cellular gene expression and activates p38 MAPK[71].

The conflicting findings for IFNγ mentioned above (see 1.5.2) play an important role in the cause of immunopathogenesis and indirect destruction of the lung. Huang et al implicate IFNγ as a key member of a proinflammatory cytokine storm including IP-10, MIG, and MCP-1 that leads to excess inflammation and lung damage. Another study

shows that IP-10 levels 1.5 times higher than the median gives an odds ratio of 3.7 (95% CI 1.5-9.2) for deterioration and an adverse outcome[55]. Lee et al, however, argue that the immunosuppressive cytokines TGFβ and PGE-2 actually cause the pathology by not allowing for an effective early clearance of the virus[57].

Virus clearance can also be hindered by the ability of SARS-CoV to block activation of the IFN regulatory pathway. Soon after IFN regulatory factor 3 (IRF-3) is transported to the nucleus, the pathway is blocked, prevent production of type I IFN[72]. The specific mechanism in which SARS-CoV blocks this pathway is currently unknown, though there is research suggesting that accessory proteins 3b and 6, along with N protein are involved. This provides a molecular mechanism for why type I IFN is noticeably absent from the immune response, and cannot even be induced *in vitro* in SARS-CoV infected cells.

Another intriguing aspect of SARS-CoV pathology is the importance of ACE2 in alleviating lung injury. Imai et al showed that ACE2 can protect against acute lung injury by its activity in inactivating angiotensin II[73]. SARS-SoV infection of mice lead to reduced ACE2 expression in the lungs, and intraperitioneal injection of recombinant S protein aggravates acute lung injury[74]. This response was seen to be specific for S protein's effects on ACE2. However, a newly discovered human coronavirus called NL63 also binds ACE2, but it is not associated with acute lung injury[75]. Therefore using ACE2 as a viral receptor does not always produce acute lung injury.

Antibody-dependent enhancement is of particular concern when developing vaccines or passive immunisation strategies. For coronoviruses, antibody-dependent enhancement has been documented in domestic cats challenged after immunisation with a

feline infectious peritonitis (FIPV) vaccine[76]. Unlike FIPV however, SARS does not seem to productively infect macrophages, a key cell type affected by antibody-dependent enhancement. As well, studies in animals using the passive transfer of anti-SARS-CoV antibodies detected no evidence of enhancement[77].

1.6 Aetiology and Epidemiology

1.6.1 Animal Reservoir

A unique feature of the epidemiology of SARS-CoV was the tight connexion been all the cases of SARS and the ability to trace back the epidemic to its source in Guangzhou, Guangdong Province, China. In particular, animal food handlers in Guangdong markets were significantly over-represented both in terms of early-onset SARS and higher titre of IgG antibodies directed against SARS-CoV[78]. Initial studies in the wet markets using ELISA, RT-PCR, and virus isolation on eight different species identified SARS-CoV like viruses in two species, *Paguma larvata* (masked palm civet) and *Nyctereutes procyonoides* (racoon dog) [79]. Sequence analysis of the isolates demonstrated a 99.8% nucleotide identity to human isolates of SARS-CoV[80]. This information, in combination with epidemiological data linking infections to connexions in the live animal trade, provided a strong argument for the transfer of the virus from civets and raccoon dogs to humans.

Further in depth studies on civets presents intriguing data suggesting civets are not the natural reservoirs of SARS-CoV. Independent studies by Tu et al[81], Kan et al[82],

Hu et al[83], Poon et al[84], and showed that the wet market civets had an abnormally high infection rate in comparison to farmed and wild civets. A possible explanation for these results is that the overcrowded conditions in market provide the prefect opportunity for a small number of infected animals to infect the group. Therefore an epidemic of the virus amongst civets occurred prior to the human epidemic. The close genetic relatedness, over 99.6%, of the civet viruses to each other supports this hypothesis by suggesting that civets as a species were not infected long enough for significant diversity to accumulate[85]. Regardless, civets are easily infected and definitively played a role in the zoonotic transmission of the disease.

Attention then turned to bats as a possible natural host. As the only flying mammals, bats comprise 20% the mammalian diversity and are generally gregarious in their social habitats, i.e. roosting[85]. These factors combined with evidence of bat hosts for many other infectious diseases triggered researchers to investigate bat populations in China for SARS-like coronaviruses. Two independent research groups, Li et al[86] and Lau et al[87], demonstrated by ELISA and RT-PCR that horsebat species of the genus *Rhinolophus* harboured SARS-like coronaviruses. Full genome sequence analysis showed 87-92% homology between the bat and human or civet viruses[85]. Unfortunately, neither groups were able to successfully isolate virus. Significant changes in the receptor binding region between bat and human/civet viruses could account for this, since the bat viruses may utilise an unknown receptor.

These differences between the bat and civet viruses are large enough that further research needs to be done to make the epidemiological connexion. Either higher identity viruses in bats or lower identity viruses in civets to SARS-CoV would provide a greater

genetic continuum between bat and civet viruses. The other major possibility is that species are missing from the studies that could link the gap, and that infection of civets with bat viruses did not occur directly.

1.6.2 Epidemiology and Genomic Evolution

The initial official recognition of infectious atypical pneumonia in Guangdong Province occurred on January 2nd, 2003 at the People's Hospital of Heyuan[1]. Retrospective studies showed that the initial case of SARS occurred in Foshan on November 16th, 2002. Scattered cases occurred during this early phase of the disease, till a super spreader event occurred at the HZS-2 Hospital in Guangzhou, starting January 18th, 2003. This super spreader event drastically increased the number of SARS cases, and led to the infection of Patient A, who was to later visit Hotel M in Hong Kong on February 21st, 2003 and start the worldwide pandemic through the infection of at least seventeen people.

Clinical isolates from these three phases of the epidemic combined with isolates and sequence data from civets and bats paint a fascinating picture of viral evolution, as it progresses both cross-species and within species. Twenty-six single nucleotides variations (SNVs) leading to amino acid mutations occurred between the civet and late phase human SARS-CoV isolates[1]. These SNVs accumulated as the epidemic progressed, since early phase human isolates resemble civet viruses more at these SNVs. Middle phase isolates contain only around four SNVs similar to civet, and they differ in all isolates from the late phase[85]. Civet and early phases isolates also share a 29 nucleotide sequence that connects ORF8a and ORF8b into one ORF, which is deleted in

the later isolates. These genetic characteristics help define the epidemiological phases, and were used to trace the path of the epidemic.

These molecular changes likely provided adaptive advantages as the virus attempted to infect human cells versus civet cells. In particular, these SNVs led to four amino acid changes in the receptor binding domain of S protein; K334R F360S, N479K, and T487S[88]. Affinity studies using TOR2 (late phase human) and SZ3 (civet) strains with human and civet ACE2 receptor demonstrated that TOR2 bound equally well to human and civet ACE2, while SZ3 binds preferentially to civet ACE2[88]. Further mutation studies elucidated that the residues critical in the affinity increase were at 479 and 487, with the T487S change being more significant that the N479K one. It has been suggested that the change at 487 was the essential step for human adaptation (animal-human), while the 479 change increase the affinity to allow for pandemic spread (human-human) [1].

Bat SARS-like coronaviruses add another dimension and raises questions as to how cross species animal-animal transmission occurs. While the bat viruses are 87-92% identical to the human and civet ones, a large variation occurs in the S protein, with homology dropping to 76-78%[85]. This homology drops even further when considering only the S1 region with the receptor binding domain (RBD). Two deletions sites in bat viruses of 5 and 12 amino acids in length fall in a critical region of the RBD, implying that bat viruses bind a completely different receptor[85]. More work on identifying the receptors of these viruses could lead to interesting conclusions regarding how a virus changes its molecular target.

1.7 Therapeutics

Based on the epidemiological data, two potential sources of human SARS-CoV infection exist. Firstly, the continued presence of SARS-like coronaviruses in the environment in known and unknown reservoirs provides a source for re-infection of the populace. Secondly, late phase laboratory strains can re-emerge through laboratory mishaps. Both types did occur in the winter of 2003 and the spring of 2004 after the official end of the epidemic. While proper clinical surveillance and laboratory management should be able to curb another epidemic, new therapeutics need to be developed in order to alleviate the symptoms of future patients. In addition, some therapeutics could be useful to help prevent transmission, lessening the impact of a future epidemic.

1.7.1 Vaccine Designs

Numerous studies have been undertaken to test the efficacy of different vaccine designs against SARS-CoV, with many showing promising results. Live attenuated vaccines have not been attempted, due to the seriousness of the disease and a lack of understanding of the specific mechanisms of pathogenesis. Ultraviolet light (UV) and formalin inactivated whole virion vaccines produced high levels of neutralising IgG antibody in mouse models[89-91]. The UV-inactivated vaccine in particular did not even require an alum adjuvant. Phase I clinical trials untaken by the Chinese government demonstrated that an inactivated vaccine led to no serious complications[92]. However, the

potential safety risks of handling the stock virus needed to produce the virus, which requires a Level 3 Biocontainment Facility, could discourage the large-scale production of this vaccine.

With the advent of molecular cloning techniques, vector-based vaccines have come of age as a safer and effective way to produce large amounts of vaccine without the risk of infection with wild-type virus. In this design, the immunodominant protein that elicits neutralising antibodies, which is usually the receptor-binding glycoprotein (in this case, S protein), is shuttled into another virus that will not cause disease in humans. Multiple virus platforms have been developed. A modified vaccina virus Ankara (MVA-S) demonstrated protective responses in mice and *Rhesus macaques* upon challenge, but it failed in a ferret model and even seemed to enhance the disease[93-95]. A chimeric bovine/human parainfluenza virus 3 (BHPIV3) based vaccine protected African green monkeys from challenge with wild virus[96]. Adenovirus type 5 virus has also been tested with various combinations of S, M, and N, and although a strong SARS-CoV specific immune response was seen no challenge experiment data has been published to date[97]. Vesicular stomatis virus (VSV) and Rabies virus (RV) platforms were also studied, with the S protein based vaccines demonstrating efficacy in mouse models[98, 99].

Although still in its developmental stages, DNA vaccination strategies are becoming increasing popular. Numerous DNA vaccines have been designed and tested in mouse models. Overall, S protein based DNA vaccines induced neutralising antibodies and some cytotoxic lymphocyte (CTL) responses[100], while N protein based ones produced CTL responses[101-103]. However, the long-term protection offered by these vaccines and their efficacy in humans is questionable.

Subunit vaccines are also being developed, using portions of the S protein. Using a baculovirus-expressed S1 protein, Bisht et al induced neutralising antibody in a mouse model, which was higher than that induced by live virus[101-103]. Zakhartchouk et al used a mammalian HEK293T expression system to develop a receptor binding domain (RBD) protein (S318-510) for mouse model experiments. In this study, they demonstrated that glycosylated S318-510 produces a greater SARS-CoV specific immune response than deglycosylated (dg) S318-510 protein[104]. The results of challenge experiments, however, have not been published.

The full weight of vaccine science to date has been used in the design of these new vaccines for SARS-CoV, ranging with inactivated viruses to DNA vaccines. However, vaccination may be not the most suitable approach to tackling this virus. It is uncertain when and if another epidemic will occur, and what population besides animal trade workers and hospital staff would be effected. Therefore, though vaccination may be beneficial for these high-risk groups, other therapeutic approaches need to be examined.

1.7.2 Antiviral Drugs

A promising area of therapeutic approaches is in the development of antiviral drugs. The vital role of the main protease (M^{pro}) in post-translational cleavage of the ORF1a/b polypeptide makes it an attractive target for protease inhibitors. The protease dimerises through a salt bridge between Glu290 and Arg4 [105]. A catalytic diad of Cys145 and His41 performs the proteolytic activity [21]. The majority of inhibitors target this catalytic function, in particular the thiol group on Cys145, using a mechanistic approach

based on the protease crystal structure. For example, the inhibitor TG-0205221 binds covalently to Cys145 via an aldehyde group [106]. Another inhibitor, based on a benzotriazole ester structure, acylates this cysteine residue [107]. Molecular docking experiments identified some commercially available compounds that also show potency in *in vitro* inhibition assays. The crystal structure of one of these inhibitors demonstrates inhibition by a conformation rearrangement of His41, abolishing the catalytic pocket [108, 109]. These protease inhibitors present new possible therapeutics for SARS.

During the epidemic ribavirin was used experimentally on SARS patients with contradictory results. Ribavirin is an inosine monophosphate (IMP) dehydrogenase inhibitor [110]. IMP dehydro is a key enzyme in de novo synthesis of purine nucleotides, making ribavirin a broad spectrum antiviral agent. A few experiments have been done post-epidemic in order to clarify the issue of its efficacy. In particular, when SARS-CoV infected mice were treated with ribavirin for 3 days they had higher viral titres and prolonged infection compared to an untreated group [110]. This suggests that ribavirin should not be used therapeutically.

1.7.3 Neutralising Antibodies

Neutralising antibodies to viruses can serve as a type of viral entry inhibitor drug when administered as prophylaxis. Prophylaxis is effective in a variety of viral infections, including varicella, hepatitis A, hepatitis B, rabies, and respiratory syncytial virus (RSV) [111]. During the SARS epidemic, hyperimmune sera from convalescent patients were used as treatment with no apparent adverse side effects[112]. An assessment of the efficacy of this treatment is hard to complete due to the small sample numbers

available, though it did seem to shorten hospitalisation time. Soon after the isolation of SARS-CoV monoclonal antibodies were developed to the native virion in mice by hybridoma techniques[124] and from memory B cells of convalescent patients by phage display and Epistein-Barr virus transformation[113]. In addition to providing essential reagents for diagnostics and screening, many potent neutralising antibodies have been isolated and characterised.

Using a single-chain variable fragment (scFv) library created from non-immune human antibodies screened against recombinant S1 protein, Su et al. isolated 80R which possesses potent *in vitro* neutralising capability (50% protection at 0.37nM) and high affinity (1.59nM) [114]. Immunoprophylaxis using 500μg of 80R in a mouse model reduced viral titres to below the point of detection [115]. Neutralisation assays using psuedotype virions contained spike variants from throughout the epidemic demonstrates that 80R can bind early and late forms of the virus, though not the 2003/04 GD03T0013 strain[115]. The crystal structure of 80R complexed with S1 protein shows that all six complementary determining region (CDR) loops are involved [116]. 80R contacts with 29 residues on S1 protein, all between aa426-492, of which 17 are shared contacts with ACE2. This reveals the structural rationale for its neutralisation, by interfering with S protein binding to the ACE2 receptor.

Similarly, Zhu et al isolated m396 from a non-immune human scFv library through screening against recombinant receptor binding domain (RBD) S protein[117, 118]. The IgG1 version of this antibody demonstrates an affinity of 4.6pM and an IC_{50} of 1μg/ml. In addition, it can neutralise the GD03T0013 isolate[117, 118]. Crystal structure

analysis of Fab m396 complexed to RBD S protein shows that m396 recognises the epitope 482-491, using CDR loops H1, H2, H3, and L3[117].

With mice transgenic for human immunoglobulin genes, Greenough et al. isolated two neutralising antibodies, MAb201 and MAb68, through immunisation with recombinant S protein[119]. While MAb201 binds in the RBD of S protein between residues 490-510, MAb68 has a unique neutralisation epitope located at aa130-150. Affinities were 34nM and 83nM respectively, and both provided 50% neutralisation *in vitro* at approximately 1nM. Both antibodies are protective in a mouse challenge model. MAb201 was further tested in a golden Syrian hamster model and shown to reduce the viral titre by 250-fold[120].

By screening a semisynthetic human scFv library against whole inactivated virion, van den Brink et al. obtained CR3014, which affords complete protection *in vitro* at 6.3μg/ml[121]. This antibody was further evaluated in a ferret infection model[122]. Virus titre in the lungs was reduced 3.3 logs compared to controls and the lung pathology was abolished. Furthermore, CR3014 eliminated viral shedding in three of the four ferrets treated. By additional screening of the phage library against SARS-CoV escape mutants of CR3014 the neutralising antibody CR3022 was discovered[123]. Neutralisation and affinity assays demonstrate that CR3014 and CR3022 work synergistically to prevent infection *in vitro*. These results offer hope for the use of antibody proprophylaxis as a way to combat the spread of SARS.

Many other laboratories have been active in the isolation of neutralising antibodies against SARS-CoV. Our laboratory has been involved since the SARS epidemic with the production and characterisation of antibodies against SARS-CoV for

use in diagnostics and therapeutics. We used mouse hybridoma technology to produce a series (F26) of monoclonal clonal antibodies generated against whole beta-propiolactone-inactivated TOR3 strain SARS-CoV[124]. The F26 series yielded six neutralising antibodies specific for S protein: G3, G7, G9, G10, G18, and G19. Genetic analysis of these clones demonstrated that the germline V_H gene J558.50 was used in all cases; however, different D and J_H genes were used[125]. The kappa chain V gene usage was different in most circumstances as well. F26G9 and F26G10 used the same V_H, D, J_H, V_κ, and J_κ suggesting that these clones developed as a result of somatic hypermutation.

mAb	Class	V_H-gene	D-gene	J_H-gene	V_κ-gene	J_κ-gene
G8	G2a/k	J558.33	n/a	J_H2	bw20	J_k4
G9	G2a/k	J558.50	SP2.3/4/5	J_H1	19-25	J_k2
G10	G2a/k	J558.50	SP2.3/4/5	J_H1	19-25	J_k2
G18	G2b/k	J558.50	FL16.2	J_H4	ce9	J_k2
G19	G2a/k	J558.50	Q52.01	J_H4	cw9	J_k1

Table 1.1 Summary of the genetic properties of the murine F26 anti-SARS-CoV mAbs.

1.8 Therapeutic Antibody Production and Immunogenicity Issues

It would be appropriate at this time to provide the reader with a brief overview of the antibody production process and some of the immunogenicity issues involved when developing an antibody therapeutic. Since monoclonal antibodies (mAbs) were discovered by Köhler and Milstein in 1975[126], development of these reagents into novel diagnostic and therapeutic uses has continued. Twenty-two mAbs are currently licensed

by the FDA for clinical use in a broad range of fields from infectious disease to allergy and cancer[127]. Many more are in clinical trials[128]. As more is discovered about antibody immunogenicity and how to avoid it, this number will continue to increase.

1.8.1 Hybridoma Methodology

Production of antibodies by immunisation of mice followed by immortalisation of the antibody producing cells through creation of a hybrid cell line has been well established. The pioneering work of Köhler and Milstein demonstrated that by chemically fusing immortal myeloma cells to short-lived B cells a hybridoma retaining the immortal and antigen-specific characteristics of these individual cell types can be created[126]. The spleen is the primary source of these B cells, since large numbers of cells are required and the immune adult mouse spleen is 54% B cells[129]. Hybridomas are believed to be created from the antigen-activated proliferating B lymphocyte blast population[130]. For rodent species, it is still considered the most efficient way of producing monoclonal antibodies. These immortalised cell lines contain both the ability to produce large amounts of antibody and the genetic information encoding the antibody. This genetic information can then by used in downstream applications like the development of therapeutic antibodies.

1.8.2 Recombinant Antibody Methodology

In contrast to hybridoma methodology, the creation of recombinant antibodies focuses on the immortalisation of the genetic information only, not the antibody producing cell itself[130]. A cDNA library of variable heavy and light (V_H and V_L) genes is

created from a lymphocyte pool which is then displayed in various combinations using phage, lentiviral, or mammalian systems. The displayed scFv or Fab is then screened against the antigen of interest through successive rounds of panning to yield mAbs with high binding affinities. The main advantage of this approach is that mAb development can be expanded to non-rodent species and specific tissues (i.e. cervical lymphocytes), where hybridoma techniques do not function as well, allowing fully human antibodies to be created[131]. However, natural V region glycosylations and V_H/V_L pairings are lost, leading to the potential for missing out on natural pairings that are important in pathogen clearance *in vivo*.

1.8.3 Immunogenicity Issues: Antibody Engineering

Antibodies for therapeutic use have been developed using both hybridoma and recombinant antibody methodologies, demonstrating the significance of both of these arms of antibody production to health care. However, the major obstacle in antibody/protein therapeutics is the inherent immunogenicity of a foreign protein to the human immune system. Though proteins from other species tend to be the major culprits in this respect, even proteins of human origin can be immunogenic[132]. So when mouse mAbs antibodies are administered to patients, human anti-mouse antibodies (HAMA) can result that led to either a decreased efficacy of the mAb or morbidity (sometimes mortality) [127]. Though human anti-human antibodies (HAHA) can result when fully human antibodies are administered, the likelihood of such an event decreases along with its intensity if it does occur.

Therefore the major focus in engineering mouse antibodies to escape such undesirable responses is to make them look more 'human'. Using recombinant DNA technology, chimeric mouse/human antibodies can be synthesized that contain the V regions from the mouse parental antibody, and the constant (CH1, CH2, CH3) regions from a human isotype. These antibodies are 75% human and significantly less immunogenic than their mouse counterparts[127]. A review on HAMA, HAHA, and human anti-chimeric antibodies (HACA) responses highlights the fact that HAHA and HACA responses are remarkably similar, and the advantages of fully human versus chimeric antibodies in terms of immunogenicity is unclear[132]. If desired, the 'human' content of a murine antibody can be further increased to 95% by framework region swapping, although loss of affinity is a common problem[128].

It is advantageous to produce a mAb with human constant regions for functional reasons as well. The Fcγ regions human antibodies are more effective at triggering effector functions then that of mouse antibodies, as related to the lower binding affinity of mouse Fcγ to human FcγR[133]. The half-life of chimeric or humanised antibodies in the serum is also increased, since the human Fcγ binds stronger to the human neonatal receptor (FcRn), which is partly responsible for protecting serum IgG from degradation[134]. In addition, by choosing the appropriate isotype different functions *in vivo* can be obtained. For example, IgG1 is particularly good at triggering immune responses and clearance of pathogens, while IgG2 or IgG4 does not[127]. Therefore for clearance of pathogens IgG1 is usually the logical choice, while IgG2 or IgG4 would be used as blocking antibodies and in radioimmunotherapy.

1.9 Project Rationale

Based on the current information on SARS-CoV virology and epidemology, antiviral agents such as therapeutic neutralising antibodies present as an attractive option to pursue in the strategy to combat this new and emergent pathogen. Possessing high specificity, potent activity at low doses, and a long serum half-life, antibodies are an ideal antiviral agent. Mathematical modelling demonstrates that antibody prophylaxis to risk groups in contact with SARS patients could significant halt disease spread[135], and *in vivo* animal studies reveal that it way also be used to relieve the severity of symptoms in infected individuals.

Antibody prophylaxis has an advantage over vaccination for a disease such as SARS since antibodies can be administered after infection, while vaccines need to be administered prior to exposure. Antibody therapy can be used after the initial super spreading event (SSE) to reach infected individuals who are still asymptotic, allowing coverage for groups that possibly had not been administered the vaccine. A combination of vaccination for known high risk groups in any SARS outbreak (i.e. health care workers) and antibody prophylaxis for populations that become high risk during the epidemic (i.e. families of infected individuals) should significantly halt the impact of this disease should it re-emerge. Although much work has been done on ferreting out the 'incubator' style conditions in wet markets that lead to the 2002-2003 epidemic, the lack of information on the animal-animal transmission chain and natural reservior of SARS-CoV makes re-emergence a likely possibility.

This paper outlines a project undertaken to develop a novel therapeutic antibody for SARS-CoV using a combination of hybridoma and recombinant DNA technologies.

Four antibodies from the F26 series previously created in lab, G9, G10, G18, and G19 demonstrated high neutralisation titres *in vitro* against wild-type virus. Further characterisation of these antibodies, along with a non-neutralising S protein specific mAb G8, was done to define their epitopes and affinities. The DNA encoding the variable regions of these mAbs was then shuffled into the pIGG vector (Rader, C NIH) with an IgG1 backbone for expression and purification of recombinant chimeric versions of these neutralising antibodies. After obtaining epitope, neutralisation, and affinity information on these chimeric antibodies, the hypothesis that these chimeric mAbs had retained the characteristics of the parental murine ones was tested. In addition chain-shuffling experiments, where the V_H of one antibody and the V_L of another are co-expressed to create a novel antibody, provide intriguing information on the antibody V gene usage for combating a pathogen such as SARS-CoV.

2 Materials and Methods

2.1 Hybridoma Cell Lines, Medium Preparation, and Growth

Hybridoma cell lines of F26G8, F26G9, F26G10, F26G18, and F26G19 were obtained in house from previous experiments as described by Berry et al. [124] Hybridoma cells were grown in BD MAb Quantum Yield Medium (BD) supplemented with 10% Fetal Bovine Serum (FBS) (HyClone), 2mM L-glutamine (Gibco), 1% antibiotic/antimycotic solution (Multicell), 1% HT Hybri-Max® (Sigma), and 2% Hybridoma Cloning Factor (BioVeris™). When antibody purification was desired, the cell lines were grown in HyQ CCM1 Serum-Free Medium (HyClone) supplemented with 2mM L-glutamine, 1% antibiotic/antimycotic solution, 1% HT Hybri-Max®, and 2% Hybridoma Cloning Factor. Cell lines were grown in Nunclon™ Surface T flasks at 37°C with 5% CO_2 as a suspension culture and passaged every 2-3 days into new medium at a density of approximately $5x10^5$ cells/mL. Cell lines were frozen down and stored at -150°C in a medium containing 80% FBS, 10% BD Mab Quantum Yield Medium, and 10% DMSO (Sigma).

2.2 Tranfection Cell Lines, Medium Preparation, and Growth

Cell lines used in transfection experiments were as follows: HEK293 (ATCC#: CRL-1573), 293T (Heinz Feldmann, NML), and 293F (Invitrogen). HEK293 and 293T cells were grown with BD Mab Quantum Yield supplemented with 10% FBS, 2mM L-glutamine, and 1% antibiotic/antimycotic solution. The cells were grown as an adherent culture at 37°C with 5% CO_2 in Nunclon™ Surface T Flasks until a monolayer culture

was achieved (approximately 2-3 days) then passaged at a surface ratio of 1:5 using 0.25% Trysin-EDTA (Gibco) to disrupt the cells. Cells were frozen in the same freezing medium described in 2.1. 293F cells were grown in Erlenmeyer Polycarbonate Sterile Flasks (VWR) using FreeStyle™ 293 Expression Medium (Gibco) to a density of 1.5-2.5x10^6 cells/mL at 37°C with 8% CO_2 and 125rpm shaking, and then passaged at 3x10^5 cells/mL (approximately every 3 days). Cells were frozen down in FreeStyle™ 293 Expression Medium with 10% DMSO at -150°C.

2.3 Enzyme Linked Immunosorbent Assay (ELISA) Determination of Murine Antibody Binding Specificity

Culture supernatants from the murine hybridoma F26 series were tested against 200ng full-length recombinant spike protein (rFS) (BEI Resources), 100ng recombinant 318-510aa spike containing the ACE2 binding domain (rACE2BDS) (James Rini, U of Toronto), or 200ng of recombinant protective antigen (rPA) (Jeremy Mogridge, U of Toronto) coated to individual wells of a MaxiSorp 96 well plate (NUNC™). Coating occurred overnight at 4°C in 60µl Phosphate Buffered Saline (PBS) pH 7.2, then in the morning the wells were blocked at 37°C for 2 hours with 200µl 0.4% w/v Bovine Serum Albumin (BSA) (Sigma) in PBS pH 7.2. The plate was washed twice with MilliQ® water (resistivity 18.2MΩ•cm) using a Power Washer 384 (TECAN) automatic washing device. All ELISA washes were carried out using this system. Next, 60µl of the culture supernatants were then applied at a dilution, determined previously, that yielded an absorbance unit of approximately OD=1 at 405nm versus rFS when the substrate is applied for an hour. The culture supernatants were incubated in the plate for 2 hours at 37°C. The plate was then washed eight times with water, and 60µl of a 1:2000 dilution

of goat anti-mouse IgG heavy chain Fc specific polyclonal antibody conjugated to the horseradish peroxidase enzyme (GαM IgG-γ HRP) (Southern Biotech) was applied and incubated for 1 hour. The plate was washed eight times again, and then incubated at room temperature with 60µl of 2,2'-azino-bis(3-ethylbenzthiazoline-6-sulphonic acid) (ABTS) substrate (Roche). Colour development was monitored at 405nm by use of a SpectroMax250 Spectrometer (Molecular Devices), with readings taken at approximately 20, 40, and 60 minutes. SoftMax Pro 4.6 Software (Molecular Devices) was used to record the readings, and all samples were performed in triplicate and averaged.

2.4 Competitive ELISA Determination of Murine Antibody Binding Specificity

200ng of rFS was coated per well on MaxiSorp 96 well plates overnight at 4°C. The plates were blocked and washed as per 2.3. Meanwhile culture supernatants from the murine hybridoma F26 series were diluted with PBS to a dilution, determined previously, that yielded an absorbance unit of approximately OD=1 at 405nm versus rFS when the substrate is applied for an hour, and incubated for 30-40 minutes with twofold serial dilutions in PBS of deglycosylated (dg) rACE2BDS (James Rini, U of Toronto), starting at .03625 mg/ml down to 1.77×10^{-5} mg/ml. 60µl of these mixtures were then applied to the wells and incubated for 2 hours at 37°C. The plates were then washed, incubated with secondary, washed again, substrate applied, and readings taken as described in 2.3. All samples were performed in triplicate, averaged, and graphed as a function of absorbance versus dgrACEBDS concentration.

2.5 Western Immunoblotting Determination of Murine Antibody Binding Specificity

For each antibody to be tested, 2μg of rFS, 0.5μg of rACE2BDS, and 1μg of rPA were mixed 1:1 with Laemmli Sample Buffer containing 0.05% betamercaptoethanol (BME) (BioRad) to a total volume of 40μl and heated at 95°C for 5-10 minutes. After cooling on ice, the samples were then loaded onto a Criterion 4-20% Tris-HCl gradient gel (BioRad) in a 25mM Tris, 192mM Glycine, 0.1% w/v sodium dodecyl sulfate (SDS) Buffer pH 8.3 (BioRad) and run at 200V for 50 minutes. Kaleidoscope Prestained Standards (BioRad) was used as the molecular weight ladder. The gel cassettes were then opened and the gel placed in a transfer apparatus containing an Immobilon-P PVDF membrane (Millipore) with 20% v/v methanol, 0.15M Tris/Glycine Buffer, pH 8.8 (BioRad). Transfer took place at 120V for 1 hour, and then the membrane was then removed and blocked with 10% w/v skim milk (BD) for 2 hours at room temperature. After blocking, the membrane was washed twice with Tris-Buffered Saline (TBS) and cut into sections for each antibody, and incubated with the appropriate culture supernatant overnight at 4°C with gentle shaking. In the morning, the supernatants were removed and the membrane washed thrice with TBS containing 0.05% Tween-20 (Sigma) (TBST). A 1:5000 dilution in TBST of GαM IgG-γ HRP (Southern Biotech) was then applied and incubated for 1 hour at room temperature. The membrane was then washed thrice with TBST. Diaminobenzidine(DAB)/Metal Substrate (Pierce) was applied to the membrane until substantial colour development could be seen, usually 0.5 to 4 minutes. Excess substrate was then washed away with water and the membrane allowed to dry prior to scanning to obtain a digital image.

2.6 Concentration of Culture Supernatant and Purification of Murine Antibody

In order to purify monoclonal antibody from the murine hybridoma culture supernatants, roller bottles (Corning, 1L) containing 500mL of serum-free hybridoma medium (described in 2.1) with a starting cell density of $5x10^5$ cells/mL were incubated for 14 days at 37°C with 5% CO_2. The supernatant was then collected by centrifugation at 2095xg for 15min in a Beckman Coulter Allegra X-12R. The supernatant was then concentrated ten to twenty fold using a Millipore ultrafiltration device with a 30kDa cut-off membrane. The concentrated supernatant was then mixed 1:1 with Pierce Binding Buffer pH 8.0 and applied to a 1mL volume HiTrap Protein G column (GE HealthCare) pre-equilibrated with 5 column volumes of Binding Buffer. The sample was passed over the column thrice, and then eluted with 7 column volumes of Pierce Elution Buffer pH 2.8 into a Amicon Centriprep Y-30 device with a 30kDa regenerated cellulose membrane containing 7mL of PBS pH 7.2 for immediate neutralisation. The Centriprep device was then used to dialyse the sample thrice against PBS at 2095xg for 30min in the Allegra X-12R Centrifuge and finally concentrate the sample volume down to 0.5-2 mL. The sample was then sterilised by passage through a low protein binding 0.2µm filter (Millipore) and stored at -20°C until used.

2.7 Quantification of Purified Antibody by the Bicinchoninic Acid (BCA) Method

Concentration of purified antibody was determined using the BCA™ Protein Assay Kit (Pierce) according to the manufacture's instructions. Briefly, 25µl of PBS was added to all wells except row A of a round-bottom 96 well plate. In row A, 50µl of PBS was added to column 1, column 2-4 received 50µl of the 2.0 mg/ml BSA standard supplied,

and columns 5-12 received 50µl of the unknown samples in duplicate. Twofold serial dilutions were then made down the plate to row H, and the last 25µl discarded. The BCA working reagent was then made by mixing reagent A with reagent B in a 50:1 ratio (for a single plate, this works out to 400µl B into 20mL A). 200µl of the working reagent was then applied to each well, starting at row H and working up to row A. The plate was gently shaken for 1-3 minutes then incubated at 37°C for 1 hour. After incubation, a SpectroMax250 Spectrometer was used to read the absorbance at 562nm, and samples compared to the standard curve. Sample dilutions that fell off the standard curve were ignored in the calculations. If the sample was extremely concentrated compared to the standards, the samples were diluted appropriately prior to the assay and run again.

2.8 Qualification of Antibody Purity by Native and Denaturing Polyacrylamide Gel Electrophoresis (PAGE)

The purity (in terms of gross contaminants) of the antibody preparations was further determined by PAGE analysis under native and denaturing conditions. In both cases, 2µg of antibody was loaded at a final volume of 40µl into a Criterion 4-20% Tris-HCl gel. For native conditions, the antibody diluted in PBS was mixed 1:1 with the Native Sample Buffer (BioRad), while for denaturing conditions it was combined 1:1 with Laemmli Sample Buffer containing 0.05% BME. The denaturing gel sample were incubated at 95°C for 5-10 minutes and cooled afterwards on ice. Native samples were run in a 25mM Tris, 192 mM Glycine Buffer pH 8.3 (BioRad), while denaturing samples were run in the denaturing buffer as described in 2.5. Both gels were run at 200V for 50 minutes. The gels were then removed from their casing and stained with 0.001% w/v Coomassie Blue in a 10% v/v acetic acid, 20% v/v methanol solution for 1 hour at room

temperature. Destaining solution (10% v/v acetic acid, 10% v/v methanol in water) was applied multiple times until the gel was significantly destained, usually overnight. The gels were then scanned using the Odyssey Infrared Imager (Li-Cor) to obtain a digital image.

2.9 BIACore Affinity Analysis

All BIACore analysis was performed on a BIACore 2000, using 0.15M NaCl, 0.005% Surfactant P20, 0.01M HEPES pH7.4 (HEPES-P) (BIACore) as the buffer with a flow rate of 5 µl/minute. Flow cell 1 was used in all cases.

2.9.1 Coating of rFS onto a CM5 Chip

A new CM5 Chip (BIACore) was docked and the following injection program established. First, 20µl of freshly mixed EDC/NHS (BIACore) was injected to activate the chip, followed by 40µl of a 1:2 dilution of rFS (65ng/µl) in a 10mM Sodium Acetate Buffer pH4.0 (BIACore), then 35µl of 1.0M ethanolamine to block the remaining sites. The blocked chip was then scrubbed with 30µl Glycine-HCl pH 1.5 (BIACore). An increase in signal from baseline (after activation) to after coating indicated that sample had been successfully coated onto the chip.

2.9.2 Sample Preparation

Antibody samples were prepared for injection by making dilutions from 89-377nN in HEPES-P. In order to account for the dual binding sites of IgG, Normal versus Molarity values were used. 200µl of each sample dilution was placed in the 0.2mL BIACore tubes

and placed accordingly in the sample rack. 3mL of Glycine-HCl pH 1.5 was placed in a 5 mL vial and placed in the sample rack for scrubbing the chip between runs.

2.9.3 BIACore Automation

The following method was then programmed into the computer using the BIACore 2000 Control Software in order to automate the affinity analysis process:

```
DEFINE LOOP cycle
  LPARAM      %sample       %position
  TIMES 1
              F26G8-89nN    r2a1
              F26G8-111nN   r2a2
              F26G8-144nN   r2a3
              F26G8-167nN   r2a4
              F26G8-200nN   r2a5
              F26G8-220nN   r2a6
              F26G8-182nN   r2b1
              F26G8-220nN   r2b2
              F26G8-272nN   r2b3
              F26G8-304nN   r2b4
              F26G8-349nN   r2b5
              F26G8-377nN   r2b6
END

DEFINE APROG kinetics

  PARAM %sample %position

  KEYWORD sample %sample
  FLOW 5
* KINJECT %position 40 840      !14 min dissociation
  INJECT r2f3 30                !Regeneration

END

MAIN

  LOOP cycle STEP
    APROG kinetics %sample %position

ENDLOOP
  APPEND continue
END
```

The method was then run for each antibody, and the information stored as a single file comprised of multiple curves.

2.9.4 Calculation of Affinity Constants

Using the BIAEvaluation program, the file containing the curves for the appropriate antibody was then opened. After Y transforming (and X transforming, if required) the data, the kinetic analysis was performed separately, starting with the k_d. The k_a value was then determined using the k_d value and the concentration for each curve. The K_A and K_D were then calculated from the equations: $K_D = k_d/k_a$ and $K_A = 1/K_D$. The average K_D value was then determined, along with the corresponding standard deviation and 95% confidence interval (CI). Sample runs with bubbles occurring during the run, which creates a spike effect, were eliminated from the analysis. A minimum of five samples runs was used for each antibody.

2.10 SARS-CoV Neutralisation Assay

Vero-E6 cells were grown in a tissue culture 96 well plate to confluence in DMEM with 2% FBS (Gibco). Antibody was diluted tenfold in the medium and heat inactivated at 56°C for 30 minutes. The Vero-E6 cells and antibody were then taken into the Biosafety Level 3 Laboratory. Various dilutions of antibody were then mixed with a $TCID_{50}$=100 of SARS-CoV TOR2 strain and incubated at 37°C for 1 hour. After incubation, 20µl of the antibody/virus dilutions were applied to six wells per dilution to the plate and incubated for 1 hour to allow for infection. Virus titers of $TCID_{50}$=10, 1, and 0.1 were used as a positive control. 100µl of medium was then added to each well and the plates

incubated at 37°C for 3-4 days, then scored under a microscope for the presence of cytopathic effect (CPE).

2.11 Epitope Mapping of F26G8 and F26G18 Using Pin Peptides

Using the region of the SARS-CoV TOR2 strain spike protein spanning from 300-700aa, forty-nine 17-mers with 9aa overlap were developed, synthesised, and attached via an extra C-terminal cysteine to pins (synthesis and attachment performed by PepScan Presto). Internal cysteine residues were replaced by alanine residues to prevent interpeptide disulphide bonding. For the assay, the pins were blocked for 2 hours with 1% skim milk and 1% Tween-20 in PBS pH 7.2 (200µl/well) at room temperature in flexible Falcon 96 well plates by lowering the pin block into the plate, and then washed with the wash solution composed of 0.9% w/v NaCl and 0.05% v/v Tween-20 in PBS pH 7.2. Next, 100µl of a 1ug/mL solution of the mAb to be mapped was diluted in 0.1% skim milk and 0.1% Tween-20 in PBS and then added to each well of a new flexi-plate and incubated overnight at 4°C. In the morning, the pins were washed thrice (as above) then incubated with a 1:5000 dilution of GαM IgG-γ HRP (Southern Biotech) in 0.1% skim milk and 0.1% Tween-20 in PBS for 1 hour. After washing thrice again, 200µl of ABTS substrate was applied to a MaxiSorp 96-well plate, the pins lowered into the plate to develop, and the readings taken at as per 2.3. The absorbance reading was then plotted versus the peptide sequence, and secondary antibody alone used as the negative control. The pin block was regenerated by sonication at 60°C for 1 hour in a phosphate solution with 1% SDS and 0.1% BME, followed by sonication for 30 minutes in water. The pins were rinsed with 70% ethanol and stored at -20°C.

2.12 Epitope Mapping of F26G8 and F26G18 Using Soluble Peptides

Based on the pin peptide analysis, soluble 17-mers of the putative binding sequence were commercially synthesised with N-terminal biotin. United Biochemical Research preformed synthesis and conjugation of the peptides. A scrambled sequence peptide was used as an irrelevant peptide control. The sequences synthesised were as follows:

G18PEP N-Biotin-KGCPWAYLSPPCTDPNF-COOH
G18PEPScr N-Biotin-FSPDGKPCTPPALNCYW-COOH

G8PEP N-Biotin-TAIHADQLTPAWRIYST-COOH
G8PEPScr N-Biotin-HITARQTPWAADLITYS-COOH

2.12.1 ELISA using Soluble Peptides as Antigen

To a MaxiSorp 96 well plate, 100ng of streptavidin (Zymed) was coated overnight in 60µl PBS at 4°C. In the morning the plate was washed twice then 200ng of the biotin peptides were added in 60µl to individual wells and incubated for 2 hours. The plates were then blocked with 0.4% BSA for 1.5 hours, then washed twice. Next, 60µl of murine hybridoma culture supernatant was then applied. Exactly as outlined in 2.3, the supernatant was incubated for 2 hours, washed, secondary applied, washed again, and developed. The samples were performed in triplicate and averaged.

2.12.2 Competitive ELISA using Soluble Peptides as Competitors

Competitive ELISA using the soluble peptides was carried out similar to 2.4, with the following modifications. Instead of dgrACE2BDS, the soluble peptides were mixed at twofold serial dilutions starting from 100µg/ml, and ending at 0.097µg/ml. The resulting data depicting the presence or absence of competition for binding by mAbs to rFS was

then graphed as absorbance @ 405 nm against soluble peptide concentration. Each antibody was tested against the peptide containing its putative binding domain, and the corresponding scrambled peptide.

2.13 Cloning and Sequencing of the Variable Light (V_L) and Variable Heavy (V_H) regions into TOPO pCR2.1

To isolate the V_L and V_H sequences, total RNA was extracted from $1x10^7$ murine hybridoma cells using an RNeasy® Mini Kit (QIAGEN). Complementary DNA (cDNA) was then made from 4µl of RNA using ThermoScript™ RT-PCR (Invitrogen) with oligo$(dT)_{20}$ priming. A 3' biotin blocked primer was designed to anneal to the CDR3 region of the endogenous aberrant variant chain kappa (AbVk) (5'TAATGTGCTGACAGTAATAGGT3-Biotin') was used to prevent cDNA creation of this common interference.[136] The GeneRacer™ System (Invitrogen) was used to perform RNA ligase-mediated rapid amplification of cDNA ends (RLM-RACE) when the blocking primer failed to prevent AbVk amplification. Polymerase Chain Reaction (PCR) was then used to amplify the V_L and V_H using combinations of the following primers:

V_H 5':

UmIgVH	TGAGGTGCAGCTGGAGGAGTC
MHcL-1	ATGGACTT(GCT)G(GAT)A(CT)TGAGCT
MHcL-2	ATGGAATGGA(GC)CTGG(GA)TCTTTCTCT
MHcL-3	ATGAAAGTGTTGAGTCTGTTGTACCTG
MHcL-4	ATG(GA)A(GC)TT(GC)(TG)GG(TC)T(AC)A(AG)CT(TG)G(GA)TT
MHC1	AGGTCCAGCTGCTCGAGTCTGG
Sheriff IgG	GCCGGTACCCAGCTCCAGCTTCAGGAGTC

V_H 3':

MG1-3Seq	AGATGGGGGTGTCGTTTTGGC
Sheriff IgG	GCGTCGACCAGGGGCCAGTGGATAGAC
MG2a/b-3Seq	GAC(TC)GATGGGG(CG)TGTTGTTTTGGC

MH125	GGATACAGTTGGTGCAGC

V_L 5':

MVL	GTGCCAGATGTGAGCTCGTGATGACCCAGTCTCCA
Sheriff Kappa	GCCGAATTCGACATTGTGCTGACCCAATCTCCAGCTTC
MKcL-1	ATGAAGTTGCCTGTTAGGCTGT
MKcL-2	ATGGACTTTCAGGTGCAGATCT
MKcL-3	TTGCTGTTCTGGGTATCTGGTA
MKcL-4	ATGGAGACAGACACACTCCTGCTAT
UmIgVK	GACATTCTGATGACCCAGTCT

V_L 3':

MK-3Seq	TACAGTTGGTGCAGCATCAGC
IgKappa	GCGCCGTCTAGAATTAACACTCATTCCTGTTGAA
MKC1	GGATACAGTTGGTGCAGC
Sheriff Kappa	GCGAATGCGGATGTTAACTGCTCACTGGATGGTGGG
AbVK	ACCTATTACTGTCAGCACATTA

Platinum® Blue PCR SuperMix (Invitrogen) was used to amplify the fragments in a 48µl total volume, with 1µl of cDNA template and 1µl of 100µM solutions of the forward and reverse primers. The reaction was cycled in a GeneAmp® PCR System 9700 thermocycler as follows: 94°C for 2 minutes; 30 cycles of 94°C for 30s, 55°C for 30s, and 72°C for 1min; final extension at 72°C for 8min; then hold at 4°C. The total volume of the reactions was run at 100V for 50 minutes in a 1.5% agarose gel with trace amounts of ethidium bromide, and viewed using a GelDoc XR (BioRad). The amplified product band (~400bp) was then cut out with a scalpel, extracted using the QIAquick® Gel Extraction Kit, and eluted in 30µl of 10mM Tris-HCl pH 8.5. 4µl of the gel-purified product was then used with TOPO TA Cloning® Kit (Invitrogen) for insertion into pCR2.1. Electrocompetent TOP10 cells were transformed with the plasmid, allowed to recover for an hour, and then plated onto Luria-Bertani (LB) medium containing 100µg/ml ampicillin. A total of 8 clones were picked and grown in 5mL LB-Amp

(100μg/ml) overnight and the plasmids isolated from the pelleted lysed *E. coli* with the QIAprep® Miniprep Kit. The ND-1000 Spectrophotometer (NanoDrop®) was used to quantify the DNA. Next, 10μl of a 150ng/ul solution was sent to the Genomics Core Facility within the NML for sequencing using M13 Reverse (5'CAGGAAACAGCTATGAC3') and T7 (5'TAATACGACTCACTATAGGG3') primers. Sequence data was analysed using DNAStar software.

2.14 Mutagenesis to remove undesired Restriction Enzyme (RE) Sites

An internal Sac I site in the V_H region that would interfere with the digestion and ligation strategy was removed via site-directed mutagenesis using the QuikChange® II XL Site-Directed Mutagenesis Kit (Strategene). The primer set developed was as follows:

SacImutF: 5'GCTCTGCCTACATGGAGCTAAGCAGCCTGAC3'
SacImutB: 5'GTCAGGCTGCTTAGCTCCATGTAGGCAGAGC3'

One heavy chain clone from 2.13 was picked and the QuikChange® protocol followed accordingly. A total of 8 clones were picked, expanded in 2mL of LB broth with 100μg/ml ampicillin overnight, and processed in a similar fashion as 2.13.

2.15 Linking of V_L and Human Kappa Constant (C_κ) using pIGG Specific Primers

Based on the sequence data obtained by 2.13, previous work done on the F26 series, along with the published human C_κ sequence, primers were developed to link the murine V_L to the human C_κ and provide the appropriate 5' and 3' RE sites (Hind III and Xba I respectively) for ligation in the pIGG vector (Christoph Rader, NIH) [137, 138]. The primers developed were as follows:

G910FHindIII	5'CCCATAAGCTTGTTGCTCTGGATCTCTGGTGCCTACGGGGA CATTCTGATGACCCAGTCTCAC3'
G18FHindIII	5'CCCCATAAGCTTGTTGCTCTGGATCTCTGGTGCCTACGGGG ACGTTGTAATGACCCAGTCTCCATCCTCC3'
G19FHindIII	5'TTCATAAGCTTGTTGCTCTGGATCTCTGGTGCCTACGGGGA CATTCTGATGACCCAGTCT3'
MHKB	5'GAAGACAGATGGTGCAGCATCAGC3'
HKCF	5'CGAACTGTGGCTGCACCATCTGTC3'
HKBXbaI	5'TCTAGAACTAACACTCTCCCCTGTTGAAGCT3'

Using 45µl Platinum® Blue PCR SuperMix, 1µl of pCR2.1 containing the V_L region (150ng/µl) was mixed with 1µl each of the MHKB and one of G910FHindIII, G18FHindIII, or G19FHindIII primers, as appropriate. SuperMix was also used to amplify C_κ from pCR2.1- C_κ using 1µl the plasmid with 1µl each of primers HKCF and HKBXbaI. The reactions were cycled and gel extracted as per 2.13. A new PCR reaction was setup using approximately 33ng of each of the purified products as template and 1µl of G910FHindIII, G18FHindIII, or G19FHindIII and 1µl of HKBXbaI. The reaction was then cycled as follows: 94°C for 2 minutes; 7 cycles of 94°C for 30s, 50°C for 45s, and 72°C for 2min; 30 cycles of 94°C for 30s, 55°C for 30s, and 72°C for 1.5min; final extension at 72°C; then hold at 4°C. The amplified product was then extracted and cloned into pCR2.1 as per 2.13. A total of 8 clones were picked and grown overnight in 2mL culture. Plasmid minipreps were screened by Hind III / Xba I restriction enzyme digest and were sequenced as above.

2.16 Insertion of V_LC_κ into pIGG

The pIGG-P14 plasmid clone was obtained as a gift from Christoph Rader (NIH) [137, 138]. Approximately 1µg pIGG-P14 DNA was digested using 1µl of each 100 units/µl Hind III and Xba I enzyme solutions (NEB), 5µl 10x Buffer 2 (NEB), and 0.5µl 100x BSA

(NEB), diluting to a total reaction volume of 50µl using autoclaved MilliQ® water. Then 1µg of pCR2.1 containing the linked V_LC_k product from 2.15 was digested in a similar fashion. The reactions were incubated for 1 hour at 37°C. Next, 1µl of calf intestinal alkaline phophatase (CIAP) (20 units/µl) (Invitrogen) was added to the pIGG-P14 digestion and incubated at 50°C for 20 minutes to prevent religation of the vector. The vector and insert reactions were then gel purified in a 1% agarose gel and extracted as per 2.13. The ligation reaction to link vector and insert was performed using 0.1µg of vector and 28ng of insert (3-fold molar excess of insert) in a 20µl reaction volume with 4µl T4 Ligase Buffer and 1µl T4 DNA Ligase (Invitrogen). The ligation was incubated overnight at 14°C, then precipitated with 2µl 3M Sodium acetate (pH 5), 2µl mussel glycogen (Sigma), and 44µl 95% ethanol on dry ice or at -80°C for 1 hour. The reaction was then spun down at maximum speed in an Eppendorf 5415R tabletop centrifuge for 20 minutes at 4°C. After washing the pellet twice with 100µl 70% ethanol, the pellet was allowed to dry for 1 hour before resuspending in 8µl sterile water. Electroporation was used to transform TOP10 electrocompentent cells (Invitrogen) with 4µl of the ligated product, and 8 clones picked for screening as described in 2.18.

2.17 Insertion of V_H into pIGG- V_LC_K

Based on the sequence data obtained by 2.13 and previous work done on the F26 series, primers were developed to provide the appropriate 5' and 3' RE sites (Sac I and Apa I respectively) for insertion of the V_H region into the pIGG vector. The primers developed were as follows:

F26FSacI 5'CCCCGAGCTCACAGCGAGGTGCAGCTGGAGGAGTCTG3'

F26BApaI 5'CGATGGGCCCTTGGTGGAGGCTGAGGAGACGGT3'

Using 150ng of pCR2.1 containing the V_H region as the template, 1µl of a 100µM solution of each primer was used with SuperMix, cycling as described in 2.13. The amplified product was then gel purified and extracted. 4µl of the solution was used with the pCR2.1 TOPO TA Cloning Kit to make pCR2.1-V_H. For immediate ligation into pIGG-V_LC_κ, the reminder (25µl) was digested with 1µl Apa I (50units/µl) (NEB), 5µl 10x Buffer 4 (NEB), and 0.5µl 100x BSA (NEB) in a total volume of 50µl at room temperature for 1 hour. Alternately, 1µg of the pCR2.1-V_H was digested in a similar fashion. For the V_H insertion 1µg of one clone of pIGG-V_LC_κ from 2.16 that passed the screening process was digested in the same way, to open up the V_H site on the vector. The reactions were then heat inactivated at 65°C for 20 minutes, cooled on ice, then 1µl of Sac I (100units/µl) (NEB) added and incubated at 37°C for 1 hour. Again, 1µl of CIAP (20units/µl) was then added to the vector reaction and incubated at 50°C for 20 minutes. The vector and insert were then gel purified in a 1% agarose gel at 100V for 50 minutes and extracted. The ligation reaction to link vector and insert was performed using 0.1µg of vector and 14ng of insert (3-fold molar excess of insert) in a 20µl reaction volume with 4µl T4 Ligase Buffer and 1µl T4 DNA Ligase. Where PCR product was used as the source of insert a 6-fold molar excess (28ng) was used to compensate for inefficient cutting. The ligation was incubated overnight at 14°C, then precipitated and transformed into TOP10 electrocompetent cells as described in 2.16. The 8 clones were screened as described in 2.18.

2.18 Screening of pIGG Clones

2.18.1 Restriction Enzyme Digest

In order to confirm presence of inserts, 3µl of a 150ng/µl dilution of each clone was digested in a 50µl total volume for 1 hour at 37°C. For V_H screening the clone was digested with 1µl of Sac I and Apa I, while for V_LC_κ screening 1µl of each Hind III and Xba I were used. The samples were then viewed in a 1.5% agarose gel with the undigested clone run in the adjacent lane (data not shown).

2.18.2 Primer Design and Sequencing

Based on the sequence of the pIGG-P14 vector supplied by Christoph Rader, primers were developed upstream and downstream from the restriction enzyme sites for use in sequencing reactions.

VHF	5'TTGGAGGAGGGTGCCAGGGGGAAGACC3'
VHB	5'CTGGAGGATCCTCTTCTTGGTGGCAGCA3'
VLF	5'CATGGTGTTGCAGACCCAGGTCTTCAT3'
VLB	5'CAGCTGGCACGACAGGTTTCCCGACTGGAA3'

These primers were then supplied to the Genomics Core Facility at the NML for use in the sequencing reactions. A volume of 10µl of a 150ng/µl dilution of plasmid was given as template for sequencing.

2.18.3 Small Scale Transfection of 293T cells

Transfection of 293T cells was carried out in a flat bottom CoStar® 24 well plate (Corning) with $2x10^5$ cells/well. On the day of transfection, approximately 1µg of pIGG

DNA was mixed gently with 25µl of LyoVec™ (InvivoGen) in a tissue culture hood and incubated at room temperature for 15-30 minutes. Meanwhile, 293T cells were seeded into the plate by trypsin digest of a tissue culture flask grown as per 2.2 followed by cell counting using a hemacytometer and dilution down to $4x10^5$ cells/ml in growth medium described in 2.2. A volume of 500µl of the cell suspension was then pipetted into each well. 25µl of the DNA:LyoVec™ solution was then added to the appropriate wells and mixed gently. The transfection plate was incubated at 37°C with 5% CO_2 for 48-72 hours, then screened by ELISA as described in 2.18.4.

2.18.4 Transfection Screening ELISA

Supernatant from transfected cells were screened for both expression and for rFS specific binding. For each transfection to be screened 200ng rFS, 100ng goat anti-human IgG $F(ab)'_2$ specific polyclonal antibody (GαH IgG-$F(ab)'_2$) (Jackson ImmunoResearch), 100ng goat anti-human IgK C_κ specific polyclonal antibody (GαH IgK-C_κ) (Southern Biotech), or 0.4% BSA was coated overnight at 4°C in a 60µl volume of PBS on a 96 well plate the day prior to screening. The plate was then blocked and washed as per 2.3, and 60µl of neat culture supernatants from the transfection wells were incubated for 2 hours at 37°C with each of the four antigens. The plate was washed as per 2.3, then incubated for 1 hour at 37°C with a goat anti-human IgG γ specific polyclonal antibody conjugated to HRP (GαH IgG-γ HRP). The plate was then washed, incubated with substrate, and read as per 2.3.

2.19 Expression Studies

2.19.1 Expression in HEK 293 versus 293T cells

HEK 293 and 293T cells were grown to confluence in a T175 flask as per 2.2. 175µl of Lipofectamine™ 2000 (Invitrogen) and 70µg pIGG-F26G18 was then mixed accordingly to the manufacture's protocol in BD MAb Medium Quantum Yield (BD) supplemented with 1% L-Glutamine and incubated for 20-30 minutes. Meanwhile the growth medium in the confluent flasks was replaced with BD MAb Medium supplemented with 1% L-Glutamine (i.e. no serum, no antibiotic) or BD MAb Medium supplemented with 1% L-Glutamine and 10% FBS (i.e. no antibiotic). The DNA:Lipofectamine™ 2000 complexes were then added to the cells and the flasks incubated at 37°C with 5% CO_2 for 3 days to allow for recombinant antibody expression. The flasks were then screened by ELISA as per 2.19.3.

2.19.2 Expression in 293F versus s293T cells

293F cells were grown as per 2.2. 293T cells were adapted to suspension, serum-free culture by passaging the cells thrice in CD 293 Medium for Suspension Cultures (Gibco), then splitting into the FreeStyle™ 293 Expression Medium. These cells were then named s293T. Transfection of both cell lines was carried out using 293fectin™ (Invitrogen) in a 125ml flask with 30ml culture volume. DNA:293fectin™ complexes were formed in OptiMEM® I Reduced Serum Medium as per the manufacture's protocol, then added to the flasks and incubated for 3 days at 37°C with 8% CO_2. The flasks were then screened as per 2.19.3, with only the first point recorded.

2.19.3 ELISA Screening of Expression Studies

Expression of mouse-human chimeric antibody was confirmed using ELISA. 100ng of goat anti-human IgK-C_κ was added to each well of a MaxiSorp 96 well plate and incubated overnight at 4°C. The plates were washed and blocked as per 2.3. Meanwhile, twofold serial dilutions of supernatant from the transfection flasks were made, starting at a fourfold dilution. 60µl of the dilutions were then applied to the plate and incubated for 2 hours at 37°C. The plates were then processed as per 2.18.4 and the absorbance at 405 nm plotted versus dilution.

2.20 Large Scale Expression of Chimeric Products

2.20.1 GigaPrep Preparation of DNA

Large amounts of pIGG DNA were prepared using the QIAprep Giga Kit (QIAGEN). The large-scale plasmid preparations were then screened for insert and sequenced as per 2.18.

2.20.2 Expression in 293F cells

The 293F cells were grown as per 2.2 to a 600ml total volume in three 500ml flasks. The cells were then transfected using 293fectin™ according to the manufacture's protocol and incubated at 37°C with 8% CO_2 for 6 days prior to collection. The supernatant was screened for antibody activity as per 2.18.4 prior to proceeding with concentration and purification.

2.21 Concentration and Purification of Chimeric Products

Supernatant from the large-scale expression described in 2.20.2 was concentrated as per 2.6. The concentrated product was then sterilised by filtration through a 0.22μm membrane and divided equally into three batches to test different purification protocols. In the first protocol, supernatant was mixed 1:1 with PBS pH7.2 and loaded onto a 1ml Protein A Column (GE Healthcare) pre-equilbrated with 5 column volumes of PBS. [137] The column was then washed with 10ml of PBS and eluted with 5ml 0.5M Acetic Acid pH 3.0 into 1.0M Tris-HCl pH 8.0. The second protocol retained the same volume amounts but was performed with a Protein G column using Pierce Protein G Binding Buffer pH 5.0 and Pierce Elution Buffer pH 2.8, eluting into PBS. In the third protocol, the sample was mixed 9:1 with 1.0M sodium acetate (NaOAc) pH 5.0 and loaded onto a Protein G column pre-equilibrated with 5ml of 0.1M NaOAc pH 5.0. The column was washed with 10ml of the same, then eluted into PBS with 5ml of 0.1M Glycine-HCl pH 2.5. All three protocols were then placed in a CentriPrep and prepared as per 2.6. The samples were analyzed by BCA (2.7), denaturing PAGE (2.8), and ELISA (2.19.3) with the following modifications. A 1:1 dilution of antibody in PBS was used as the starting concentration in BCA, 20μl of neat sample was run in a total volume of 40μl in denaturing SDS-PAGE, and a 1:19 dilution was used as the starting concentration for ELISA.

2.22 Characterisation of Chimeric Products

2.22.1 ELISA, cELISA, Western Blotting, BIACore Affinity

The protocols outlined in 2.3, 2.4, 2.5, and 2.9 were followed for characterisation of the chimeric antibody with the following modifications. In ELISA, cELISA, and Western Blotting the GαH IgG-γ HRP antibody was substituted for the anti-mouse secondary. BIACore analysis was performed in an identical fashion to that recorded in 2.9.

2.22.2 Epitope Mapping of 18H18L and Neutralisation Assay

Epitope Mapping was performed on the 18H18L chimeric monoclonal antibody using pin peptides (2.11) and soluble peptides (2.12) identical to the methods described, except substituting the GαH IgG-γ HRP antibody for the anti-mouse secondary. The neutralisation assay for 18H18L was identical to that in 2.10.

3 Results

3.1 Characterisation of Murine F26 Series mAbs

3.1.1 ELISA Epitope Characterisation

At the time of the development of the F26 series mAbs, only whole inactivated virions or infected Vero-E6 cell lysate were available for screening. Using this information, it was determined by ELISA that G8, G9, G10, G18, and G19 all were specific for SARS-CoV. Since then, many recombinant forms SARS-CoV proteins have become available, allowing for ELISA screening for specific SARS-CoV proteins. Figure 3.1 shows the results of an ELISA and cELISA performed to further characterise the protein and epitope specificity of these mAbs using recombinant S proteins. F20G7-5, a mAb specific for the protective antigen (PA) protein of *Bacillus anthracis,* was used as a negative control.

As can be seen from 3.1a, all five of the F26 series mAbs bind to a recombinant full-length S protein (rFS), while only the neutralising mAbs (G9, G10, G18, G19) bind a fragment (rACE2BDS) spanning the receptor-binding domain (RBD) from aa318-510. In addition these four neutralising mAbs bind a deglycosylated version (dgrACE2BDS), suggesting that binding is non-glycosylation dependent. All five F26 series mAbs do not recognise rPA compared to F20G7-5 control mAb, which does. Therefore binding of the antibodies in this assay is specific to rFS.

Next, a competitive ELISA (cELISA) was developed to see if soluble dgrACE2BDS could compete with rFS coated onto the plate for antibody binding. As

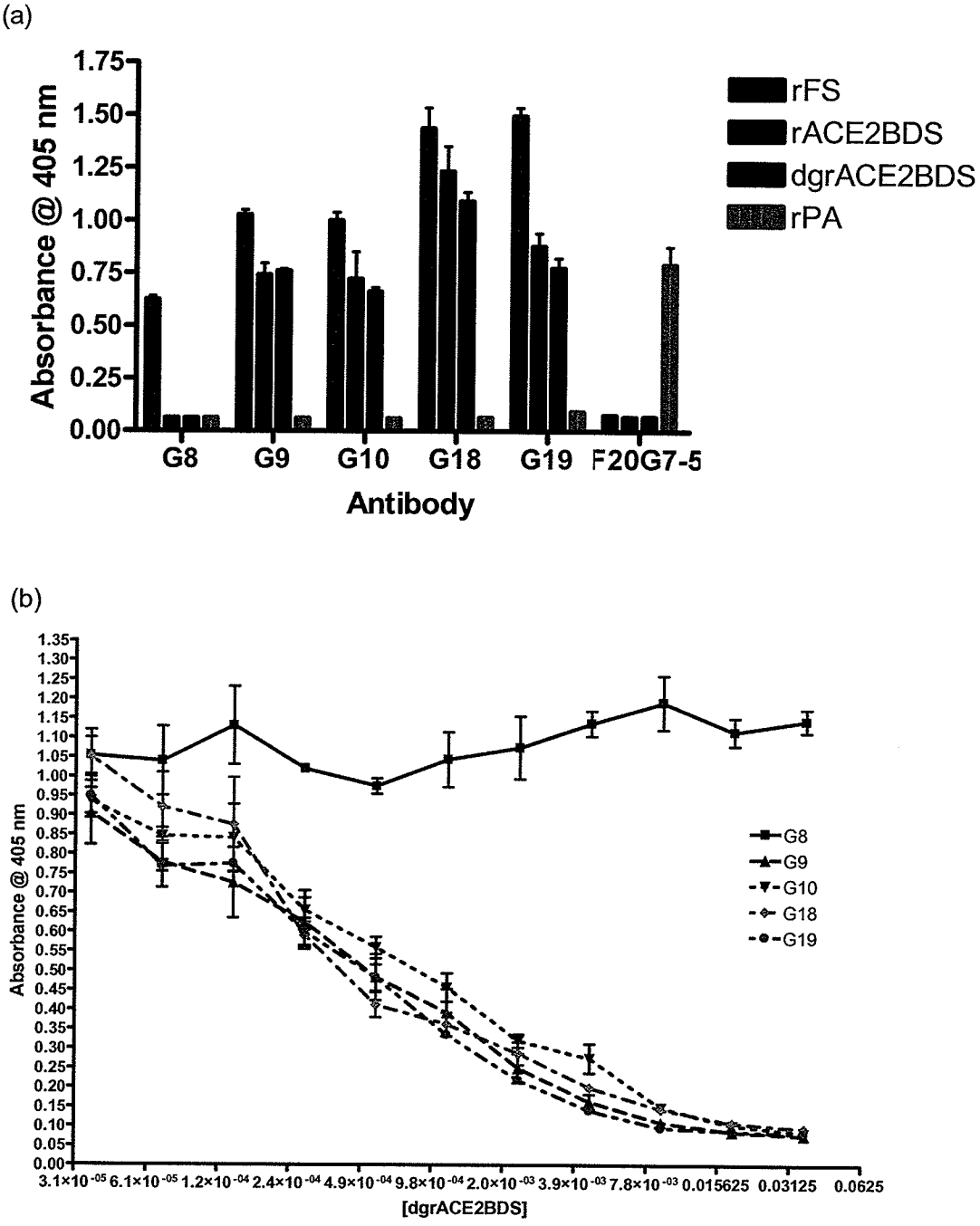

Figure 3.1: ELISA Epitope Characterisation of Murine F26 Series mAbs. All the F26 series mAbs tested bind to rFS, while G8 is the only one that does not bind in the ACE2BD region, as demonstrated by lack of binding to either rACE2BDS or dgACE2BDS (a). These results were confirmed by a competitive ELISA with rFS coating and dgACE2BDS inhibition (b).

Figure 3.1b demonstrates, the four neutralising mAbs are inhibited in their binding to rFS by increasing concentrations of dgrACE2BDS. G8 binding, on the other hand, is unaffected.

3.1.2 Western Immunoblot Epitope Characterisation

Previous western immunoblotting with SARS-CoV infected Vero-E6 cell lysate demonstrated that G8, G18, and G19 bound to a linear epitope on the S protein, while G9 and G10 did not bind. This experiment was repeated using the recombinant S proteins. Figure 3.2 shows that G8 and G18 do indeed bind rFS by western blot, while G9, G10, and G19 do not. G19 was retested twice (not shown), varying the concentration of antibody applied to confirm this result. G18 binds to rACE2BDS, confirming the ELISA and cELISA data. rPA was applied to the third lane with only the F20G7-5 negative control binding it.

3.1.3 SDS-PAGE Analysis of Purity

In order to continue with affinity analysis, purified mAbs must be obtained. Using a protein G column with pH-based binding and elution, high concentrations of purified antibody were obtained. Purity was tested by native (Figure 3.3a) and SDS (Figure 3.3b) PAGE. Figure 3.3a shows that the antibody is uncontaminated and both heavy and light chains are associated with each other and that the purification process has not denatured the antibodies. The SDS-PAGE in Figure 3.3b demonstrates that the band observable in the native gel is indeed antibody, since upon denaturing with the detergent and beta-mercaptoethanol it separates into its heavy (~60kiloDaltons) and light (~30kilo

Daltons) chains. G18 migrates differently in Figure 3.3a and has a different MW in 3.3b because it is an IgG2b isotype, versus IgG2a like the others.

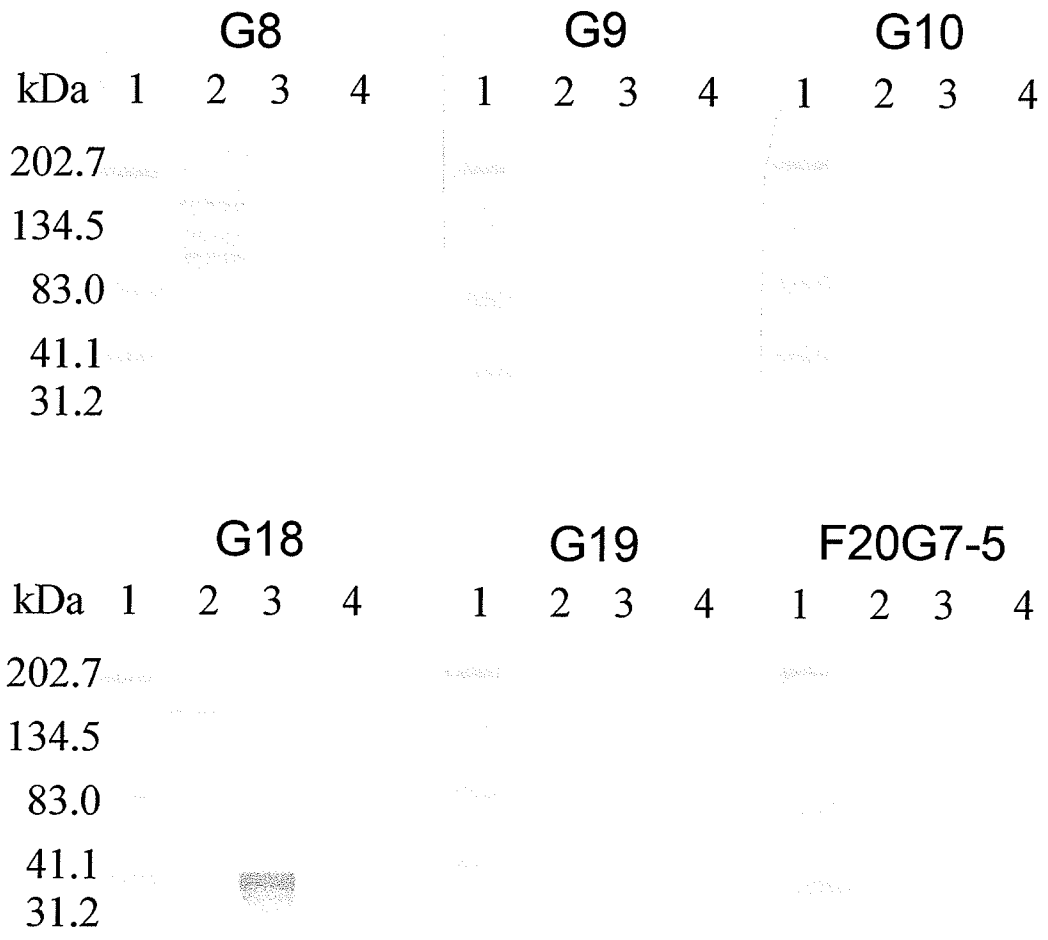

Figure 3.2: Western Immunoblotting on rFS (2), rACE2BDS (3) and rPA (4) using F26 Series mAbs. Both G8 and G18 bind to rFS, while only G18 binds to rACE2BDS. G9, G10, and G19 fail to bind to either form of S protein in this assay, suggesting a conformational epitope. The F20G7-5 negative control binds rPA, while none of the other antibodies do. Lane 1 is the molecular weight marker, with the values in kiloDaltons (kDa) on the left hand side.

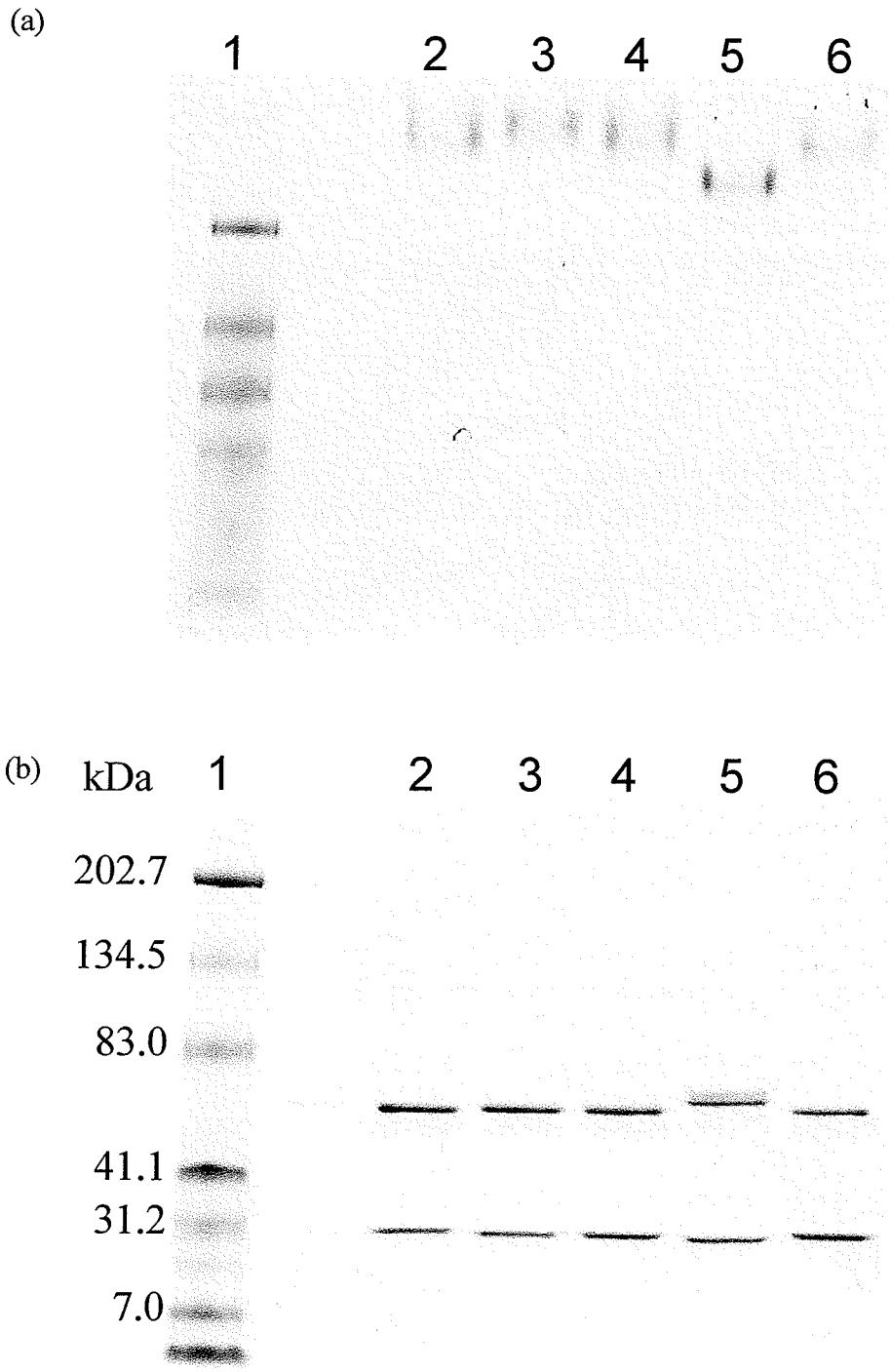

Figure 3.3: PAGE analysis for purity of the murine F26 mAbs. Native- (a) and SDS- (b) PAGE analysis demonstrates that all five antibodies are clean of gross contaminants. Lanes in both gels are as follows: Molecular Weight Marker (1), G8 (2), G9 (3), G10 (4), G18 (5), and G19 (6).

3.1.4 BIACore Affinity Analysis

In order to perform affinity analysis the BIACore 2000 surface plasmon resonance (SPR) technique was used, the gold standard for antibody affinity determination. The surface of a CM5 chip was successfully coated with rFS (Figure 3.4a). Varying concentrations of the F26 series mAbs were flowed over the chip for association to occur, then disassociation was measured by the drop in resonance over time when only buffer was flowing. Figure 3.4b-f demonstrates the curves that were generated by this method for each murine mAb. Calculation of the kinetic constants (k_a and k_d) and affinity constant (K_D) was performed using the BIAEvalution Software assuming 1:1 Langmuir binding. The results are listed in Table 3.1. As can be seen, all the antibodies have nM level affinities. G8 binds very strongly, with an affinity of 0.83(±0.36)nM. G18 has the next highest affinity, at 1.78(±0.63)nM. G9 and G10 have similar affinities, at 10.3(±0.52) and 7.49(±0.40)nM respectively. G19 has an affinity of 4.05(±1.01)nM.

3.1.5 Peptide Mapping of G8 and G18

Since western blotting suggested that G8 and G18 recognised linear epitopes, further epitope mapping was undertaken to localise the binding area. In the first experiment, 17-mer peptides with 9-mer overlaps that covered the S protein region aa300-700 were synthesized and attached to pins. Antibody binding to these pins was then monitored and plotted, as shown in Figure 3.5a. The signal for G8 spikes at two pins, 604-620 and 612-628, suggesting that the epitope lays with the 9-mer overlap region, whose sequence is ADQLTPAWR. Some binding also seems to occur at aa444-

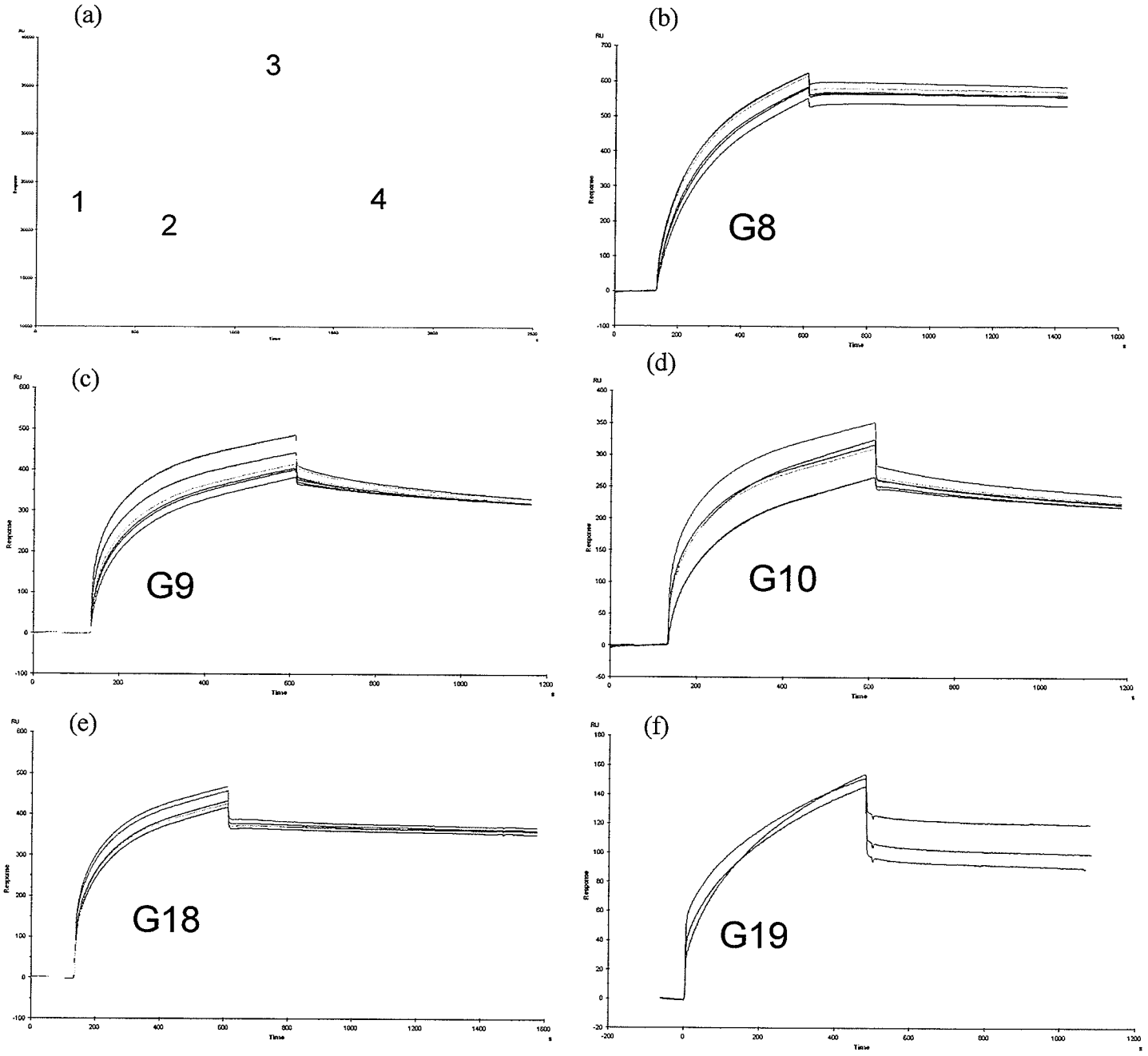

Figure 3.4: BIACore Affinity Analysis on murine F26 series mAbs using rFS. Activation (1), Coating (2), Blocking (3), and Scrubbing (4) were performed on a CM5 chip with rFS (a). The resonance signal level increased from before and after coating, indicating the reaction was successful. Curves (b-f) were then generated by flowing different concentrations from 87-250nN over the coated chip surface. Affinity data in Table 3.1.

460, which can be discounted as an artificial background since ELISA with whole proteins (Figure 3.1) demonstrates G8 does not bind in this region. Another spike of similar value occurs at pin aa540-556. Although it is most probably background, it is hard to discount immediately, since the sequence does lay outside of aa318-510.

The G18 epitope, on the other hand, seems to be located at aa460-476, whose sequence is FSPDGKPATPPALNAYW. This novel epitope is located within the binding domain region, as the ELISA and western blotting experiments predicted it would. Secondary antibody alone (GαM IgG-γ HRP) was used as background signal.

Based on this pin peptide information four soluble peptides were synthesized; two identical to the respective epitope regions, and two scrambled versions of the epitopes. In an ELISA (Figure 3.5b), both antibodies recognise their respective epitopes and do not bind to the scrambled versions. A cELISA (Figure 3.5c) was then performed with rFS coated to the plate and the soluble peptides used as binding competitors. Both G8PEP and G18PEP compete in a concentration dependent manner with rFS for binding to G8 and G18 respectively while G8PEPScr and G18PEPScr do not affect binding.

F26 Series Antibody	ka (1/Ms)	kd (1/s)	KD (nM)	Neutralisation Titre (μg/ml)[a]
G8	$2.87(\pm0.49)\times10^{4}$	$2.19(\pm0.38)\times10^{-5}$	0.83(±0.26)	n/a
G9	$3.30(\pm0.81)\times10^{4}$	$2.83(\pm0.33)\times10^{-4}$	10.2(±3.5)	n.d.
G10	$3.87(\pm1.32)\times10^{4}$	$2.33(\pm0.25)\times10^{-4}$	7.5(±2.7)	n.d.
G18	$2.68(\pm0.51)\times10^{4}$	$4.71(\pm0.62)\times10^{-5}$	1.79(±0.50)	0.31
G19	$2.09(\pm0.41)\times10^{4}$	$8.24(\pm1.16)\times10^{-5}$	4.05(±1.01)	n.d.

Table 3.1: BIACore affinities and neutralisation titres on the F26 series murine mAbs. [a]Not determined for this project.

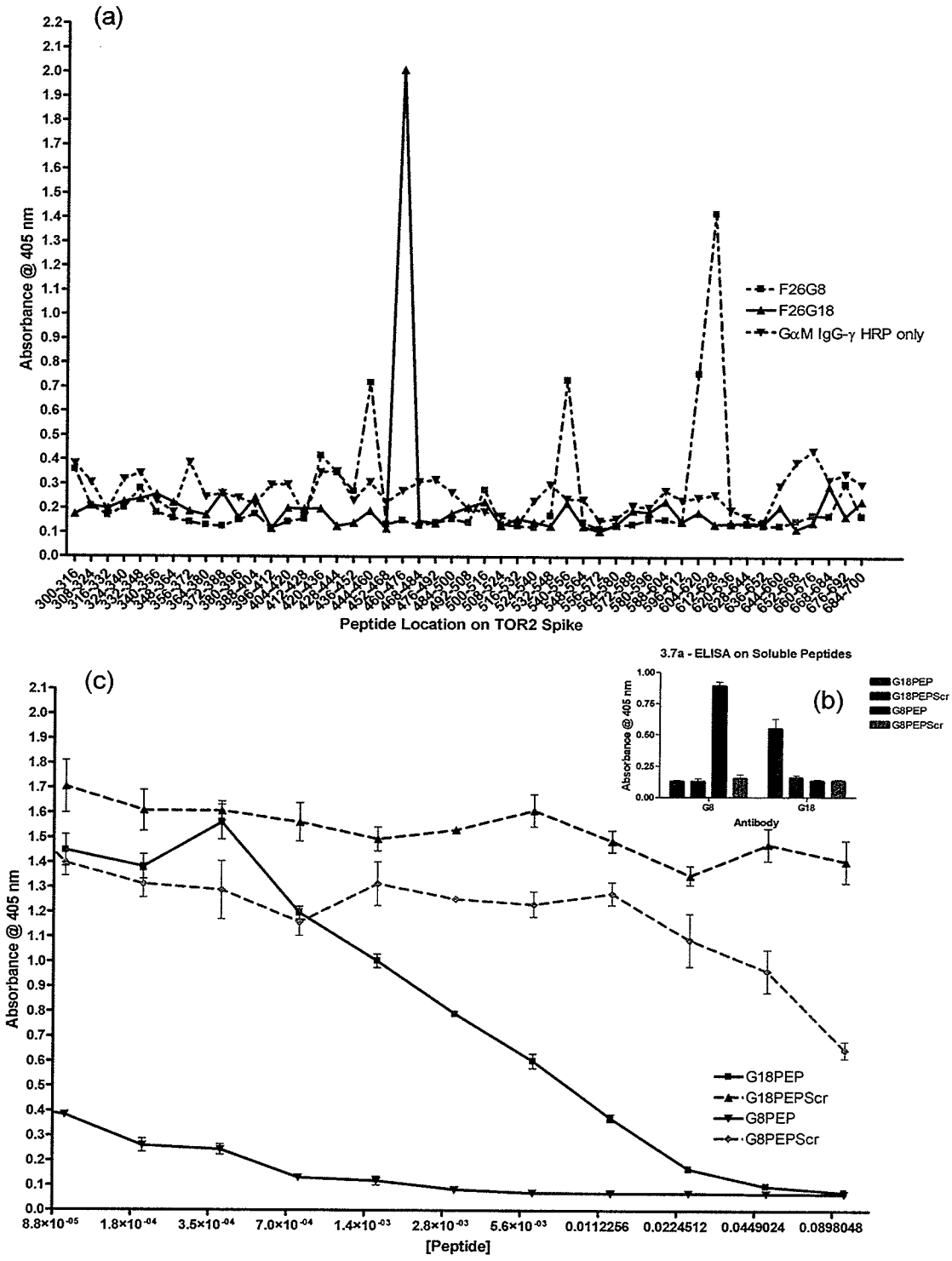

Figure 3.5: Peptide Mapping of F26G8 and F26G18. Pin Peptide Mapping (a), Soluble peptide ELISA (b), and competitive ELISA (c) demonstrate that G8 and G18 bind regions aa612-620 and aa460-476 respectively.

3.2 Development of Chimeric mAbs

Sequence data on the variable regions (V_H and V_L) of the F26 mAbs was obtained by Gubbins et al. in 2004. Comparison of the sequence data for heavy and light chains demonstrates that G9, G10, G18, and G19 all share the same germline V_H gene, J588.50, while the light chain V_L gene usage is varied. In order to see if the light and heavy chain V genes of G9, G10, G18, and G19 can be interchanged, I created chimeric pIGG constructs that have both the original pairings (i.e. 18H18L) and uniquely assembled pairings (i.e. 9H10L). While the original pairings could be used as a novel therapeutic, the uniquely built pairings could provide tools to address the relative contributions of both heavy and light chain V genes to binding.

3.2.1 Chimeric Construct Development and Screening

Reverse transcriptase polymerase chain reaction (RT-PCR) was performed on fresh total RNA preparations from G18 and G19 hybridomas using oligodT priming. The cDNA created was amplified for V_H and V_L regions in separate PCRs. For G18, UmIgVH(5') and MG2a/bSeq(3') amplified V_H. G19 amplification was obtained with UmIgVH(5') and MG2a/bSeq(3') for V_H, and MVL(5') and MK3-Seq(3') for V_L. For the G18 V_L, rapid amplification of cDNA ends (RACE) was employed using Gene-Racer (Invitrogen), since aberrant kappa (AbVk) interference prevented regular amplification techniques. These V_H and V_L regions were then placed into the pCR2.1 vector and eight clones sequenced. Sequence data (not shown) demonstrates that the V_H and V_L regions were identical to the ones outlined by Gubbins et al. G9 and G10 V regions were already present in a pCR2.1 vector from previous work.

An internal Sac I site was then removed from the framework 3 V_H region of G9, G18, and G19 by site-directed mutagenesis. A synonymous mutation was performed, conserving the amino acid sequence in the region to be MELS. Sequence data (not shown) demonstrates that the clones picked contained the synonymous mutation and no other mutations. Mutation was unnecessary for G10, since it contains no Sac I site in the V_H region.

Linking PCR was then used to link the V_L regions of G9, G10, G18, and G19 to the human constant kappa (C_κ) region. The linked products were then inserted into pCR2.1 using the TOPO-TA reaction, and eight clones were sequenced. Of the eight clones, two had the V_L and C_κ correctly linked and in-frame, giving a 25% success rate for the linking reaction. Since Hind III and Xba I restriction enzyme sites were present in the linking PCR primer design, a double restriction enzyme digest of the pCR2.1-V_LC_κ vectors using these two enzymes yielded the product for insertion into Hind III / Xba I digested pIGG (Figure 3.6a). Eight clones of the ligation reaction were screened by sequencing for each V_LC_κ inserted. In addition, transfection of 293T cells with the clones followed by ELISA demonstrated that the constructs could still produce antibody (Figure 3.6b). This is shown by the binding to α-Igγ and α-Igκ coated wells, demonstrating that the heavy and light chains respectively are produced.

The heavy chain V_H regions were then amplified from the pCR2.1-V_H vectors (or sometimes cDNA) with primers for the Sac I / Apa I digestion and ligation into pIGG-V_LC_κ vectors created. 9H and 10H were paired with all four possible combinations (9L, 10L, 18L, and 19L), while 18H and 19H were each paired with 18L and 19L only. This

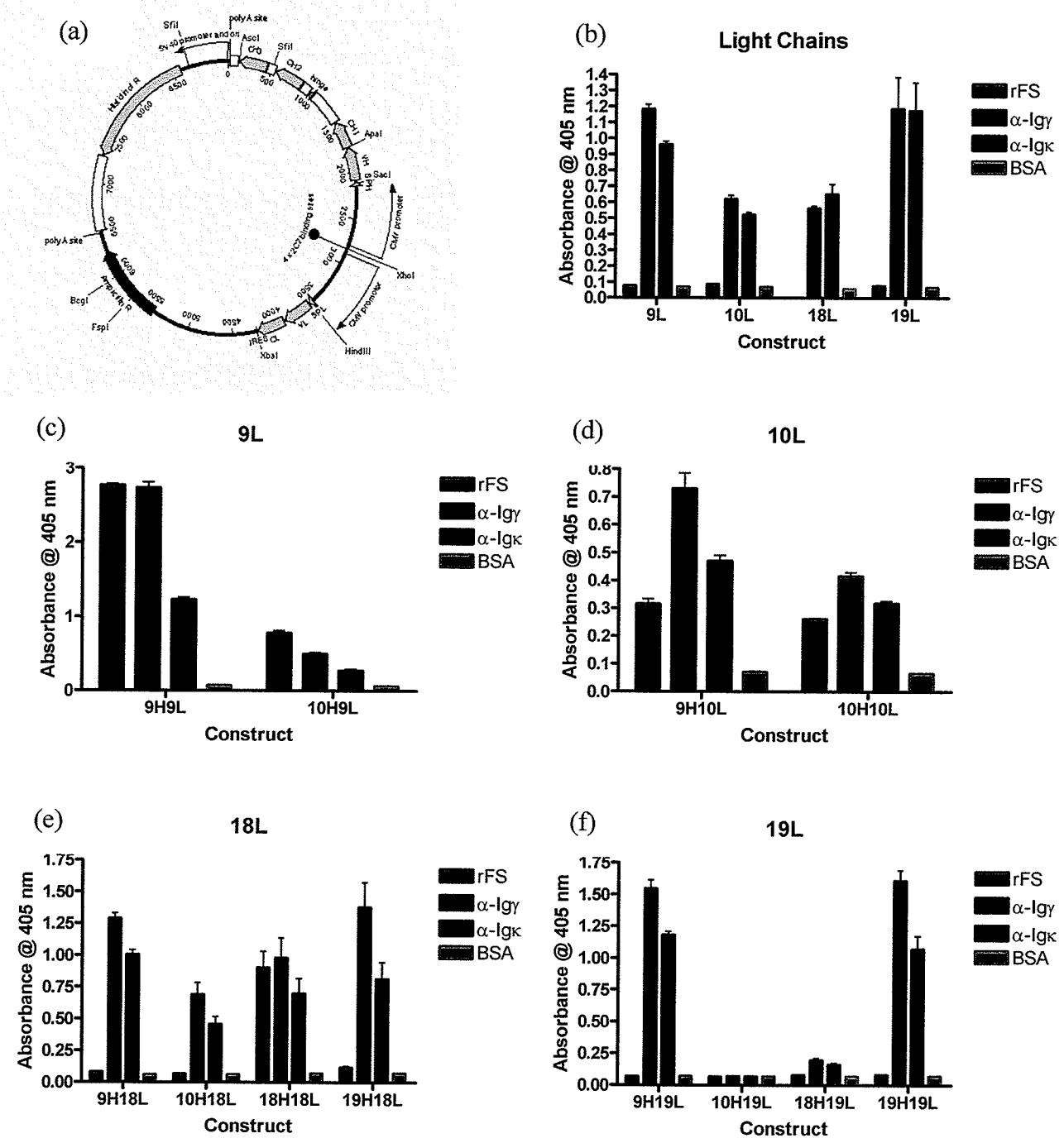

Figure 3.6: Development of chimeric mAbs from the F26 series using pIGG vector. The pIGG vector (a). Production of antibody when the light chain (9L, 10L, 18L, or 19L) is inserted into the vector (b). When the heavy chains (9H, 10H, 18H, 19H) were inserted into constructs containing the various light chains, the following combinations were productive: 9H9L, 10H9L, 10H10L, 9H10L, and 18H18L (c-f).

gave a total of 12 constructs, with 4 original pairings and 8 uniquely assembled pairs. Eight clones of the ligation reactions were screened by sequencing, showing that all the constructs created were correct and in-frame (data not shown).

Transfection of 293T cells followed by ELISA screening demonstrates that 3 of the original pairs (9H9L, 10H10L, and 18H18L) and 2 of the uniquely assembled ones (9H10L and 10H9L) produce antibody that binds to rFS (Figure 3.6c-f). 10H19L and 18H19L are the only constructs that seem to not produce antibody, although there is a slight increase in the α-Igγ and α-Igκ signal for 18H19L. Interestingly, 19H19L (Figure 3.6f) is producing a significant amount of antibody but does not bind rFS. This is the only original pairing where rFS binding is lost.

3.2.2 Production of Chimeric Antibody

The plasmids expressing the five constructs that produced antibody against rFS were then prepared on a large scale using QiaGen Giga Prep kit. Sequencing and restriction enzyme digest on the large scale preparations tested the integrity of the constructs. Sequencing data (not shown) demonstrated that the insert V regions were identical to the V_H and V_L regions previously described. Restriction enzyme digestion (Figure 3.7) showed the expected bands at approximately 370bp for V_H and 700bp for V_LC_κ. The Hind III / Xba I digestion for plasmids harbouring 9H9L, 10H9L, 10H10L, and 9H10L creates another band at approximately 1700bp due to the fact that 9H and 10H contain a known Hind III site.

Since serum-free medium is necessary for purification of antibody, expression studies were done using the 18H18L construct to determine the ideal

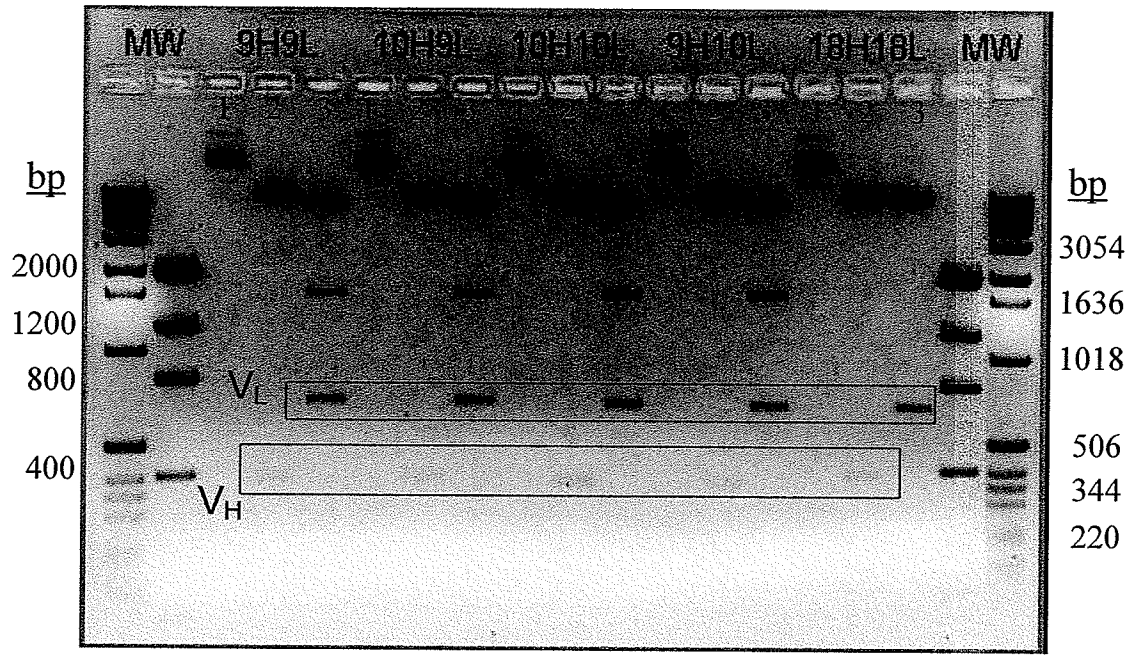

Figure 3.7: Restriction Enzyme digestion of chimeric constructs. Comparison of uncut (1), SacI/ApaI cut (2), and HindIII/XbaI cut (3) digestions for each construct. Lane 2 shows the V_H band at approximately 370bp, while lane 3 demonstrates the $C\kappa$-V_L band at 700bp. Molecular weight markers flank the samples, with the size in bp of specific bands given on the sides of the gel: left – low weight ladder; right – high weight ladder.

conditions for producing large amounts of antibody. First, adherent 293 and 293T cells were compared with and without serum by ELISA (Figure 3.8a). Both cell types are commonly used in antibody production, with 293T being 293 cells that contain the SV40 large T antigen. As can be seen, 293T cells produce more antibody then the 293 cells. As well, the addition of serum increases production, although the effect is more drastic for 293 cells. Therefore adherent 293T cells without serum would be the best of these options.

However, this adherent 293T cell culture is difficult to maintain in serum-free conditions (author's personal observations). Therefore the 293F cell line, a suspension 293 cell line that has already been adapted to serum-free medium, was compared to the

293T culture. In order to make a comparison, the 293T cells were adapted to suspension growth using CD293 medium, making s293T. These cells were then adapted to the same

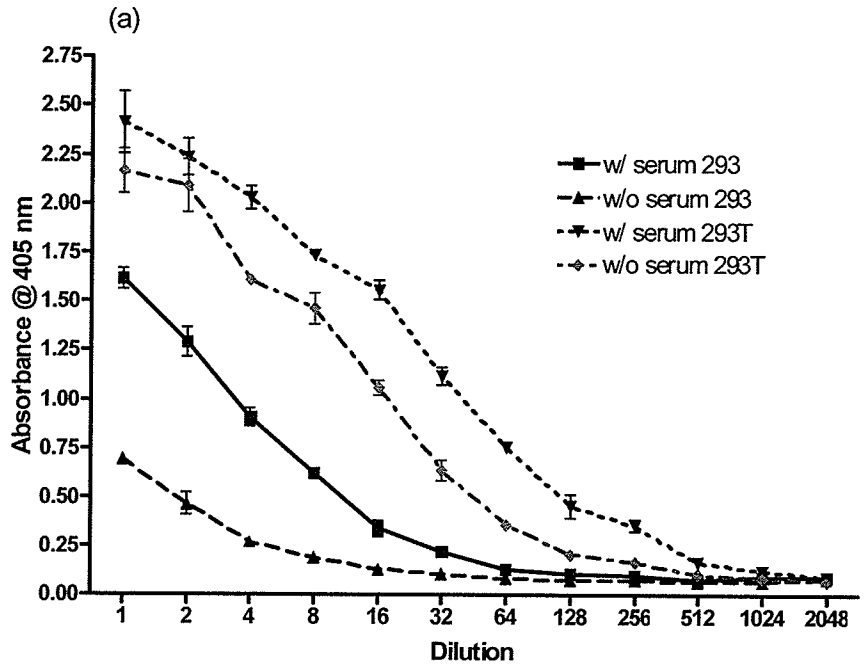

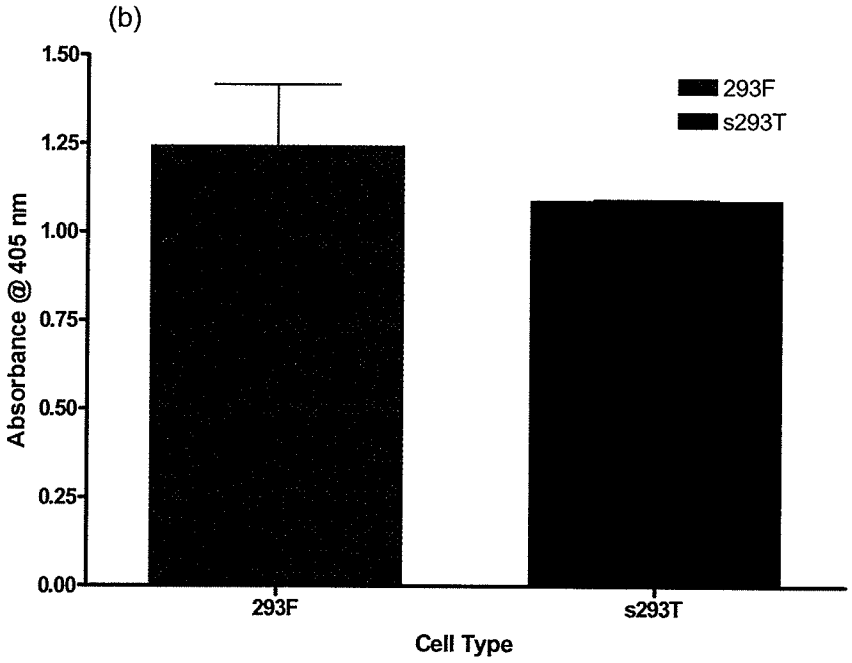

Figure 3.8: Testing of different cell line conditions for chimeric antibody production. For adherent cells, 2 93T cells with and without serum behaved relatively identical, while 293 cells required serum to produce significant levels of antibody (a). 293F and s293T cells in the FreeStyle™ Serum-Free medium behave similar (b).

medium as 293F cells. Transfection of s293T and 293T cells with 18H18L was then screened by ELISA (Figure 3.8b). From the results, it is inconclusive which cell system is better from a production stand point. Since the 293F cells required less maintenance and clumped less, this system was chosen to continue with purification.

Three different purification protocols (as described in the Materials and Methods) were attempted and compared using the same batch of supernatant from transfection of 293F cells with 18H18L. By ELISA (Figure 3.9a), protocols 1 and 2 produced approximately the same amount of antibody. A μBCA on the preparations for protein concentration gave 340, 360, and 40 μg/ml for protocols 1, 2, and 3 respectively. As shown by the SDS-PAGE in Figure 3.9b, protocol 1 creates a higher quality preparation in terms of purity. Therefore protocol 1 was used to purify the remaining chimeric antibodies.

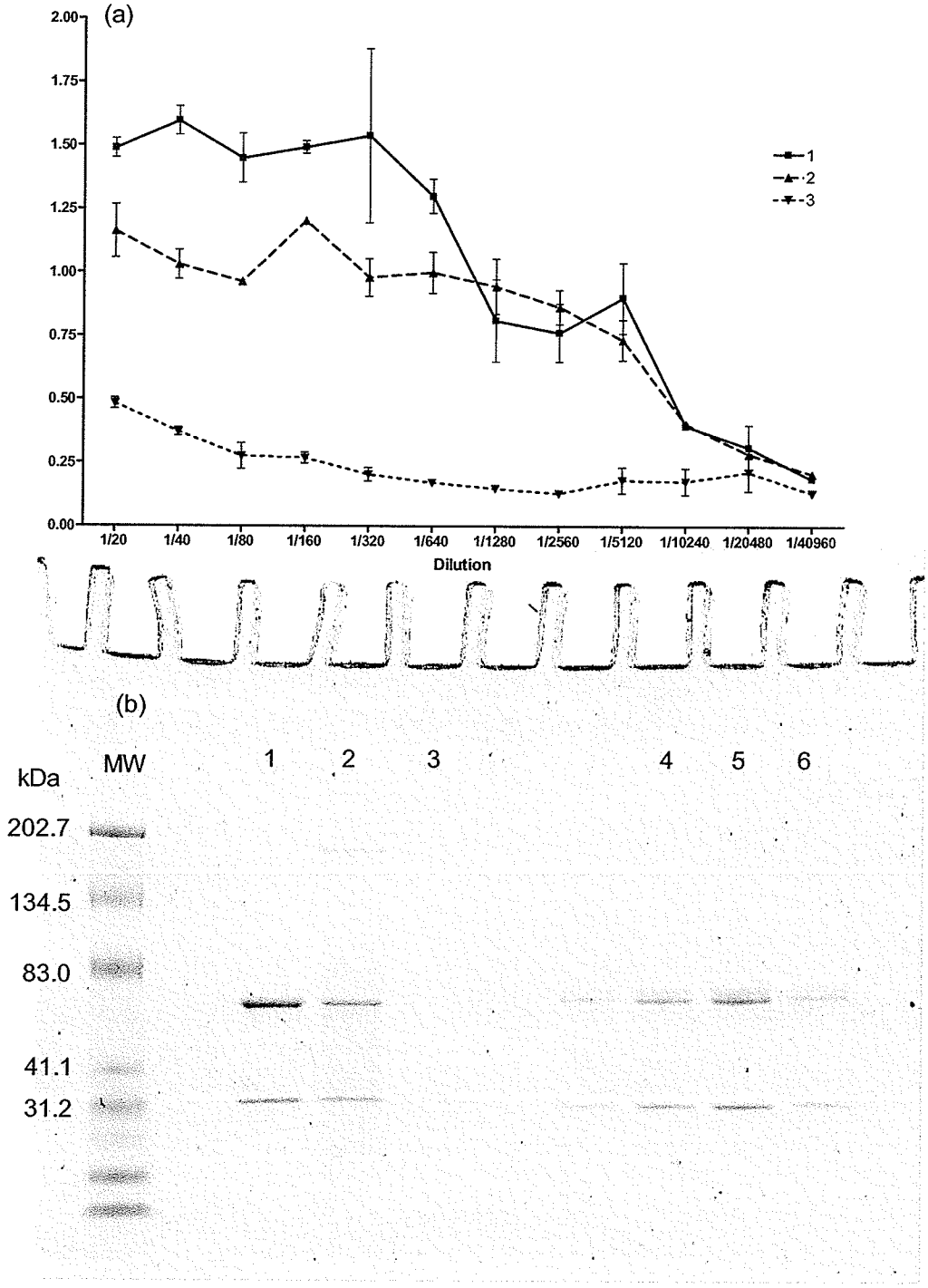

Figure 3.9: The efficacy of three different purification protocols on 18H18L. Protocols 1 and 2 show the most promise by ELISA (a), while an SDS-PAGE (b) analysis demonstrates that protocol 2 yields more impurities than protocol 1, leading to protocol 1 being chosen. The protocols are described in 2.21. Lanes in (b) are as follows: (1), (2), (3) are protocols 1-3 respectively, while 4-6 are varying concentrations of the murine G18 antibody run as a control.

3.3 Characterisation of Chimeric mAbs

In order to compare the chimeric mAbs to the original murine ones, all the characterisation experiments performed on the latter were repeated with the chimeric antibodies.

3.3.1 ELISA Epitope Characterisation

Figure 3.10 shows the results of an ELISA and cELISA performed to characterise the epitope of these mAbs using recombinant S proteins. As can be seen from Figure 3.10a, all five of the chimeric mAbs bind to rFS, rACE2BDS and dgrACE2BDS, although binding to rACE2BDS and the deglycosylated form is lower for 10H9L and 9H10L. A cELISA was then done to confirm these results (Figure 3.10b), which demonstrates that all of the chimeric antibodies are inhibited in their binding to rFS by increasing concentrations of dgrACE2BDS.

3.3.2 Western Immunoblot Epitope Characterisation

Since Western Immunoblotting on the murine F26 series mAbs demonstrated that only G8 and G18 bound, western blotting was repeated for the chimerics only for 18H18L. Looking at Figure 3.11, it can be seen that 18H18L shows the same binding pattern in western blot that G18 does, binding to both rFS and rACE2BDS and not rPA.

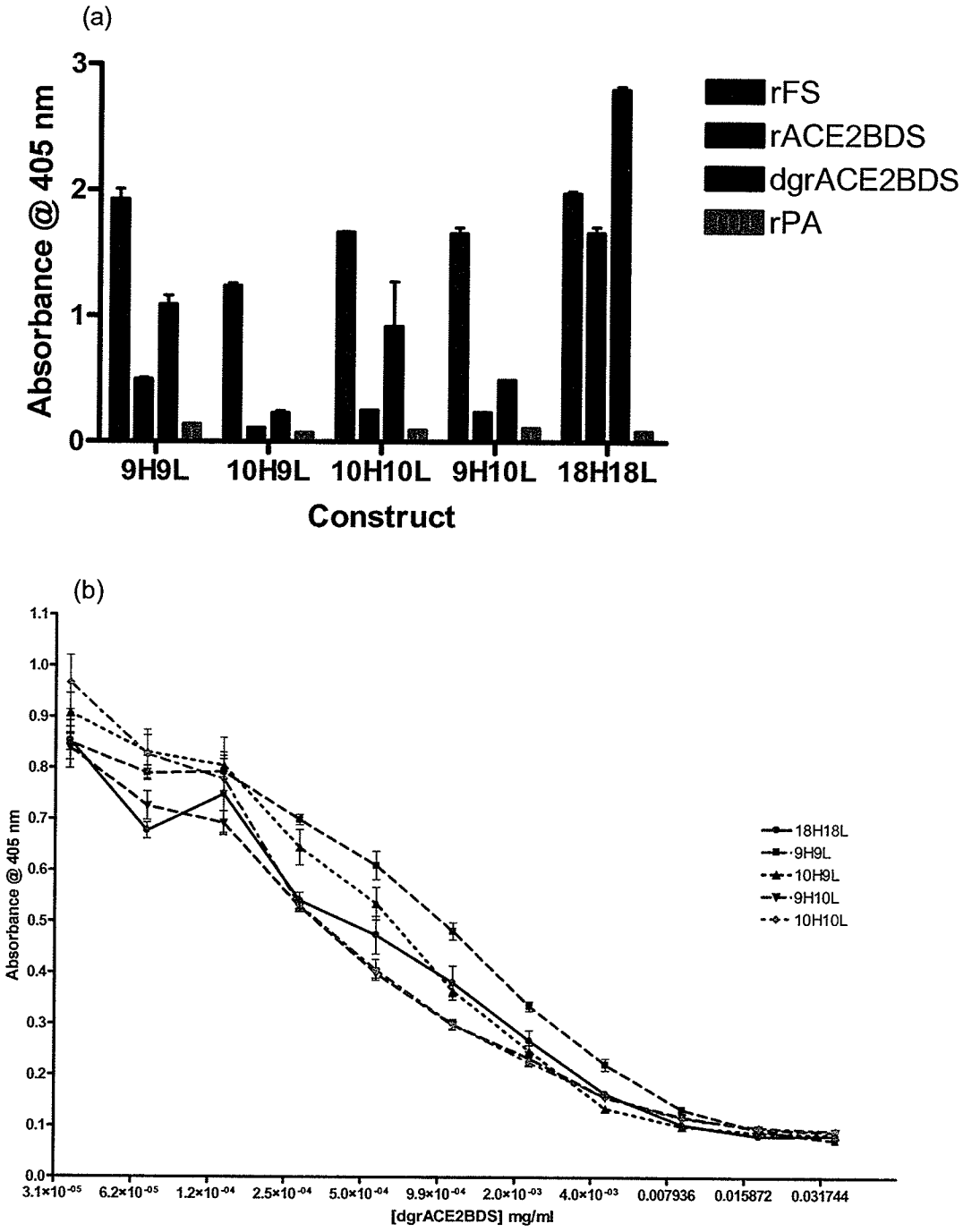

Figure 3.10: ELISA epitope characterisation of chimeric mAbs. Direct ELISA (a) shows that all the chimeric mAbs bind strongly to rFS, while rACE2BDS and rdgACE2BDS bind with varying degrees. Competitive ELISA (b) shows that rdgACE2BDS successfully competes with rFS for antibody binding for all the chimerics.

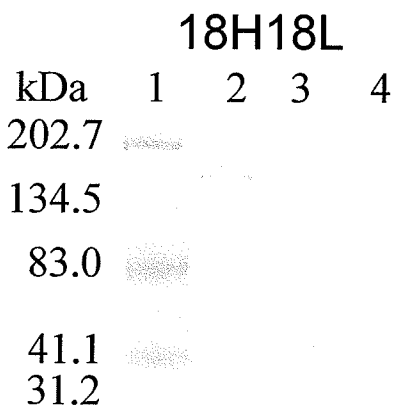

Figure 3.11: Western Immunoblotting on rFS (2), rACE2BDS (3) and rPA (4) using chimeric antibody 18H18L. The chimeric antibody binds to both rFS and rACE2BDS, without binding rPA. Lane 1 is the molecular weight marker, with the values in kiloDaltons (kDa) on the left hand side.

3.3.3 SDS-PAGE Analysis of Purity and μBCA Assay for Concentration

Using protocol 1, all five chimeric antibodies were purified and run on SDS-PAGE and native PAGE gels. As can be seen from Figure 3.12a and 3.12b, 9H9L, 10H10L, and 18H18L are produced in amounts that can be seen in both the denaturing and native conditions. 10H9L and 9H10L production, on the other hand, is significantly lower, with 9H10L visible only in the SDS-PAGE, and 10H9L not visible at all. Results from the μBCA assay (see Table 3.2) demonstrate that even though the same number of cells and starting volume of supernatant was used for all the chimerics, the chain-switched pairs were both produced at lower levels. In fact, 9H10L production is only visible by ELISA, and 10H9L is at the lower limit of the μBCA detection range. 9H10L production was attempted a second time with the same result.

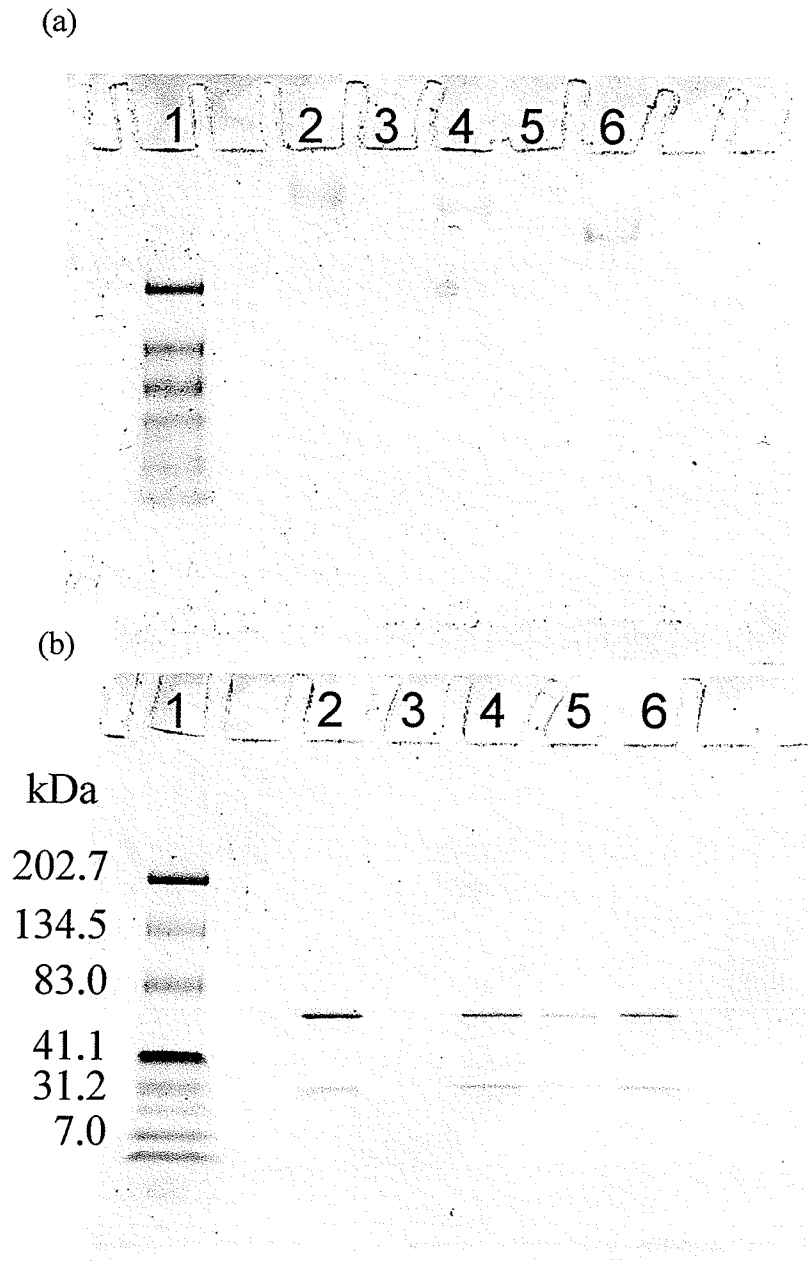

Figure 3.12: PAGE analysis for purity of the chimeric mAbs. Native- (a) and SDS- (b) PAGE analysis demonstrates that all antibodies are pure, but 9H10L is barely visible (5) and 10H9L is not visible at all (3), suggesting low concentrations of these two antibodies. Lanes in both gels are as follows: Molecular Weight Marker (1), 9H9L (2), 10H9L (3), 10H10L (4), 9H10L (5), and 18H18L (6).

3.3.4 BIACore Affinity Analysis

BIACore affinity analysis was performed on the four chimeric antibodies that a concentration was available for; 9H9L, 10H10L, 10H9L, and 18H18L. Varying concentrations of the chimeric antibodies were flowed over the rFS-coated CM5chip for association to occur, then disassociation was measured by the drop in SPR over time when only buffer was flowing. Figure 3.13a-d demonstrates the curves that were generated by this method for each antibody. Calculation of the kinetic constants (k_a and k_d) and affinity constant (K_D) was performed using the BIAEvalution Software assuming 1:1 Langmuir binding, and the results are listed in Table 3.2. 10H10L, 9H9L, and 9H10L all have similar affinities, at 3.62(±2.31), 2.69(±0.99), and 5.23(±2.90) nM respectively. 18H18L has an affinity of 1.28(±1.02) nM.

Antibody	Concentration (µg/ml)	ka (1/Ms)	kd (1/s)	KD (nM)	Neutralisation Titre (µg/ml)[a]
9H9L	137	$3.98(\pm0.71)\times10^{4}$	$9.73(\pm1.29)\times10^{-5}$	2.69(±0.50)	n.d.
10H9L	n.d.	n/a	n/a	n/a	n/a
10H10L	86	$4.01(\pm1.14)\times10^{4}$	$1.12(\pm0.20)\times10^{-4}$	3.62(±1.46)	n.d.
9H10L	15.4	$6.15(\pm2.34)\times10^{4}$	$2.49(\pm0.36)\times10^{-4}$	5.23(±2.05)	n.d.
18H18L	1000	$2.81(\pm0.73)\times10^{4}$	$2.90(\pm0.80)\times10^{-5}$	1.28(±0.78)	0.37

Table 3.2: Concentration, affinity, and neutralisation results for chimeric mAbs.
[a]Not determined for this project.

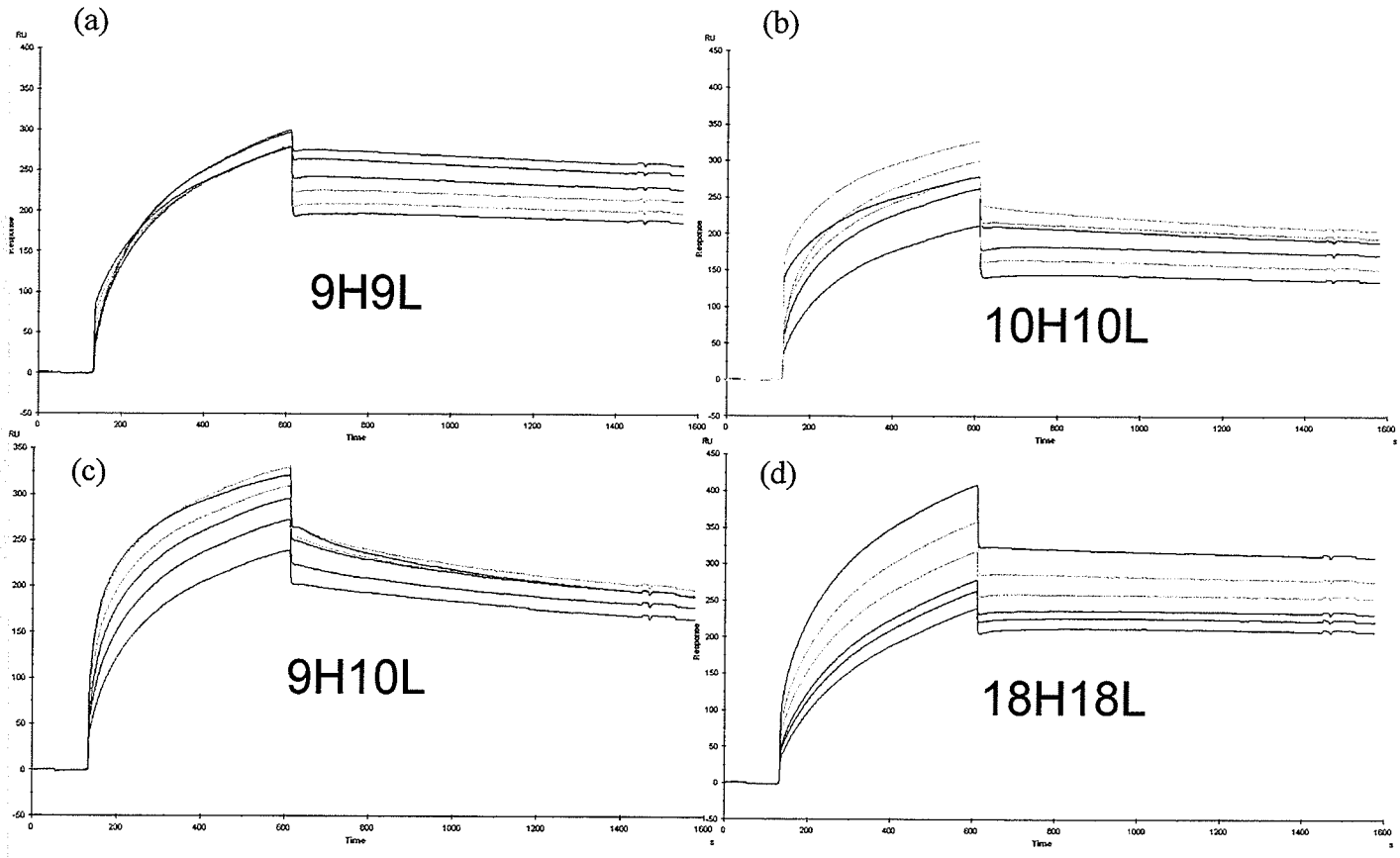

Figure 3.13: BIACore Affinity Analysis on chimeric mAbs using rFS. Curves (a-d) were generated by flowing different concentrations from 87-250nN over a previously coating (see Figure 3.4) CM5-rFS chip. The affinity data is presented in Table 3.2.

3.3.5 Neutralisation Assay on G18 and 18H18L

Neutralisation assay were then performed on the both G18 and 18H18L in parallel so as to limit errors due to different viral stocks. Both G18 (murine) and 18H18L (chimeric) successfully neutralised the wild-type TOR2 strain of SARS-CoV. The titres for the murine antibodies are shown in Table 3.1, while the chimeric antibody data is presented in Table 3.2. G18 had a 100% neutralisation titre of 0.3137μg/ml, while 18H18L had a neutralisation titre of 0.37μg/ml.

3.3.6 Peptide Mapping of 18H18L

As for G18, peptide mapping was performed on 18H18L using 17-mer pin peptides with 9-mer overlaps and soluble G18PEP and G18PEPScr. Figure 3.14a demonstrates that pin peptide mapping was unable to locate the epitope for the chimeric version. The readings were identical to baseline (GαH 2° alone). This experiment was repeated thrice with the same result each time. The soluble peptides were then tried in a normal ELISA, with inconclusive results. 18H18L did not bind to G18PEP stronger than to background (G18PEPScr, G8PEP, G8PEPScr).

However, a competitive ELISA using G18PEP and G18PEPScr as competitors for 18H18L demonstrates that G18PEP inhibits 18H18L binding to rFS in a concentration dependent fashion. G18PEPScr, on the other hand, produces no inhibitory effect. This demonstrates that 18H18L binds to the specific sequence in G18PEP.

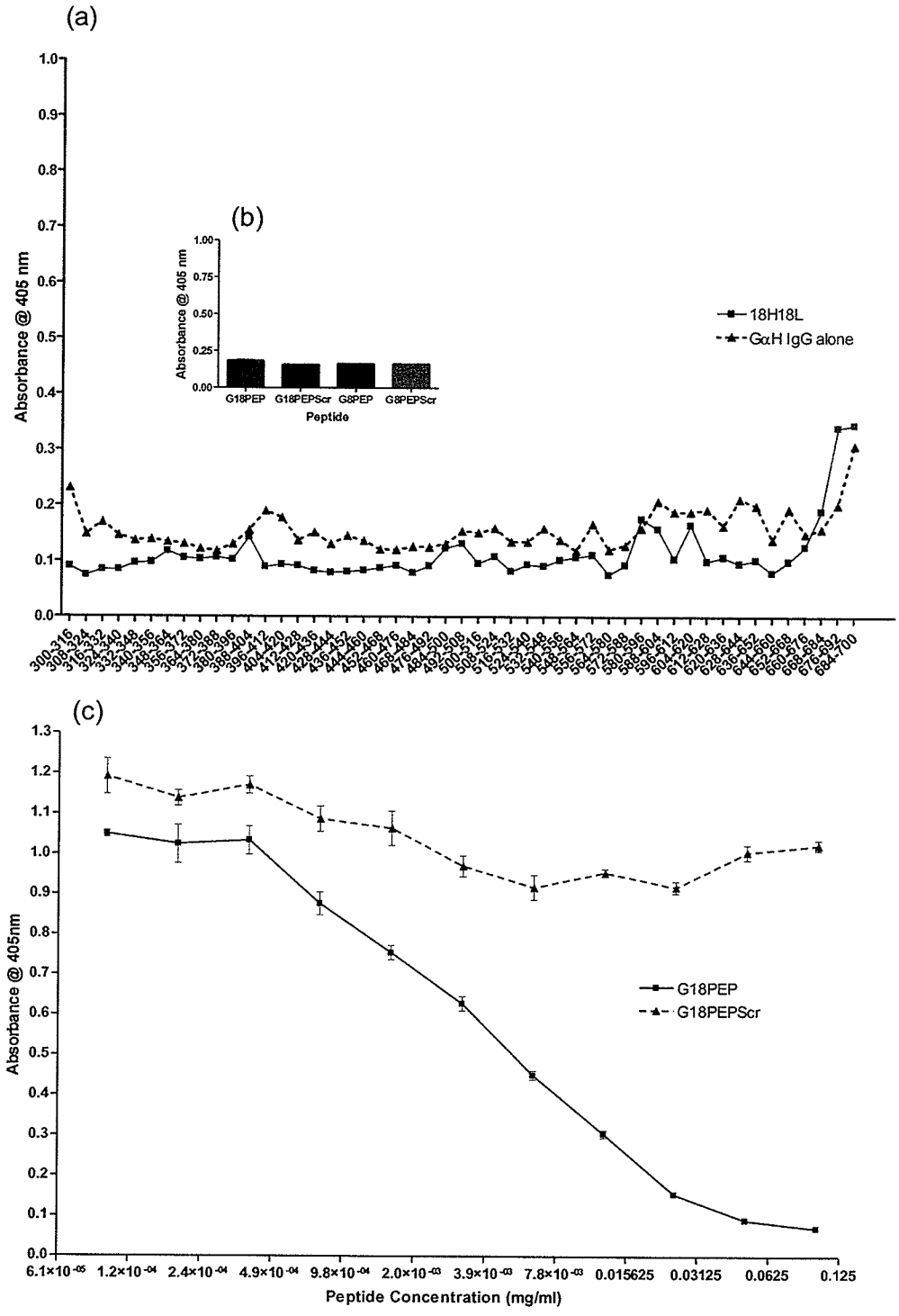

Figure 3.14: Peptide Mapping of 18H18L. Pin Peptide Mapping (a) and soluble peptide ELISA (b) results are inconclusive, while the competitive ELISA (c) demonstrates that 18H18L binds the aa460-476 peptide.

4 Discussion

4.1 Introduction

The potential for using monoclonal antibodies (mAb) in therapeutics has been recognised since the 1980s. However, the inherent immunogenicity of the majority of murine mAbs in humans limited their therapeutic application. Recent advances in molecular cloning techniques have enabled the immunogenicity of mAbs to be significantly reduced, leading to an explosion of mAbs in development and clinical trials to treat diseases from cancer to asthma. These immuno-engineering techniques have focussed on increasing the 'human' content of the mAbs, with one of the most dramatic changes seen when the murine constant regions are replaced with human constant regions to make a chimeric mAb.

Chimeric mAb therapy could be used to combat the spread of infectious agents such as SARS-CoV. Studies by other groups demonstrated the effectiveness of antibody prophylaxis in infected individuals[112] and of mAb therapy *in vivo* in animal models.[115,120,122] In addition, mathematical modeling outlines and supports the utility of mAb therapy to contain an epidemic.[135] Administration of mAb therapy to infected individuals would be simplified due to the short-lived nature of the infection, requiring probably only one dose. Therefore, application of therapeutic mAbs to combat the spread of SARS-CoV in case of another epidemic is a realistic possibility.

With this in mind, neutralising chimeric mAbs derived from the F26 series that target SARS-CoV have been developed and characterised in our lab. In order to perform

an analysis of the success of this project, further characterisation of the parental murine mAbs properties was undertaken. Chimeric constructs were then produced using the pIGG vector, screened, and the viable constructs produced for characterisation. The results were then compared to the murine versions.

4.2 Murine mAb Properties

Previous work had confirmed that G9, G10, G18, and G19 of the F26 series neutralised SARS-CoV, while G8 did not. However, epitope and affinity information were lacking, with the exception of Western immunoblotting information that suggested G8, G18, and G19 bound to the S protein. The first series of experiments undertaken was done to confirm this binding, as well as to characterise whether or not the interaction took place within the receptor-binding domain (RBD) of S protein, the region where ACE2 binds. If so, it would provide a molecular mechanism whereby the antibodies neutralise SARS-CoV.

ELISA experiments demonstrated that all of the neutralising mAbs bound not only to a recombinant full-length version of S protein (rFS), but also to a recombinant S protein that spans the only RBD (rACE2BDS). On the other hand, the non-neutralising mAb G8 bound only rFS and therefore not in the RBD. Therefore it is rational to assume that the ability to neutralise SARS-CoV for this set of antibodies is due to interference with the S protein and ACE2 interface. The lack of neutralisation ability by G8 can similarly be summarised by the fact that the binding site clearly exists outside of the RBD. Importantly, all the neutralising mAbs also bound the deglycosylated version of

rACE2BDS, demonstrating that binding of the antibodies to S protein does not depend upon the glycosylation of the epitope.

Western immunoblotting experiments with these recombinant proteins confirmed the results previously obtained used whole cell lysate, with the notable exception of G19. The previous work showed G19 binding to S protein, while even upon repetition of the experiments G19 did not bind rFS or rACE2BDS in western blot. While this suggests that G19 binds a less linear and more conformation epitope, previous immunoblotting experiments were performed using whole cell lysate instead of a recombinant baculovirus form, which could possibly explain the discrepancies in the results.

Recently, work with collaborators has resolved the crystal structure of the G19:rACE2BDS complex (James Rini, University of Toronto, manuscript submitted). This demonstrates that G19 does indeed bind a conformation epitope across many regions of rACE2BDS using the H1, H2, H3 and L3 loops in the complimentary determining regions (CDR). Therefore G8 and G18 are the only antibodies that target a linear epitope on S protein; G8 outside the RBD and G18 inside it.

Further mapping of these two epitopes demonstrates that G8 and G18 bind the aa612-620 and aa460-476 regions respectively. Both pin peptides and soluble peptides were used to confirm this analysis. Scrambled control versions of the peptides were not bound by the mAbs, showing that the binding was sequence specific. Since G8 bound to two of the pin peptides in order, the shorter sequence (ADQLTPAWR) where the pin peptide sequence overlap occurs forms the minimal epitope. The epitope for G8 has also been further confirmed by a collaborator to locate to the aa612-620 region, using a random phage display peptide library (Linfa Wang, CSIRD Aus, unpublished data). For

G18, however, only the pin with the aa460-476 peptide (FSPDGKPATPPALNAYW) bound.

When using this approach to map an epitope it is important to keep in mind that other protein-protein interactions may be occurring; only the necessary and minimally sufficient epitope for antibody binding is demarcated. For example, G18 could have contacts with other regions, but if those interactions are not strong enough on their own to lead to a signal the method will not be able to pick it up. Therefore from the data presented G18 definitely binds the aa460-476 sequence, but one cannot discount the possibility that G18 interacts at other regions; only that those interactions are not necessary and sufficient in and of themselves for antibody-antigen binding to be detectable.

All of the antibodies demonstrated affinity to recombinant full-length S protein in the nanomolar range, with G8 having the highest affinity and G9 the lowest (Table 3.1). These affinities are normative for antibody-antigen interactions. Overall, there does not seem to be a large correlation between affinity and the neutralisation titre. For example, G9 and G19 have a greater than 6nM difference in affinity, but no difference in neutralisation titre. G18 is 2nM stronger than G19 in affinity, but thirteen times stronger in terms of neutralising titre in the assay performed previously.[125] Amongst the neutralising mAbs, however, G18 is the strongest in terms of both neutralising capability and affinity.

4.3 Chimeric Construct Screening

Chimeric constructs were created using cDNA from hybridomas of the F26 series. In the cloning strategy, the pIGG plasmid (C. Rader, NIH) was used which is capable of expressing kappa chain and IgG1 heavy chain. The main benefit of using this vector was that both light and heavy chains could be present on the same vector, eliminating the need for dual transfection. That being said, one then must put both heavy and light chain DNA on the same vector, adding time and difficulty to the cloning process.

The cloning strategy involved a SacI / ApaI digestion to insert the heavy chain, and a HindIII / XbaI digestion to insert the kappa chain. Since the starting construct, pIGG-P14, had a Sac I site in the variable light chain region, the light chains of the F26 series needed to be added prior to the heavy chain. These intermediate constructs (9L, 10L, 18L, 19L) were able to produce antibody by combining with the heavy chain of P14, but not able to bind to S protein. This result was expected, since theoretically most light and heavy chains should be able to associate and thereby leave the cell. The chains are associated and not simply being co-expressed because when an ELISA is performed with α-Igκ coated onto the plate, a secondary that is α-Igγ leads to a signal. This demonstrates that both antibody chains must be present and associated with one another. A reverse of this experiment (ELISA plate coated with α-Igγ, secondary that is α-Igκ) leads to the same result (data not shown).

Screening of the constructs containing both light and heavy chains from the F26 series demonstrates the specificity of the antibody-antigen interaction and the need for the

natural pairings. Every natural pairing tested except 19H19L lead to production of an antibody that bound S protein. 10H9L and 9H10L were the only chain-mixed constructs that produced S protein-binding antibody. One can also infer from the negative results for the swapped constructs (i.e. 9H18L, 10H18L, 19H18L, and 18H19L) that the heavy chain alone is insufficient for antigen binding. In other words, contact regions on both the heavy and light chains are required for the antibody-antigen interaction. Again, the x-ray crystal structure of G19:rACE2BDS supports this notion, since it was seen that both heavy and kappa chains interact with S protein.

By returning to the variable region sequences (Figure 1.1) a rational explanation can be formed for these results. Looking closely at the sequences, it can be seen that even though the same V_H germline gene is used, different D and J_H genes are used, leading to variability in the CDR3 region amongst the antibodies. For the vast majority of antibodies, the CDR3 region is the predominate part involved in antibody-antigen binding. Therefore despite the similarity amongst the heavy chains in the CDR1 and CDR2 regions, the variability in CDR3 has greater significance in this case. The 9H and 10H heavy chains are interchangeable since they contain the same D and J_H germline genes, thereby making similar CDR3 regions in these antibodies. The combination of the heavy chain CDR3 with regions on the light chain is therefore necessary for this series of antibodies to bind S protein.

Unlike the rest of the natural pairs, 19H19L does not bind S protein despite both heavy and light chains clearly being expressed. Sequencing of the clones was performed in order to ensure that mutations (such as a stop codon) were not introduced through the cloning process. Three possible explanations could account for the lack of binding

ability. One reason could be that a posttranslational modification such as glycosylation occurring in the variable region is not being properly added in the transfection cell system. It is also known that culture conditions can effect the glycosylation patterns of antibodies.[139] The other major reason could be that even though the antibody molecule forms, a slight difference in sterics due to slight misfolding could lead to abrogation of binding. Despite the fact that 293T and murine hybridomas are both mammalian cells, differences in expression levels of glycosylation enzymes and chaperone proteins between the human and murine cells could exist, leading to either of these two difficulties.

4.4 Chimeric mAb Production

In order to perform affinity and neutralisation analysis on the chimeric mAbs, a protocol needed to be developed in order to produce larger amounts of antibody. Two major options existed: either large scale transient transfection or the development of a cell line stably expressing the antibody genes. Large-scale transient transfection was chosen since screening of the product was still the desired outcome, and stable expression would require a lot of time and energy put into a construct that may not pass the affinity and neutralisation screening assays. Therefore a protocol was desired to rapidly produce and purify antibody produced by a large-scale transfection.

The first transfection system assessed was an adherent cell culture system. 293 and 293T cells are standard human mammalian cells that are easily transfectable. Derived from adenovirus transformed human epithelial kidney cells, they are well

characterised and commonly used in laboratories. 293T cells differ from regular 293 cells in that they stably express the large T antigen from SV40. This allows for episomal replication of a plasmid that contains the SV40 origin of replication. Therefore 293T cells transfected with a plasmid that has a SV40ori will replicate the plasmid, leading to higher expression of the transfected gene. This accounts for the superior performance of the pIGG vector in 293T over 293 cells, since pIGG has a SV40ori.

The presence of serum also increases the production of antibody, especially in the 293 cells. This result is expected since serum deprivation places stress on the cells leading to lower protein synthesis overall. In addition, serum deprivation led to a greater degree of cell detachment and death. However, serum-free conditions are necessary since the presence of bovine antibody in the serum causes impurities in the purification process. A more reliable serum-free system needed to be developed.

Two options were pursued in this regard, both serum-free suspension cell systems. In the first case, the FreeStyle™ 293F Cell System developed by Invitrogen was used. This system uses a defined serum-free medium to grow a clonal line of 293 cells called 293F. 293F is adapted to the serum-free conditions and produces high levels of protein when transfected. The second system was developed by adapting 293T cells to suspension serum-free growth, called s293T. Using CD293 media, the 293T cells were gradually adapted to the suspension serum-free growth. Due to interference of transfection reagents with CD293 media (according to the Invitrogen product information), the s293T cells were then adapted to the FreeStyle™ 293 medium.

The rationale for proceeding with the second option was that the 293F cells do not contain the large T antigen from SV40. Therefore if the 293T cell type could be adapted

to the serum-free conditions, this cell type could potentially be superior to the 293F cells for this particular plasmid. However, any gain in production achieved by having the large T antigen seemed to be counteracted by the fact that 293F cells still grow to a higher cell density without clustering in the FreeStyle™ 293 medium and probably are easier to transfect. One clear example of this is that the 293T cells tend to form clusters, while 293F cells grew as individual cells. The transfection reagent used, 293fectin™, works better for single cells versus clusters (Invitrogen, Product Info Sheet). Therefore it was decided that the 293F cell system would be used, due to ease of working with this cell type and the ability to grow the cells at a higher density without aggregation.

Once the cell type was chosen, a protocol needed to be developed to purify the antibody from the supernatant. Searching literature on purification protocols allowed me to choose three different approaches to attempt. The first protocol was developed by Rader et al, and was used to purify chimeric antibodies that were created using pIGG. In this protocol, a protein A column was used, with binding at pH 7.4 and elution at pH 3.0. The second protocol was the commercially available binding (pH 5.0) and elution (pH 2.8) buffers from Pierce that were used to purify the murine antibodies on a protein G column. A textbook on antibody purification provided the last protocol, with binding at pH 5.0 and elution at pH 2.5.

By making one large batch of 18H18L supernatant and splitting it into three, the protocols could be compared relative to each other. While both the Rader and Pierce protocols purified out similar levels of antibody, the third protocol failed to produce a significant quantity. When the purified antibody was tested in SDS-PAGE, however, it could be seen that the Rader protocol is superior in terms of actually purifying the

antibody, creating the distinct two band format for the heavy (~70kDa) and light (~32kDa) chains respectively. This protocol was then used to purify the reminder of the antibodies.

4.5 Chimeric mAb Properties: Comparison to Murine mAbs

In order to compare the characteristics of the chimeric antibodies, all the testing done on the murine versions were completed on the chimerics. While the ELISA screening performed ensured that the antibodies that were scaled-up bound S protein, it did not demonstrate where on S protein the interaction took place. An ELISA was setup similar to that performed for the murine mAbs to determine if the chimerics bound the RBD. Like the murine results, chimeric mAbs 9H9L, 10H10L, 9H10L, and 18H18L bound to the rACE2BDS protein. However, binding in the simple ELISA was hard to determine for some antibodies; for example, 10H9L looks like it does not bind rACE2BDS but could be binding rdgACE2BDS. This is where the competitive ELISA becomes significant in sorting out the false negatives. If 10H9L truly does bind in the RBD, even small amounts of rdgACE2BDS should inhibit its binding to the full-length version. This plays itself out, as binding of each of the five chimeric antibodies (9H9L, 10H9L, 9H10L, 10H10L, 18H18L) to full length S protein is inhibited by ACE2BDS, demonstrating that all bind in the RBD.

Since the only neutralising murine antibody that bound in western immunoblot to S protein was G18, blotting was performed only on the 18H18L chimeric. The results

demonstrate that 18H18L retains the ability to bind both full length S protein and rACE2BDS.

Upon purification of the antibodies, 9H9L, 10H10L, and 18H18L demonstrated high expression and were able to be purified in large enough amounts to obtain antibody for both affinity and neutralisation assays. 9H10L, however, yielded only enough antibody to perform affinity assay on, while 10H9L produced unquantifiable amounts. Since 10H9L could not be quantified, even affinity analysis could not be undertaken since concentration is a key variable to enter in to the calculation of the kinetic constants. This low concentration of antibody produced by the chain switched constructs was consistent upon repetition (data not shown), suggesting that incompatibility exists between these two chains. This could be due to the fact that there exists some small amino acid variation between G9 and G10 in both V_H and V_L, and these may be needed in order to have proper folding of the chains with each other.

The anti-SARS-CoV chimeric antibodies have essentially identical affinities to the parental murine ones. As can be seen in Table 4.1, the difference between G18 and 18H18L is not considered statistically significant ($p=0.2020$, unpaired non-parametric Mann-Whitney test). The affinity of 10H10L seems to be slightly greater than that of G10 ($p=0.0481$, unpaired t-test, Welch-corrected) but since the p value is so close to $p=0.05$, this result may not be significant realistically. Likewise, 9H10L is on the cusp of $p=0.05$ when comparing it to G9 ($p=0.0497$), while it is clearly not significant compared to G10 ($p=0.3544$). With the comparison of G9 and 9H9L, however, the results become clearly significant ($p=0.0030$) that 9H9L has a greater affinity than G9.

It was expected that the chimeric antibodies overall have a similar K_D value to the parental murine ones. Interestingly, however, is that fact that there seems to be a general trend for the affinity to increase upon chimerisation. With G9 to 9H9L this difference becomes significant. It is hard to form a hypothesis as to why this tendency seems to be occurring. A variety of factors such as small differences in folding could be at play. As well, any hypothesis would likely not be generalisable to all Abs, since the chimerisation process is empirical and dependent largely on the individual antibody involved.

	K_D (nM) Mean (95%CI)	Unpaired t-test (p-value)	Neutralising Titre (ug/ml)[a]
G18	1.79(±0.50)		0.31
18H18L	1.28(±0.78)	0.2020 (to G18)	0.37
G9	10.2(±3.5)		n.d.
9H9L	2.69(±0.50)	0.0030 (to G9)	n.d.
G10	7.5(±2.7)		n.d.
10H10L	3.62(±1.46)	0.0481 (to G10)	n.d.
9H10L	5.23(±2.05)	0.0497 (to G9)	n.d.
		0.3544 (to G10)	

Table 4.1: Comparison of Affinities and Neutralising Titres between Murine and Chimeric Antibodies. [a]Not determined for this project.

Looking again at Table 4.1, it can be seen that G18 and 18H18L have a similar neutralising titre. This demonstrates that the chimerisation process was successful, since the functionally of the murine mAb to neutralise SARS-CoV was maintained.

Since G18 could be mapped by pin and soluble peptides to the aa460-476, the same approach was used to map the human 18H18L epitope. Unfortunately, multiple attempts at mapping using pins failed, with a signal identical to background. This actually is a common problem experienced in our lab when attempt to pin peptide map human antibodies and sera (Berry JD, personal experience). Use of the soluble peptides

also failed to achieve a signal when used in a simple ELISA. However, when the competitive ELISA was performed 18H18L binding to rFS was inhibited in a dose-dependent fashion by the G18PEP. G18PEPScr did not interfere with binding. Therefore 18H18L binds the same epitope that the parental G18 antibody does.

As well, this epitope is unique when compared to other potential therapeutic antibodies for SARS-CoV in development. For example, 80R contacts on 29 residues in the aa426-492 region[116], while m396 (aa482-491)[117] and MAb201 (aa490-510)[119] epitopes both lay further upstream of the 18H18L binding site.

4.6 Path Forward

Characterisation work on the murine and chimeric mAbs continues. Besides its location in the RBD, little is known about the epitope that G9 and G10 bind, and whether or not it is the exact same epitope that is being bound for both antibodies. Since the epitope seems to be conformational, different approaches need to be used. For example, since G9 and G10 can both bind the deglycosylated version of ACE2BDS protein, mass spectrometry is a potential approach. Another possibility is the use of x-ray crystallography. Our collaborator at the University of Toronto, James Rini, has successfully crystallised G19 with dgrACE2BDS, suggested that it may be possible with G9 and G10. Although they are powerful tools both mass spectrometry and x-ray crystallography are time-consuming and expensive. This type of analysis was beyond the scope of this project.

Another important experiment that could be performed with both the murine and chimeric mAbs is to test their neutralisation profiles to various strains of SARS-CoV to determine if these are 'broad-spectrum' binders. In order to accomplish this, strains for the early, middle, and late stages of the epidemic would need to be obtained. Therefore this makes this experiment a little more difficult to do on a practical basis. Another possibility is the testing of the mAbs on virus strains that have been created in laboratory settings by repeated passaging. Anton Andonov has started to do some work in this regard concerning the murine mAbs.

18H18L retains the epitope, affinity, and high neutralising capability of G18. Therefore the next logical step in order to develop 18H18L into a therapeutic product would be to characterise the ability of both G18 and 18H18L to inhibit virus replication in an animal model. Although there is considerable debate over what constitutes a good animal model for SARS-CoV, work done in ferrets and old mice tends to mimic the pathogenesis in humans the most. Therefore a challenge of virus pre- and post- antibody injection in one of these models would a significant step forward.

4.7 Conclusion

Neutralising chimeric monoclonal antibodies specific for the S protein of SARS-CoV have been developed and characterised. Based on the characterisation, these antibodies are essentially identical in terms of their epitope and affinity to the parental murine versions. Neutralisation experiments performed on G18 and 18H18L demonstrate that the high titre is maintained. In order to perform this comparison,

extensive characterisation was also carried out the murine antibodies themselves. The chimeric antibody 18H18L could be effective as a therapeutic agent. Although some neutralising antibodies already exist for SARS-CoV that could be used therapeutically, a combination 'cocktail' approach would be more effective in light of the ability of RNA viruses to mutate and create quasi-species. Since 18H18L binds a novel sequence, it could be combined with other antibodies (i.e. 80R, or even some of the other chimerics of the F26 series that were produced) to produce an additive or even synergetic effect.

5 References

1. Zhao GP. SARS molecular epidemiology: A chinese fairy tale of controlling an emerging zoonotic disease in the genomics era. Philos Trans R Soc Lond B Biol Sci 2007 Jun 29;362(1482):1063-81.

2. Peiris JS, Yuen KY, Osterhaus AD, Stohr K. The severe acute respiratory syndrome. N Engl J Med 2003 Dec 18;349(25):2431-41.

3. Poon LL, Guan Y, Nicholls JM, Yuen KY, Peiris JS. The aetiology, origins, and diagnosis of severe acute respiratory syndrome. Lancet Infect Dis 2004 Nov;4(11):663-71.

4. Poutanen SM, Low DE, Henry B, Finkelstein S, Rose D, Green K, Tellier R, Draker R, Adachi D, Ayers M, Chan AK, Skowronski DM, Salit I, Simor AE, Slutsky AS, Doyle PW, Krajden M, Petric M, Brunham RC, McGeer AJ, National Microbiology Laboratory, Canada, Canadian Severe Acute Respiratory Syndrome Study Team. Identification of severe acute respiratory syndrome in canada. N Engl J Med 2003 May 15;348(20):1995-2005.

5. Drosten C, Gunther S, Preiser W, van der Werf S, Brodt HR, Becker S, Rabenau H, Panning M, Kolesnikova L, Fouchier RA, Berger A, Burguiere AM, Cinatl J, Eickmann M, Escriou N, Grywna K, Kramme S, Manuguerra JC, Muller S, Rickerts V, Sturmer M, Vieth S, Klenk HD, Osterhaus AD, Schmitz H, Doerr HW. Identification of a novel coronavirus in patients with severe acute respiratory syndrome. N Engl J Med 2003 May 15;348(20):1967-76.

6. Ksiazek TG, Erdman D, Goldsmith CS, Zaki SR, Peret T, Emery S, Tong S, Urbani C, Comer JA, Lim W, Rollin PE, Dowell SF, Ling AE, Humphrey CD, Shieh WJ, Guarner J, Paddock CD, Rota P, Fields B, DeRisi J, Yang JY, Cox N, Hughes JM, LeDuc JW, Bellini WJ, Anderson LJ, SARS Working Group. A novel coronavirus associated with severe acute respiratory syndrome. N Engl J Med 2003 May 15;348(20):1953-66.

7. Marra MA, Jones SJ, Astell CR, Holt RA, Brooks-Wilson A, Butterfield YS, Khattra J, Asano JK, Barber SA, Chan SY, Cloutier A, Coughlin SM, Freeman D, Girn N, Griffith OL, Leach SR, Mayo M, McDonald H, Montgomery SB, Pandoh PK, Petrescu AS, Robertson AG, Schein JE, Siddiqui A, Smailus DE, Stott JM, Yang GS, Plummer F, Andonov A, Artsob H, Bastien N, Bernard K, Booth TF, Bowness

D, Czub M, Drebot M, Fernando L, Flick R, Garbutt M, Gray M, Grolla A, Jones S, Feldmann H, Meyers A, Kabani A, Li Y, Normand S, Stroher U, Tipples GA, Tyler S, Vogrig R, Ward D, Watson B, Brunham RC, Krajden M, Petric M, Skowronski DM, Upton C, Roper RL. The genome sequence of the SARS-associated coronavirus. Science 2003 May 30;300(5624):1399-404.

8. Rota PA, Oberste MS, Monroe SS, Nix WA, Campagnoli R, Icenogle JP, Penaranda S, Bankamp B, Maher K, Chen MH, Tong S, Tamin A, Lowe L, Frace M, DeRisi JL, Chen Q, Wang D, Erdman DD, Peret TC, Burns C, Ksiazek TG, Rollin PE, Sanchez A, Liffick S, Holloway B, Limor J, McCaustland K, Olsen-Rasmussen M, Fouchier R, Gunther S, Osterhaus AD, Drosten C, Pallansch MA, Anderson LJ, Bellini WJ. Characterization of a novel coronavirus associated with severe acute respiratory syndrome. Science 2003 May 30;300(5624):1394-9.

9. Peiris JS, Chu CM, Cheng VC, Chan KS, Hung IF, Poon LL, Law KI, Tang BS, Hon TY, Chan CS, Chan KH, Ng JS, Zheng BJ, Ng WL, Lai RW, Guan Y, Yuen KY, HKU/UCH SARS Study Group. Clinical progression and viral load in a community outbreak of coronavirus-associated SARS pneumonia: A prospective study. Lancet 2003 May 24;361(9371):1767-72.

10. Ketai L, Paul NS, Wong KT. Radiology of severe acute respiratory syndrome (SARS): The emerging pathologic-radiologic correlates of an emerging disease. J Thorac Imaging 2006 Nov;21(4):276-83.

11. Chen J, Subbarao K. The immunobiology of SARS*. Annu Rev Immunol 2007;25:443-72.

12. Gu J, Korteweg C. Pathology and pathogenesis of severe acute respiratory syndrome. Am J Pathol 2007 Apr;170(4):1136-47.

13. Donnelly CA, Ghani AC, Leung GM, Hedley AJ, Fraser C, Riley S, Abu-Raddad LJ, Ho LM, Thach TQ, Chau P, Chan KP, Lam TH, Tse LY, Tsang T, Liu SH, Kong JH, Lau EM, Ferguson NM, Anderson RM. Epidemiological determinants of spread of causal agent of severe acute respiratory syndrome in hong kong. Lancet 2003 May 24;361(9371):1761-6.

14. Herridge MS, Cheung AM, Tansey CM, Matte-Martyn A, Diaz-Granados N, Al-Saidi F, Cooper AB, Guest CB, Mazer CD, Mehta S, Stewart TE, Barr A, Cook D, Slutsky AS, Canadian Critical Care Trials Group. One-year outcomes in survivors of

the acute respiratory distress syndrome. N Engl J Med 2003 Feb 20;348(8):683-93.

15. Tansey CM, Louie M, Loeb M, Gold WL, Muller MP, de Jager J, Cameron JI, Tomlinson G, Mazzulli T, Walmsley SL, Rachlis AR, Mederski BD, Silverman M, Shainhouse Z, Ephtimios IE, Avendano M, Downey J, Styra R, Yamamura D, Gerson M, Stanbrook MB, Marras TK, Phillips EJ, Zamel N, Richardson SE, Slutsky AS, Herridge MS. One-year outcomes and health care utilization in survivors of severe acute respiratory syndrome. Arch Intern Med 2007 Jun 25;167(12):1312-20.

16. Lai MM, Perlman S, Anderson LJ. Coronaviridae. In: D. M. Knipe, P. M. Howley, D. E. Griffin, et al, editors. Fields virology. 5th ed ed. Lippincott Williams & Wilkins; 2007. .

17. Stadler K, Masignani V, Eickmann M, Becker S, Abrignani S, Klenk HD, Rappuoli R. SARS--beginning to understand a new virus. Nat Rev Microbiol 2003 Dec;1(3):209-18.

18. Perlman S, Dandekar AA. Immunopathogenesis of coronavirus infections: Implications for SARS. Nat Rev Immunol 2005 Dec;5(12):917-27.

19. Satija N, Lal SK. The molecular biology of SARS coronavirus. Ann N Y Acad Sci 2007 Apr;1102:26-38.

20. Connor RF, Roper RL. Unique SARS-CoV protein nsp1: Bioinformatics, biochemistry and potential effects on virulence. Trends Microbiol 2007 Feb;15(2):51-3.

21. Yeung KS, Meanwell NA. Recent developments in the virology and antiviral research of severe acute respiratory syndrome coronavirus. Infect Disord Drug Targets 2007 Mar;7(1):29-41.

22. Imbert I, Guillemot JC, Bourhis JM, Bussetta C, Coutard B, Egloff MP, Ferron F, Gorbalenya AE, Canard B. A second, non-canonical RNA-dependent RNA polymerase in SARS coronavirus. EMBO J 2006 Oct 18;25(20):4933-42.

23. Nal B, Chan C, Kien F, Siu L, Tse J, Chu K, Kam J, Staropoli I, Crescenzo-Chaigne B, Escriou N, van der Werf S, Yuen KY, Altmeyer R. Differential maturation and subcellular localization of severe acute respiratory syndrome coronavirus surface

proteins S, M and E. J Gen Virol 2005 May;86(Pt 5):1423-34.

24. Li F, Li W, Farzan M, Harrison SC. Structure of SARS coronavirus spike receptor-binding domain complexed with receptor. Science 2005 Sep 16;309(5742):1864-8.

25. Liu S, Xiao G, Chen Y, He Y, Niu J, Escalante CR, Xiong H, Farmar J, Debnath AK, Tien P, Jiang S. Interaction between heptad repeat 1 and 2 regions in spike protein of SARS-associated coronavirus: Implications for virus fusogenic mechanism and identification of fusion inhibitors. Lancet 2004 Mar 20;363(9413):938-47.

26. Li W, Moore MJ, Vasilieva N, Sui J, Wong SK, Berne MA, Somasundaran M, Sullivan JL, Luzuriaga K, Greenough TC, Choe H, Farzan M. Angiotensin-converting enzyme 2 is a functional receptor for the SARS coronavirus. Nature 2003 Nov 27;426(6965):450-4.

27. Jeffers SA, Tusell SM, Gillim-Ross L, Hemmila EM, Achenbach JE, Babcock GJ, Thomas WD,Jr, Thackray LB, Young MD, Mason RJ, Ambrosino DM, Wentworth DE, Demartini JC, Holmes KV. CD209L (L-SIGN) is a receptor for severe acute respiratory syndrome coronavirus. Proc Natl Acad Sci U S A 2004 Nov 2;101(44):15748-53.

28. Yang ZY, Huang Y, Ganesh L, Leung K, Kong WP, Schwartz O, Subbarao K, Nabel GJ. pH-dependent entry of severe acute respiratory syndrome coronavirus is mediated by the spike glycoprotein and enhanced by dendritic cell transfer through DC-SIGN. J Virol 2004 Jun;78(11):5642-50.

29. Wilson L, McKinlay C, Gage P, Ewart G. SARS coronavirus E protein forms cation-selective ion channels. Virology 2004 Dec 5;330(1):322-31.

30. Oostra M, de Haan CA, de Groot RJ, Rottier PJ. Glycosylation of the severe acute respiratory syndrome coronavirus triple-spanning membrane proteins 3a and M. J Virol 2006 Mar;80(5):2326-36.

31. de Haan CA, Rottier PJ. Molecular interactions in the assembly of coronaviruses. Adv Virus Res 2005;64:165-230.

32. Yount B, Roberts RS, Sims AC, Deming D, Frieman MB, Sparks J, Denison MR, Davis N, Baric RS. Severe acute respiratory syndrome coronavirus group-specific

open reading frames encode nonessential functions for replication in cell cultures and mice. J Virol 2005 Dec;79(23):14909-22.

33. Tan YJ, Lim SG, Hong W. Understanding the accessory viral proteins unique to the severe acute respiratory syndrome (SARS) coronavirus. Antiviral Res 2006 Nov;72(2):78-88.

34. Shen S, Lin PS, Chao YC, Zhang A, Yang X, Lim SG, Hong W, Tan YJ. The severe acute respiratory syndrome coronavirus 3a is a novel structural protein. Biochem Biophys Res Commun 2005 Apr 29;330(1):286-92.

35. Tan YJ. The severe acute respiratory syndrome (SARS)-coronavirus 3a protein may function as a modulator of the trafficking properties of the spike protein. Virol J 2005 Feb 10;2:5.

36. Khan S, Ng ML, Tan YJ. Expression of the severe acute respiratory syndrome coronavirus 3a protein and the assembly of coronavirus-like particles in the baculovirus expression system. Methods Mol Biol 2007;379:35-50.

37. Yuan X, Yao Z, Shan Y, Chen B, Yang Z, Wu J, Zhao Z, Chen J, Cong Y. Nucleolar localization of non-structural protein 3b, a protein specifically encoded by the severe acute respiratory syndrome coronavirus. Virus Res 2005 Dec;114(1-2):70-9.

38. Yuan X, Shan Y, Zhao Z, Chen J, Cong Y. G0/G1 arrest and apoptosis induced by SARS-CoV 3b protein in transfected cells. Virol J 2005 Aug 17;2:66.

39. Pewe L, Zhou H, Netland J, Tangadu C, Olivares H, Shi L, Look D, Gallagher T, Perlman S. A SARS-CoV-specific protein enhances virulence of an attenuated strain of mouse hepatitis virus. Adv Exp Med Biol 2006;581:493-8.

40. Yuan X, Wu J, Shan Y, Yao Z, Dong B, Chen B, Zhao Z, Wang S, Chen J, Cong Y. SARS coronavirus 7a protein blocks cell cycle progression at G0/G1 phase via the cyclin D3/pRb pathway. Virology 2006 Mar 1;346(1):74-85.

41. Simmons G, Gosalia DN, Rennekamp AJ, Reeves JD, Diamond SL, Bates P. Inhibitors of cathepsin L prevent severe acute respiratory syndrome coronavirus entry. Proc Natl Acad Sci U S A 2005 Aug 16;102(33):11876-81.

42. Hofmann H, Pohlmann S. Cellular entry of the SARS coronavirus. Trends Microbiol 2004 Oct;12(10):466-72.

43. Graham RL, Sims AC, Brockway SM, Baric RS, Denison MR. The nsp2 replicase proteins of murine hepatitis virus and severe acute respiratory syndrome coronavirus are dispensable for viral replication. J Virol 2005 Nov;79(21):13399-411.

44. Hsieh PK, Chang SC, Huang CC, Lee TT, Hsiao CW, Kou YH, Chen IY, Chang CK, Huang TH, Chang MF. Assembly of severe acute respiratory syndrome coronavirus RNA packaging signal into virus-like particles is nucleocapsid dependent. J Virol 2005 Nov;79(22):13848-55.

45. Hamming I, Timens W, Bulthuis ML, Lely AT, Navis GJ, van Goor H. Tissue distribution of ACE2 protein, the functional receptor for SARS coronavirus. A first step in understanding SARS pathogenesis. J Pathol 2004 Jun;203(2):631-7.

46. Sims AC, Baric RS, Yount B, Burkett SE, Collins PL, Pickles RJ. Severe acute respiratory syndrome coronavirus infection of human ciliated airway epithelia: Role of ciliated cells in viral spread in the conducting airways of the lungs. J Virol 2005 Dec;79(24):15511-24.

47. Ding Y, He L, Zhang Q, Huang Z, Che X, Hou J, Wang H, Shen H, Qiu L, Li Z, Geng J, Cai J, Han H, Li X, Kang W, Weng D, Liang P, Jiang S. Organ distribution of severe acute respiratory syndrome (SARS) associated coronavirus (SARS-CoV) in SARS patients: Implications for pathogenesis and virus transmission pathways. J Pathol 2004 Jun;203(2):622-30.

48. Leung WK, To KF, Chan PK, Chan HL, Wu AK, Lee N, Yuen KY, Sung JJ. Enteric involvement of severe acute respiratory syndrome-associated coronavirus infection. Gastroenterology 2003 Oct;125(4):1011-7.

49. Li L, Wo J, Shao J, Zhu H, Wu N, Li M, Yao H, Hu M, Dennin RH. SARS-coronavirus replicates in mononuclear cells of peripheral blood (PBMCs) from SARS patients. J Clin Virol 2003 Dec;28(3):239-44.

50. Law HK, Cheung CY, Ng HY, Sia SF, Chan YO, Luk W, Nicholls JM, Peiris JS, Lau YL. Chemokine up-regulation in SARS-coronavirus-infected, monocyte-derived human dendritic cells. Blood 2005 Oct 1;106(7):2366-74.

51. Chen JH, Chang YW, Yao CW, Chiueh TS, Huang SC, Chien KY, Chen A, Chang FY, Wong CH, Chen YJ. Plasma proteome of severe acute respiratory syndrome analyzed by two-dimensional gel electrophoresis and mass spectrometry. Proc Natl Acad Sci U S A 2004 Dec 7;101(49):17039-44.

52. Zhang H, Zhou G, Zhi L, Yang H, Zhai Y, Dong X, Zhang X, Gao X, Zhu Y, He F. Association between mannose-binding lectin gene polymorphisms and susceptibility to severe acute respiratory syndrome coronavirus infection. J Infect Dis 2005 Oct 15;192(8):1355-61.

53. Jiang Y, Xu J, Zhou C, Wu Z, Zhong S, Liu J, Luo W, Chen T, Qin Q, Deng P. Characterization of cytokine/chemokine profiles of severe acute respiratory syndrome. Am J Respir Crit Care Med 2005 Apr 15;171(8):850-7.

54. Wong CK, Lam CW, Wu AK, Ip WK, Lee NL, Chan IH, Lit LC, Hui DS, Chan MH, Chung SS, Sung JJ. Plasma inflammatory cytokines and chemokines in severe acute respiratory syndrome. Clin Exp Immunol 2004 Apr;136(1):95-103.

55. Huang KJ, Su IJ, Theron M, Wu YC, Lai SK, Liu CC, Lei HY. An interferon-gamma-related cytokine storm in SARS patients. J Med Virol 2005 Feb;75(2):185-94.

56. Zhang Y, Li J, Zhan Y, Wu L, Yu X, Zhang W, Ye L, Xu S, Sun R, Wang Y, Lou J. Analysis of serum cytokines in patients with severe acute respiratory syndrome. Infect Immun 2004 Aug;72(8):4410-5.

57. Lee CH, Chen RF, Liu JW, Yeh WT, Chang JC, Liu PM, Eng HL, Lin MC, Yang KD. Altered p38 mitogen-activated protein kinase expression in different leukocytes with increment of immunosuppressive mediators in patients with severe acute respiratory syndrome. J Immunol 2004 Jun 15;172(12):7841-7.

58. Cheung CY, Poon LL, Ng IH, Luk W, Sia SF, Wu MH, Chan KH, Yuen KY, Gordon S, Guan Y, Peiris JS. Cytokine responses in severe acute respiratory syndrome coronavirus-infected macrophages in vitro: Possible relevance to pathogenesis. J Virol 2005 Jun;79(12):7819-26.

59. Tseng CT, Perrone LA, Zhu H, Makino S, Peters CJ. Severe acute respiratory syndrome and the innate immune responses: Modulation of effector cell function without productive infection. J Immunol 2005 Jun 15;174(12):7977-85.

60. Wang YD, Sin WY, Xu GB, Yang HH, Wong TY, Pang XW, He XY, Zhang HG, Ng JN, Cheng CS, Yu J, Meng L, Yang RF, Lai ST, Guo ZH, Xie Y, Chen WF. T-cell epitopes in severe acute respiratory syndrome (SARS) coronavirus spike protein elicit a specific T-cell immune response in patients who recover from SARS. J Virol 2004 Jun;78(11):5612-8.

61. Yang LT, Peng H, Zhu ZL, Li G, Huang ZT, Zhao ZX, Koup RA, Bailer RT, Wu CY. Long-lived effector/central memory T-cell responses to severe acute respiratory syndrome coronavirus (SARS-CoV) S antigen in recovered SARS patients. Clin Immunol 2006 Aug;120(2):171-8.

62. Chen H, Hou J, Jiang X, Ma S, Meng M, Wang B, Zhang M, Zhang M, Tang X, Zhang F, Wan T, Li N, Yu Y, Hu H, Yang R, He W, Wang X, Cao X. Response of memory CD8+ T cells to severe acute respiratory syndrome (SARS) coronavirus in recovered SARS patients and healthy individuals. J Immunol 2005 Jul 1;175(1):591-8.

63. Glass WG, Subbarao K, Murphy B, Murphy PM. Mechanisms of host defense following severe acute respiratory syndrome-coronavirus (SARS-CoV) pulmonary infection of mice. J Immunol 2004 Sep 15;173(6):4030-9.

64. Hsueh PR, Huang LM, Chen PJ, Kao CL, Yang PC. Chronological evolution of IgM, IgA, IgG and neutralisation antibodies after infection with SARS-associated coronavirus. Clin Microbiol Infect 2004 Dec;10(12):1062-6.

65. Liu W, Fontanet A, Zhang PH, Zhan L, Xin ZT, Baril L, Tang F, Lv H, Cao WC. Two-year prospective study of the humoral immune response of patients with severe acute respiratory syndrome. J Infect Dis 2006 Mar 15;193(6):792-5.

66. Buchholz UJ, Bukreyev A, Yang L, Lamirande EW, Murphy BR, Subbarao K, Collins PL. Contributions of the structural proteins of severe acute respiratory syndrome coronavirus to protective immunity. Proc Natl Acad Sci U S A 2004 Jun 29;101(26):9804-9.

67. Akerstrom S, Tan YJ, Mirazimi A. Amino acids 15-28 in the ectodomain of SARS coronavirus 3a protein induces neutralizing antibodies. FEBS Lett 2006 Jul 10;580(16):3799-803.

68. Lu L, Manopo I, Leung BP, Chng HH, Ling AE, Chee LL, Ooi EE, Chan SW, Kwang J. Immunological characterization of the spike protein of the severe acute

respiratory syndrome coronavirus. J Clin Microbiol 2004 Apr;42(4):1570-6.

69. Law PT, Wong CH, Au TC, Chuck CP, Kong SK, Chan PK, To KF, Lo AW, Chan JY, Suen YK, Chan HY, Fung KP, Waye MM, Sung JJ, Lo YM, Tsui SK. The 3a protein of severe acute respiratory syndrome-associated coronavirus induces apoptosis in vero E6 cells. J Gen Virol 2005 Jul;86(Pt 7):1921-30.

70. Tan YJ, Fielding BC, Goh PY, Shen S, Tan TH, Lim SG, Hong W. Overexpression of 7a, a protein specifically encoded by the severe acute respiratory syndrome coronavirus, induces apoptosis via a caspase-dependent pathway. J Virol 2004 Dec;78(24):14043-7.

71. Kopecky-Bromberg SA, Martinez-Sobrido L, Palese P. 7a protein of severe acute respiratory syndrome coronavirus inhibits cellular protein synthesis and activates P38 mitogen-activated protein kinase. J Virol 2006 Jan;80(2):785-93.

72. Spiegel M, Pichlmair A, Martinez-Sobrido L, Cros J, Garcia-Sastre A, Haller O, Weber F. Inhibition of beta interferon induction by severe acute respiratory syndrome coronavirus suggests a two-step model for activation of interferon regulatory factor 3. J Virol 2005 Feb;79(4):2079-86.

73. Imai Y, Kuba K, Rao S, Huan Y, Guo F, Guan B, Yang P, Sarao R, Wada T, Leong-Poi H, Crackower MA, Fukamizu A, Hui CC, Hein L, Uhlig S, Slutsky AS, Jiang C, Penninger JM. Angiotensin-converting enzyme 2 protects from severe acute lung failure. Nature 2005 Jul 7;436(7047):112-6.

74. Kuba K, Imai Y, Rao S, Gao H, Guo F, Guan B, Huan Y, Yang P, Zhang Y, Deng W, Bao L, Zhang B, Liu G, Wang Z, Chappell M, Liu Y, Zheng D, Leibbrandt A, Wada T, Slutsky AS, Liu D, Qin C, Jiang C, Penninger JM. A crucial role of angiotensin converting enzyme 2 (ACE2) in SARS coronavirus-induced lung injury. Nat Med 2005 Aug;11(8):875-9.

75. Hofmann H, Pyrc K, van der Hoek L, Geier M, Berkhout B, Pohlmann S. Human coronavirus NL63 employs the severe acute respiratory syndrome coronavirus receptor for cellular entry. Proc Natl Acad Sci U S A 2005 May 31;102(22):7988-93.

76. Gillim-Ross L, Subbarao K. Emerging respiratory viruses: Challenges and vaccine strategies. Clin Microbiol Rev 2006 Oct;19(4):614-36.

77. Subbarao K, McAuliffe J, Vogel L, Fahle G, Fischer S, Tatti K, Packard M, Shieh WJ, Zaki S, Murphy B. Prior infection and passive transfer of neutralizing antibody prevent replication of severe acute respiratory syndrome coronavirus in the respiratory tract of mice. J Virol 2004 Apr;78(7):3572-7.

78. Zhong NS, Zheng BJ, Li YM, Poon, Xie ZH, Chan KH, Li PH, Tan SY, Chang Q, Xie JP, Liu XQ, Xu J, Li DX, Yuen KY, Peiris, Guan Y. Epidemiology and cause of severe acute respiratory syndrome (SARS) in guangdong, people's republic of china, in february, 2003. Lancet 2003 Oct 25;362(9393):1353-8.

79. Guan Y, Zheng BJ, He YQ, Liu XL, Zhuang ZX, Cheung CL, Luo SW, Li PH, Zhang LJ, Guan YJ, Butt KM, Wong KL, Chan KW, Lim W, Shortridge KF, Yuen KY, Peiris JS, Poon LL. Isolation and characterization of viruses related to the SARS coronavirus from animals in southern china. Science 2003 Oct 10;302(5643):276-8.

80. Song HD, Tu CC, Zhang GW, Wang SY, Zheng K, Lei LC, Chen QX, Gao YW, Zhou HQ, Xiang H, Zheng HJ, Chern SW, Cheng F, Pan CM, Xuan H, Chen SJ, Luo HM, Zhou DH, Liu YF, He JF, Qin PZ, Li LH, Ren YQ, Liang WJ, Yu YD, Anderson L, Wang M, Xu RH, Wu XW, Zheng HY, Chen JD, Liang G, Gao Y, Liao M, Fang L, Jiang LY, Li H, Chen F, Di B, He LJ, Lin JY, Tong S, Kong X, Du L, Hao P, Tang H, Bernini A, Yu XJ, Spiga O, Guo ZM, Pan HY, He WZ, Manuguerra JC, Fontanet A, Danchin A, Niccolai N, Li YX, Wu CI, Zhao GP. Cross-host evolution of severe acute respiratory syndrome coronavirus in palm civet and human. Proc Natl Acad Sci U S A 2005 Feb 15;102(7):2430-5.

81. Tu C, Crameri G, Kong X, Chen J, Sun Y, Yu M, Xiang H, Xia X, Liu S, Ren T, Yu Y, Eaton BT, Xuan H, Wang LF. Antibodies to SARS coronavirus in civets. Emerg Infect Dis 2004 Dec;10(12):2244-8.

82. Kan B, Wang M, Jing H, Xu H, Jiang X, Yan M, Liang W, Zheng H, Wan K, Liu Q, Cui B, Xu Y, Zhang E, Wang H, Ye J, Li G, Li M, Cui Z, Qi X, Chen K, Du L, Gao K, Zhao YT, Zou XZ, Feng YJ, Gao YF, Hai R, Yu D, Guan Y, Xu J. Molecular evolution analysis and geographic investigation of severe acute respiratory syndrome coronavirus-like virus in palm civets at an animal market and on farms. J Virol 2005 Sep;79(18):11892-900.

83. Hu W, Bai B, Hu Z, Chen Z, An X, Tang L, Yang J, Wang H, Wang H. Development and evaluation of a multitarget real-time taqman reverse transcription-PCR assay for detection of the severe acute respiratory syndrome-associated coronavirus and surveillance for an apparently related coronavirus found in masked

palm civets. J Clin Microbiol 2005 May;43(5):2041-6.

84. Poon LL, Chu DK, Chan KH, Wong OK, Ellis TM, Leung YH, Lau SK, Woo PC, Suen KY, Yuen KY, Guan Y, Peiris JS. Identification of a novel coronavirus in bats. J Virol 2005 Feb;79(4):2001-9.

85. Shi Z, Hu Z. A review of studies on animal reservoirs of the SARS coronavirus. Virus Res 2007 Apr 20.

86. Li W, Shi Z, Yu M, Ren W, Smith C, Epstein JH, Wang H, Crameri G, Hu Z, Zhang H, Zhang J, McEachern J, Field H, Daszak P, Eaton BT, Zhang S, Wang LF. Bats are natural reservoirs of SARS-like coronaviruses. Science 2005 Oct 28;310(5748):676-9.

87. Lau SK, Woo PC, Li KS, Huang Y, Tsoi HW, Wong BH, Wong SS, Leung SY, Chan KH, Yuen KY. Severe acute respiratory syndrome coronavirus-like virus in chinese horseshoe bats. Proc Natl Acad Sci U S A 2005 Sep 27;102(39):14040-5.

88. Li W, Zhang C, Sui J, Kuhn JH, Moore MJ, Luo S, Wong SK, Huang IC, Xu K, Vasilieva N, Murakami A, He Y, Marasco WA, Guan Y, Choe H, Farzan M. Receptor and viral determinants of SARS-coronavirus adaptation to human ACE2. EMBO J 2005 Apr 20;24(8):1634-43.

89. Takasuka N, Fujii H, Takahashi Y, Kasai M, Morikawa S, Itamura S, Ishii K, Sakaguchi M, Ohnishi K, Ohshima M, Hashimoto S, Odagiri T, Tashiro M, Yoshikura H, Takemori T, Tsunetsugu-Yokota Y. A subcutaneously injected UV-inactivated SARS coronavirus vaccine elicits systemic humoral immunity in mice. Int Immunol 2004 Oct;16(10):1423-30.

90. Xiong S, Wang YF, Zhang MY, Liu XJ, Zhang CH, Liu SS, Qian CW, Li JX, Lu JH, Wan ZY, Zheng HY, Yan XG, Meng MJ, Fan JL. Immunogenicity of SARS inactivated vaccine in BALB/c mice. Immunol Lett 2004 Sep;95(2):139-43.

91. Zhang CH, Lu JH, Wang YF, Zheng HY, Xiong S, Zhang MY, Liu XJ, Li JX, Wan ZY, Yan XG, Qi SY, Cui Z, Zhang B. Immune responses in Balb/c mice induced by a candidate SARS-CoV inactivated vaccine prepared from F69 strain. Vaccine 2005 May 2;23(24):3196-201.

92. Tsunetsugu-Yokota Y, Ohnishi K, Takemori T. Severe acute respiratory syndrome (SARS) coronavirus: Application of monoclonal antibodies and development of an effective vaccine. Rev Med Virol 2006 Mar-Apr;16(2):117-31.

93. Bisht H, Roberts A, Vogel L, Bukreyev A, Collins PL, Murphy BR, Subbarao K, Moss B. Severe acute respiratory syndrome coronavirus spike protein expressed by attenuated vaccinia virus protectively immunizes mice. Proc Natl Acad Sci U S A 2004 Apr 27;101(17):6641-6.

94. Chen Z, Zhang L, Qin C, Ba L, Yi CE, Zhang F, Wei Q, He T, Yu W, Yu J, Gao H, Tu X, Gettie A, Farzan M, Yuen KY, Ho DD. Recombinant modified vaccinia virus ankara expressing the spike glycoprotein of severe acute respiratory syndrome coronavirus induces protective neutralizing antibodies primarily targeting the receptor binding region. J Virol 2005 Mar;79(5):2678-88.

95. Weingartl H, Czub M, Czub S, Neufeld J, Marszal P, Gren J, Smith G, Jones S, Proulx R, Deschambault Y, Grudeski E, Andonov A, He R, Li Y, Copps J, Grolla A, Dick D, Berry J, Ganske S, Manning L, Cao J. Immunization with modified vaccinia virus ankara-based recombinant vaccine against severe acute respiratory syndrome is associated with enhanced hepatitis in ferrets. J Virol 2004 Nov;78(22):12672-6.

96. Bukreyev A, Lamirande EW, Buchholz UJ, Vogel LN, Elkins WR, St Claire M, Murphy BR, Subbarao K, Collins PL. Mucosal immunisation of african green monkeys (cercopithecus aethiops) with an attenuated parainfluenza virus expressing the SARS coronavirus spike protein for the prevention of SARS. Lancet 2004 Jun 26;363(9427):2122-7.

97. Gao W, Tamin A, Soloff A, D'Aiuto L, Nwanegbo E, Robbins PD, Bellini WJ, Barratt-Boyes S, Gambotto A. Effects of a SARS-associated coronavirus vaccine in monkeys. Lancet 2003 Dec 6;362(9399):1895-6.

98. Faber M, Lamirande EW, Roberts A, Rice AB, Koprowski H, Dietzschold B, Schnell MJ. A single immunization with a rhabdovirus-based vector expressing severe acute respiratory syndrome coronavirus (SARS-CoV) S protein results in the production of high levels of SARS-CoV-neutralizing antibodies. J Gen Virol 2005 May;86(Pt 5):1435-40.

99. Kapadia SU, Rose JK, Lamirande E, Vogel L, Subbarao K, Roberts A. Long-term protection from SARS coronavirus infection conferred by a single immunization

with an attenuated VSV-based vaccine. Virology 2005 Sep 30;340(2):174-82.

100. Yang ZY, Kong WP, Huang Y, Roberts A, Murphy BR, Subbarao K, Nabel GJ. A DNA vaccine induces SARS coronavirus neutralization and protective immunity in mice. Nature 2004 Apr 1;428(6982):561-4.

101. Kim TW, Lee JH, Hung CF, Peng S, Roden R, Wang MC, Viscidi R, Tsai YC, He L, Chen PJ, Boyd DA, Wu TC. Generation and characterization of DNA vaccines targeting the nucleocapsid protein of severe acute respiratory syndrome coronavirus. J Virol 2004 May;78(9):4638-45.

102. Zhu MS, Pan Y, Chen HQ, Shen Y, Wang XC, Sun YJ, Tao KH. Induction of SARS-nucleoprotein-specific immune response by use of DNA vaccine. Immunol Lett 2004 Apr 15;92(3):237-43.

103. Zhao P, Cao J, Zhao LJ, Qin ZL, Ke JS, Pan W, Ren H, Yu JG, Qi ZT. Immune responses against SARS-coronavirus nucleocapsid protein induced by DNA vaccine. Virology 2005 Jan 5;331(1):128-35.

104. Zakhartchouk AN, Sharon C, Satkunarajah M, Auperin T, Viswanathan S, Mutwiri G, Petric M, See RH, Brunham RC, Finlay BB, Cameron C, Kelvin DJ, Cochrane A, Rini JM, Babiuk LA. Immunogenicity of a receptor-binding domain of SARS coronavirus spike protein in mice: Implications for a subunit vaccine. Vaccine 2007 Jan 2;25(1):136-43.

105. Chou CY, Chang HC, Hsu WC, Lin TZ, Lin CH, Chang GG. Quaternary structure of the severe acute respiratory syndrome (SARS) coronavirus main protease. Biochemistry 2004 Nov 30;43(47):14958-70.

106. Yang S, Chen SJ, Hsu MF, Wu JD, Tseng CT, Liu YF, Chen HC, Kuo CW, Wu CS, Chang LW, Chen WC, Liao SY, Chang TY, Hung HH, Shr HL, Liu CY, Huang YA, Chang LY, Hsu JC, Peters CJ, Wang AH, Hsu MC. Synthesis, crystal structure, structure-activity relationships, and antiviral activity of a potent SARS coronavirus 3CL protease inhibitor. J Med Chem 2006 Aug 10;49(16):4971-80.

107. Wu CY, King KY, Kuo CJ, Fang JM, Wu YT, Ho MY, Liao CL, Shie JJ, Liang PH, Wong CH. Stable benzotriazole esters as mechanism-based inactivators of the severe acute respiratory syndrome 3CL protease. Chem Biol 2006 Mar;13(3):261-8.

108. Lu IL, Mahindroo N, Liang PH, Peng YH, Kuo CJ, Tsai KC, Hsieh HP, Chao YS, Wu SY. Structure-based drug design and structural biology study of novel nonpeptide inhibitors of severe acute respiratory syndrome coronavirus main protease. J Med Chem 2006 Aug 24;49(17):5154-61.

109. Tsai KC, Chen SY, Liang PH, Lu IL, Mahindroo N, Hsieh HP, Chao YS, Liu L, Liu D, Lien W, Lin TH, Wu SY. Discovery of a novel family of SARS-CoV protease inhibitors by virtual screening and 3D-QSAR studies. J Med Chem 2006 Jun 15;49(12):3485-95.

110. Barnard DL, Day CW, Bailey K, Heiner M, Montgomery R, Lauridsen L, Winslow S, Hoopes J, Li JK, Lee J, Carson DA, Cottam HB, Sidwell RW. Enhancement of the infectivity of SARS-CoV in BALB/c mice by IMP dehydrogenase inhibitors, including ribavirin. Antiviral Res 2006 Aug;71(1):53-63.

111. Zhu Z, Dimitrov AS, Chakraborti S, Dimitrova D, Xiao X, Broder CC, Dimitrov DS. Development of human monoclonal antibodies against diseases caused by emerging and biodefense-related viruses. Expert Rev Anti Infect Ther 2006 Feb;4(1):57-66.

112. Stockman LJ, Bellamy R, Garner P. SARS: Systematic review of treatment effects. PLoS Med 2006 Sep;3(9):e343.

113. Traggiai E, Becker S, Subbarao K, Kolesnikova L, Uematsu Y, Gismondo MR, Murphy BR, Rappuoli R, Lanzavecchia A. An efficient method to make human monoclonal antibodies from memory B cells: Potent neutralization of SARS coronavirus. Nat Med 2004 Aug;10(8):871-5.

114. Sui J, Li W, Murakami A, Tamin A, Matthews LJ, Wong SK, Moore MJ, Tallarico AS, Olurinde M, Choe H, Anderson LJ, Bellini WJ, Farzan M, Marasco WA. Potent neutralization of severe acute respiratory syndrome (SARS) coronavirus by a human mAb to S1 protein that blocks receptor association. Proc Natl Acad Sci U S A 2004 Feb 24;101(8):2536-41.

115. Sui J, Li W, Roberts A, Matthews LJ, Murakami A, Vogel L, Wong SK, Subbarao K, Farzan M, Marasco WA. Evaluation of human monoclonal antibody 80R for immunoprophylaxis of severe acute respiratory syndrome by an animal study, epitope mapping, and analysis of spike variants. J Virol 2005 May;79(10):5900-6.

116. Hwang WC, Lin Y, Santelli E, Sui J, Jaroszewski L, Stec B, Farzan M, Marasco WA, Liddington RC. Structural basis of neutralization by a human anti-severe acute

respiratory syndrome spike protein antibody, 80R. J Biol Chem 2006 Nov 10;281(45):34610-6.

117. Prabakaran P, Gan J, Feng Y, Zhu Z, Choudhry V, Xiao X, Ji X, Dimitrov DS. Structure of severe acute respiratory syndrome coronavirus receptor-binding domain complexed with neutralizing antibody. J Biol Chem 2006 Jun 9;281(23):15829-36.

118. Zhu Z, Chakraborti S, He Y, Roberts A, Sheahan T, Xiao X, Hensley LE, Prabakaran P, Rockx B, Sidorov IA, Corti D, Vogel L, Feng Y, Kim JO, Wang LF, Baric R, Lanzavecchia A, Curtis KM, Nabel GJ, Subbarao K, Jiang S, Dimitrov DS. Potent cross-reactive neutralization of SARS coronavirus isolates by human monoclonal antibodies. Proc Natl Acad Sci U S A 2007 Jul 17;104(29):12123-8.

119. Greenough TC, Babcock GJ, Roberts A, Hernandez HJ, Thomas WD,Jr, Coccia JA, Graziano RF, Srinivasan M, Lowy I, Finberg RW, Subbarao K, Vogel L, Somasundaran M, Luzuriaga K, Sullivan JL, Ambrosino DM. Development and characterization of a severe acute respiratory syndrome-associated coronavirus-neutralizing human monoclonal antibody that provides effective immunoprophylaxis in mice. J Infect Dis 2005 Feb 15;191(4):507-14.

120. Roberts A, Thomas WD, Guarner J, Lamirande EW, Babcock GJ, Greenough TC, Vogel L, Hayes N, Sullivan JL, Zaki S, Subbarao K, Ambrosino DM. Therapy with a severe acute respiratory syndrome-associated coronavirus-neutralizing human monoclonal antibody reduces disease severity and viral burden in golden syrian hamsters. J Infect Dis 2006 Mar 1;193(5):685-92.

121. van den Brink EN, Ter Meulen J, Cox F, Jongeneelen MA, Thijsse A, Throsby M, Marissen WE, Rood PM, Bakker AB, Gelderblom HR, Martina BE, Osterhaus AD, Preiser W, Doerr HW, de Kruif J, Goudsmit J. Molecular and biological characterization of human monoclonal antibodies binding to the spike and nucleocapsid proteins of severe acute respiratory syndrome coronavirus. J Virol 2005 Feb;79(3):1635-44.

122. ter Meulen J, Bakker AB, van den Brink EN, Weverling GJ, Martina BE, Haagmans BL, Kuiken T, de Kruif J, Preiser W, Spaan W, Gelderblom HR, Goudsmit J, Osterhaus AD. Human monoclonal antibody as prophylaxis for SARS coronavirus infection in ferrets. Lancet 2004 Jun 26;363(9427):2139-41.

123. ter Meulen J, van den Brink EN, Poon LL, Marissen WE, Leung CS, Cox F, Cheung CY, Bakker AQ, Bogaards JA, van Deventer E, Preiser W, Doerr HW, Chow VT, de

Kruif J, Peiris JS, Goudsmit J. Human monoclonal antibody combination against SARS coronavirus: Synergy and coverage of escape mutants. PLoS Med 2006 Jul;3(7):e237.

124. Berry JD, Jones S, Drebot MA, Andonov A, Sabara M, Yuan XY, Weingartl H, Fernando L, Marszal P, Gren J, Nicolas B, Andonova M, Ranada F, Gubbins MJ, Ball TB, Kitching P, Li Y, Kabani A, Plummer F. Development and characterisation of neutralising monoclonal antibody to the SARS-coronavirus. J Virol Methods 2004 Sep 1;120(1):87-96.

125. Gubbins MJ, Plummer FA, Yuan XY, Johnstone D, Drebot M, Andonova M, Andonov A, Berry JD. Molecular characterization of a panel of murine monoclonal antibodies specific for the SARS-coronavirus. Mol Immunol 2005 Jan;42(1):125-36.

126. Kohler G, Milstein C. Continuous cultures of fused cells secreting antibody of predefined specificity. Nature 1975 Aug 7;256(5517):495-7.

127. Teillaud JL. Engineering of monoclonal antibodies and antibody-based fusion proteins: Successes and challenges. Expert Opin Biol Ther 2005 Sep;5 Suppl 1:S15-27.

128. Groner B, Hartmann C, Wels W. Therapeutic antibodies. Curr Mol Med 2004 Aug;4(5):539-47.

129. Thompson MA, Cancro MP. Dynamics of B cell repertoire formation: Normal patterns of clonal turnover are altered by ligand interaction. J Immunol 1982 Dec;129(6):2372-6.

130. Berry JD. Rational monoclonal antibody development to emerging pathogens, biothreat agents and agents of foreign animal disease: The antigen scale. Vet J 2005 Sep;170(2):193-211.

131. Berry JD, Rutherford J, Silverman GJ, Kaul R, Elia M, Gobuty S, Fuller R, Plummer FA, Barbas CF,3rd. Development of functional human monoclonal single-chain variable fragment antibody against HIV-1 from human cervical B cells. Hybrid Hybridomics 2003 Apr;22(2):97-108.

132. Hwang WY, Foote J. Immunogenicity of engineered antibodies. Methods 2005 May;36(1):3-10.

133. Hulett MD, Hogarth PM. Molecular basis of fc receptor function. Adv Immunol 1994;57:1-127.

134. Ghetie V, Ward ES. Transcytosis and catabolism of antibody. Immunol Res 2002;25(2):97-113.

135. Bogaards JA, Putter H, Jan Weverling G, Ter Meulen J, Goudsmit J. The potential of targeted antibody prophylaxis in SARS outbreak control: A mathematic analysis. Travel Med Infect Dis 2007 Mar;5(2):70-8.

136. Yuan X, Gubbins MJ, Berry JD. A simple and rapid protocol for the sequence determination of functional kappa light chain cDNAs from aberrant-chain-positive murine hybridomas. J Immunol Methods 2004 Nov;294(1-2):199-207.

137. Hofer T, Tangkeangsirisin W, Kennedy MG, Mage RG, Raiker SJ, Venkatesh K, Lee H, Giger RJ, Rader C. Chimeric rabbit/human fab and IgG specific for members of the nogo-66 receptor family selected for species cross-reactivity with an improved phage display vector. J Immunol Methods 2007 Jan 10;318(1-2):75-87.

138. Chung J, Rader C, Popkov M, Hur YM, Kim HK, Lee YJ, Barbas CF,3rd. Integrin alphaIIbbeta3-specific synthetic human monoclonal antibodies and HCDR3 peptides that potently inhibit platelet aggregation. FASEB J 2004 Feb;18(2):361-3.

139. Werner RG, Kopp K, Schlueter M. Glycosylation of therapeutic proteins in different production systems. Acta Paediatr Suppl 2007 Apr;96(455):17-22.